Anatase to Rutile Transition in Titanium Dioxide Photocatalytic Nanomaterials

by

Ciara Byrne, B.Sc.

Supervisor:

Prof. Suresh C. Pillai

Submitted to the Institute of Technology Sligo, December 2018
for the award of Doctor of Philosophy.

Declaration Page

Title: Anatase to Rutile Transition in Titanium Dioxide Photocatalytic Nanomaterials

Name: Ciara Byrne

ID Number: S00106961

Supervisor: Suresh Pillai

Declaration:

"*I hereby declare that this Doctoral Research Degree Thesis is entirely my own work and that it has not been submitted for any other academic award, or thereof, at this or any other education establishment*"

_____

Ciara Byrne

_____

Prof. Suresh Pillai

Abstract

Anatase and brookite are both considered metastable phases and transition irreversibly into the thermodynamically stable rutile phase at elevated temperatures (600-700°C in pure synthetic TiO_2). Anatase TiO_2 is widely accepted as the most photocatalytically active phase. However, TiO_2 is only active under Ultraviolet (UV) light (~4% sunlight). A chemical precursor modifier, chemical additive or dopant can be used to alter the transition temperature and increase the photocatalytic activity of TiO_2. These chemical additives/dopants/modifiers can result in a higher transition temperature and photocatalytic activity. However, some additives/dopants/modifiers have been known to reduce both. This work examined the effects benzoic acid, tungsten and boron nitride had on the transition temperature and the photodegradation of 1,4-dioxane. Benzoic acid and tungsten doping all increased the transition temperature compared to the control, with anatase still present at 800°C and 950°C respectively. All doped boron nitride samples were 100% rutile by 700°C, however the 0% BN-TiO_2 was 100% rutile from 600°C. There were varying results when examining the percent removal of 1,4-dioxane. Benzoic acid, tungsten and boron nitride showed increased photocatalytic activity. Out of all of the samples examined, only 3 samples showed 100% removal of 1,4-dioxane, these were 2% W-TiO_2, 4% W-TiO_2 and 8% W-TiO_2 at 800°C. When comparing the results for the transition temperature and photocatalytic activity of all dopants studied, 8% W-TiO_2 is considered the optimim dopant and concentration. This is due to 26% anatase still being present at 950°C and it showed 100% and ~80% 1,4-dioxane removal when calcined at 800°C and 900°C respectively. The current investigation therefore showed that using the sol-gel method for doping with tungsten, benzoic acid and boron nitride successfully improved the anatase to rutile transition temperature and photocatalytic activity of TiO_2.

Dedication Page

I would like to dedicate this thesis in memory of my granddad, John Brierton. His quick wit and great sense of humour brightened even some of my hardest days during the completion of this work. It was his immense pride and firm belief in me that spurred on my determination to complete this thesis to the best of my ability and in a timely manner. He will be forever loved and missed.

Acknowledgements

I would like to thank the following:

- The Institute of Technology Sligo for providing financial support, in the form of the IT Sligo President's Bursary, while completing this research.
- Prof. Suresh Pillai at Institute of Technology Sligo
- Dr Steven Hinder in the University of Surrey, UK
- Prof. Daphne Hermosilla from the University of Valladolid, Spain
- Dr Noemí Merayo and Dr Ángeles Blanco at Complutense University of Madrid, Spain
- Dr Rachel Fagan at the Centre for Research in Engineering Surface Technology (CREST), FOCAS Institute, Dublin Institute of Technology.
- Dr Luke O'Neill Centre for Research in Engineering Surface Technology (CREST), FOCAS Institute, Dublin Institute of Technology.
- Ms. Saoirse Dervin at Institute of Technology Sligo
- Mrs. Susan O'Rourke
- Mr. Philip Byrne
- John Keegan Jnr, Amy Keegan, Steven Byrne and John Keegan Snr.

Table of Contents

List of Abbrevations

A	Anatase
ABT	Anatase to Brookite Transition
ART	Anatase to Rutile Transition
at. %	Atomic %
BA	Benzoic Acid
BAT	Brookite to Anatase Transition
BET	Brunauer-Emmett-Teller analysis
BN	Boron Nitride
BRT	Brookite to Rutile Transition
C	Carbon
CB	Conduction Band
CO_2	Carbon Dioxide
e^-	Electrons
e^-_{CB}	'excited' electron in the condition band
E. Coli	Escherichia coli
E_a	Activation Energy
EPA	Environmental Protection Agency
eV	Electron volts
FTIR	Fourier Transform Infrared spectrometer
FTIR-ATR	Fourier Transform Infrared spectrometer used with an Attenuated Total Reflection accessory
GC	Gas Chromatography
$^{\bullet}HO_2$	Hydroperoxide radicals
H^+	Hydrogen ion
h^+_{VB}	Positive hole in the valence band
H_2O_4W	Tungstic Acid
*h*BN	Hexagonal Boron Nitride
N	Nitrogen
IPA	Isopropyl Alcohol/isopropanol
O	Oxygen
$^{\bullet}O_2^-$	Superoxide radicals

$^{\bullet}OH$	Hydroxyl radicals
$^{1}O_2$	Singlet Oxygen
$O_2^{\bullet-}$	Superoxide Anion radicals
N	Nitrogen
P25	TiO_2 reference. Previously manufactured by Degussa but now made by Evonik Industries, contains 75% anatase and 25% rutile.
PDT	Photodynamic Therapy
R	Rutile
Rh B	Rhodamine B
ROS	Reactive Oxygen Species
SEM	Scanning Electron Microscope
SEM-EDX	SEM-EDX -Scanning Electron Microscope with Energy Dispersive X-ray analyser
Ti	Titanium
TiO_2	Titanium Dioxide/Titania
TTIP/$Ti(OPr)_4$	Titanium Tetraisopropoxide
UV	Ultraviolet
VB	Valence Band
W	Tungsten
WO_3	Tungsten Trioxide
WWTP	Waste Water Treatment Plant
XPS	X-ray Photoelectron Spectroscopy
XRD	X-Ray Diffraction

List of Schemes, Figures and Tables

List of Schemes

List of Figures

List of Tables

Chapter 1 - Introduction

1.1 Background

Titanium dioxide (TiO_2) has many applications, which include photocatalysis, batteries, UV blockers, pigments for paint and filling material in cosmetics, textiles and papers.[1-3] TiO_2 is a metal-oxide semiconductor that has gained increasing interest in recent years because of its use in photocatalysis, its chemical stability and its large band gap energy.[4-6] TiO_2 is used as a photocatalyst because of its nontoxicity, ease of preparation and strong oxidising ability.[7] Photocatalysis is a method, which utilises light in order to activate a semiconductor (photocatalyst), which alters the rate of the chemical reaction without being used up during the reaction.[8-10] The use of TiO_2 as photocatalyst has a wide range of applications and has been used for environmental purposes (e.g. air and water purification). TiO_2 occurs in nature in three main polymorphs,[11-14] these are anatase (tetragonal, a=b=3.785Å, c=9.54Å), brookite (rhombohedral, a=5.143Å, b=5.456Å, c=9.182Å) and rutile (tetragonal, a=b=4.593Å, c=2.959Å).[1, 6-8, 11-19] The TiO_2 phases consist of $[TiO_6]^{2-}$ octahedral that are arranged by sharing edges, corners or both depending on the phase, while maintaining an overall stoichiometry of TiO_2.[6, 7, 20] Out of the three phases of TiO_2, anatase is widely regarded as the most photocatalytically active phase.[6, 7] Rutile has a high refractive index and UV absorptivity and is used for solar creams and pigments.[1] Anatase and brookite are both thermodynamically metastable and transition irreversibly into rutile at elevated temperatures.[4]

It should be noted that the anatase-rutile transition (ART) temperature is not well defined, however in pure synthetic TiO_2, this transition usually occurs between 600°C and 700°C.[16, 21] Dopants, chemical modifiers and chemical additives can be used in order to improve the photocatalytic activity and alter the transition temperature.[4] It is important to note in the design of nanomaterials that particle size surface area and volume play a vital part in catalysis, while contrasting photonic crystals rely on particle size and shape.[1] At present, TiO_2 can only utilise the UV light (<390nm) in solar irradiation due to its large band gap (3.2 eV). Solar light is made up of only 4% UV light but visible light counts for approximately 42% of solar light.[8, 22] A visible light (400-700nm) active, high temperature (≥1000°C) stable anatase phase is required for several applications, especially at the processing temperature of ceramic substrates.[6, 19, 23-25] This is important

for range of building material applications such as anti-bacterial tiles, self-cleaning ceramics, *etc.*.[6, 19, 23, 24]

1.2 Electronic Structure of TiO_2

As with all semiconductors, the TiO_2 electronic structure is comprised of occupied electron states and unoccupied electron states, the valence band (VB) and conduction band (CB) respectively.[26] Band gap value is the determining factor in indicating where in the solar spectrum semiconductors will absorb light.[26]

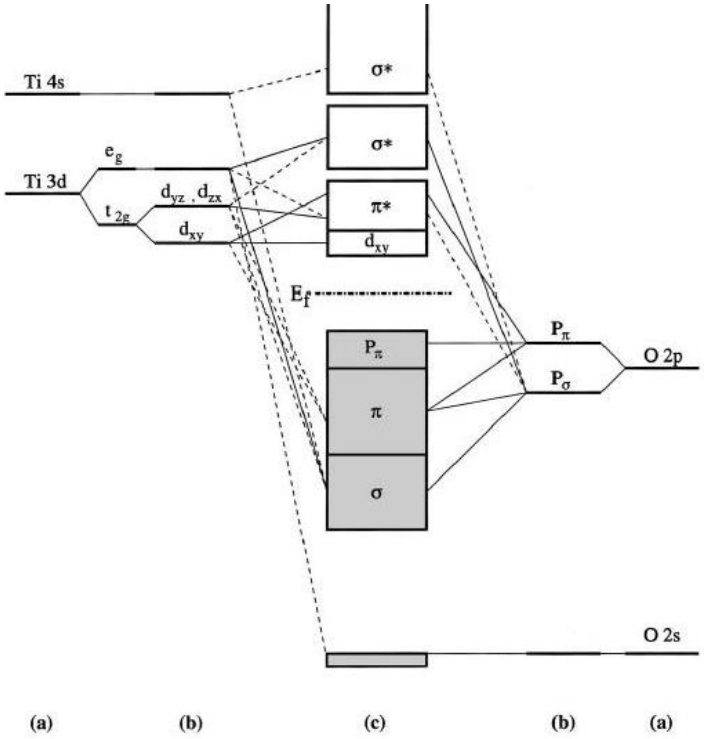

Figure 1.1: Electronic structure of anatase TiO_2, showing the (a) atomic levels, (b) crystal-field split levels, and (c) final interaction states.[27] Reprinted with permission from Asahi, R., Taga, Y., Mannstadt, W. & Freeman, A. J., *Physical Review B,* 61**,** 7459-7465, 2000. Copyright 2000 by the American Physical Society.

After completing a study into the chemical bonding in anatase TiO_2, Asahi *et al.* (2000) were able to form a diagram showing the molecular orbital bonding energy in anatase TiO_2.[27, 28] Figure 1.1 shows the chemical bonds between Titanium (Ti) and Oxygen (O) in TiO_2 and the hybridisation of the various energy levels.[27, 28] The main states involved in the CB and the VB in TiO_2 are O *2p*, Ti *3d* and Ti *4s.* The Ti *3d* and *4s* states compose the CB. Due to the crystal field splitting of Ti *3d*, the lower energy regions of the CB are comprised of the degenerate e_g-like and threefold t_{2g}-like states.[27, 28] While the VB is

formed from the O *2p* higher energy (O pπ), intermediate energy (pσ and pπ) and lower energy (pσ) regions.[27, 28]

1.3 TiO_2 Polymorphs

The vast majority of research previously performed on TiO_2 polymorphs has included examining the anatase and/or rutile phase. In nature, brookite is the rarest polymorph of TiO_2 and it is very difficult to synthesize it synthetically, there has been no significant research on brookite for these reasons.[4, 29] There are other polymorphs of TiO_2.[4] These TiO_2 polymorphs have been prepared synthetically at various pressures and temperatures,[1, 4, 12, 29, 30] and they include:

- Cotunnite - is a titanium nine-coordinated to oxygen in the cotunnite ($PbCl_2$) structure and is one the hardest oxides that exists.[31] It is a orthorhombic crystal.[30]
- Cubic TiO_2 – includes titanium fluorite and titanium pyrite. Cubic TiO_2 is obtained using a laser-heated diamond-anvil cell at 1900-2100K (~1627-1827°C) under 48 GPa.[17, 32-34]
- Srilankite (or TiO_2 II) – is a high pressure polymorph which can be made from anatase, rutile or brookite, is orthorhombic, is metastable and will convert to rutile once it has been heated to 600°C under atmosphere pressure for a few hours.[35]
- Hollamdite (or TiO_2 (H)) – The complete oxidation of K_xTiO_2 (x is close to 0.5) results in the formation of TiO_2 (H). It is a tetragonal phase and transforms into anatase at 410°C.[36, 37]

These polymorphs are of minor importance for research and development purposes, and will not be discussed in any detail in this thesis.[4]

The basic structure of TiO_2 consists of a titanium atom surrounded by six oxygen atoms in a distorted octahedral. [1] The two bonds between the Ti and the O at the apices of each octahedral are slightly longer than the other bonds.[1] $[TiO_6]^{2-}$ octahedra are interconnected differently for each phase, each phase has a different spatial arrangement sharing corners and edges in a different manner. Anatase shares corners, rutile shares edges and brookite shares edges and corners, Figures 1.2 & 1.3. The manner in which the $[TiO_6]^{2-}$ octahedra are shared gives an overall stoichiometry of TiO_2.[1]

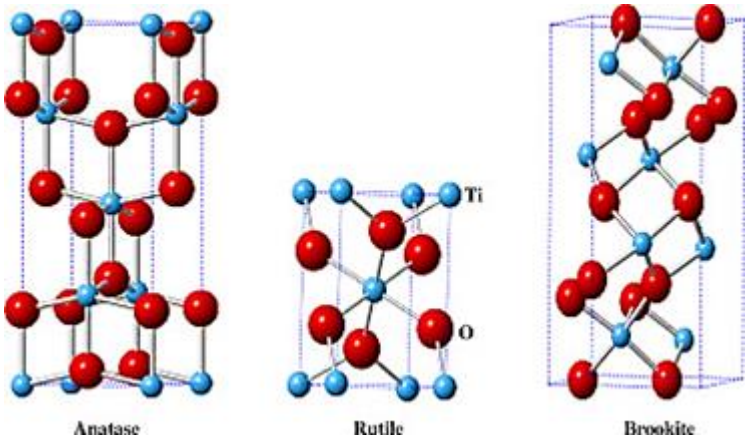

Figure 1.2: The arrangement of atoms in the anatase, rutile and brookite phases of TiO_2.[38] Reprinted from Journal of Photochemistry and Photobiology C: Photochemistry Reviews, 25, Etacheri, V., Di Valentin, C., Schneider, J., Bahnemann, D., & Pillai, S. C, Visible-light activation of TiO_2 photocatalysts: Advances in theory and experiments, 1–29, Copyright 2015, with permission from Elsevier.

The relaxation of the Ti-O-Ti bonds is achieved in the linear rutile phase, as a result it is thermodynamically favoured. However, anatase/brookite is a result of the less relaxed right angle configuration.[1] Kumar and Rao (2014) define the transformation between titania phases as "*co-operative movement of titanium and oxygen atoms, in contrast to struct diffusion mechanism.*" [1]

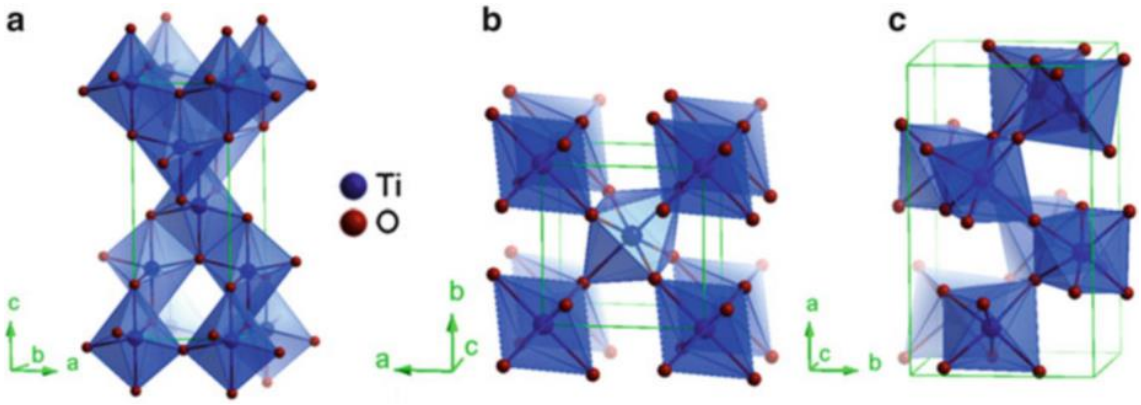

Figure 1.3: Arrangement of crystals in the (a) anatase, (b) brookite and (c) rutile phases of TiO_2. Reprinted by permission from Springer Nature, In: Colmenares J., Xu YJ. (eds) Heterogeneous Photocatalysis. Green Chemistry and Sustainable Technology. Guo Q., Zhou C., Ma Z., Ren Z., Fan H., Yang X., Fundamental Processes in Surface Photocatalysis on TiO_2.), COPYRIGHT (2016).

Scheme 1.1, shows the possible pathways for the phase transition between the three major phases of TiO_2.[1]

Rutile ⟵ Anatase ⟷ Brookite ⟶ Rutile

Scheme 1.1: Possible transition pathways for TiO_2 phases.[1, 39]

As brookite is considered more stable than anatase but less stable than rutile, lower energy is required for anatase-brookite transition (ABT) than brookite-rutile transition (BRT) while ART requires the most energy: 11.9 kJ/mol, 163.8 kJ/mol and 400 kJ/mol (for bulk) respectively.[40]

1.3.1 Anatase

In the synthesis of TiO_2, anatase is generally the major product of inorganic synthesis and is the main constituent of nanocrystalline TiO_2 materials. Anatase crystallises in a tetragonal system. The anatase phase is a low-temperature metastable polymorph with a density of 3.894g/cm^3, [41] however there are two papers that state that the density is 3.840g/cm^3, [1, 6] an optical band gap of 3.25eV, a refractive index of 2.5 and an absorption threshold that corresponds to 280nm. Anatase can be transformed into rutile during calcination as anatase in thermodynamically unstable.

Anatase can be regarded to be built up from octahedra that are connected by their vertices, i.e. each octahedral shares its corners (Figures 1.2 and 1.3). In anatase, the [TiO_6] is surrounded by eight octahedra.[1] The interstitial spaces between octahedra are larger in anatase then in rutile, making rutile denser than anatase.

Anatase shows a better photocatalytic activity and antibacterial performance than the other phases of TiO_2.[6, 25] The higher photocatalytic activity is due to anatase having high crystallinity and a large specific surface area, which are desirable parameters in photocatalytic reactions.[4, 6, 8, 12, 42]

1.3.2 Brookite

Relatively little is known about the brookite phase of TiO_2.[43] It is rare to find this TiO_2 phase in nature and a pure sample can only be synthesized under very sensitive conditions.[1] Brookite is present as a minority product during the synthesis of TiO_2.[11, 44] Brookite has an orthorhombic structure (Figures 1.2 and 1.3).[1, 6, 7, 41, 45] It is metastable at

all temperatures and transitions into rutile at elevated temperatures.[4, 7, 11, 46] Brookite's structural characteristics are an intermediate between anatase and rutile.[1, 43] Brookite has a density of 4.11g/cm^3, an optical band gap of 3.11 eV, an indirect band gap of 2.85 and a refractive index of 2.63.[1]

Brookite is most stable (thermodynamically) for crystal sizes between 11-35nm.[11, 12] Brookite tends to transfer directly into rutile, while anatase may transform either directly to rutile or into brookite and then into rutile.[11] Brookite crystals are connected by the edges and corners of the crystalline structure.[1, 7, 12] The ability to produce a pure brookite sample remains a challenge as there tends be a co-existence or remains of anatase.[1]

1.3.3 Rutile

Rutile is produced from anatase after the samples has been heated at elevated temperatures. When rutile is synthesized, it crystallises in a tetragonal system (Figure 1.2 and 1.3). Rutile is the only stable phase of TiO_2 at all temperatures and pressures. Rutile is thermodynamically more stable, is the densest TiO_2 phase at 4.25 to 4.26g/cm^3,[1, 6, 41] has an optical band gap of 3.0-3.05eV[41] also stated as 3.02eV,[47] a refractive index of 2.7 and an absorption threshold which corresponds to 410nm. Rutile has the best dielectric and optical properties of the TiO_2 polymorphs.[17] For many years, rutile has been studied comprehensively as it is the most stable phase at high temperatures and is produced in most attempts to grow TiO_2 crystals.[48] Rutile is generally less active compared to anatase, due to a lower surface affinity from any organic compounds and higher rates of recombination of photogenerated charge pairs.

The rutile structure is composed of corner-sharing octahedra, with each octahedron surrounded by ten octahedra.[1, 4] Rutile is more symmetric and compacted when compared to the other TiO_2 polymorphs.[1, 4] As rutile has a high refractive index, excellent light scattering efficiency and UV absorptivity, it is utilised as a filter in sun cream, pigments and optical communication devices.[1, 4]

1.4 Anatase to Rutile Transition (ART)

1.4.1 Formation of Titania and Phase Transition

Although the only thermodynamically stable phase is rutile, the initial crystalline TiO_2 phase generally formed in a sol-gel preparation is anatase, which transforms to rutile when calcined at high temperatures.[49] In terms of the structure, it is easier to arrange the

$[TiO_6]^{2-}$ octahedral into the anatase configuration in comparison to rutile.[4, 49-51] From a thermodynamic view, when anatase has a lower surface free energy it can lead to an increased recrystallisation of the phase.[4, 52, 53] Rutile can be formed at temperatures close to room temperatures by controlling the hydrothermal synthesis (with precipitation of a crystalline phase).[4, 51, 54-56] The only other method of producing rutile is by heating TiO_2 at elevated temperatures.

The control of the kinetic conditions that influence the anatase to rutile phase transition is one area of research that is important. Understanding this is vital when using TiO_2 for high temperature applications or when elevated temperatures are required for the production of materials (*e.g.* sintering of tiles).[4] It is important to know the stability of each of the three phases, the kinetics that is involved in the transition between each phase (phase transitions pathways shown in Scheme 1) and how to manipulate this in order to obtain the required phase.[4] The parameters during the synthesis of TiO_2 has a major impact on the resulting phase in the product.[4]

The kinetics of the transition includes the temperature of the phase transition and how long it takes.[4] Generally, the transition from anatase to rutile is considered to begin at approximately 600°C and is considered to be completed at 700°C.[14] There have been studies that have shown that this transition temperature can occur between 400-1200°C depending on a number of conditions, *e.g.* raw materials and method of synthesis.[12, 15, 48, 57-60] The phase transition does not occur immediately, this is determined by the time it takes for the crystals to reform.[4] There are numerous factors that will influence these kinetic conditions (time, activation energy and temperature),[1, 4] for example the particle size, purity, nature of Ti precursor, addition of modifiers, *etc*.[1, 4, 61-64] These factors will be discussed in Sections 1.4.2, 1.4.3, 1.4.4 & 1.5.

During ART, the bonds of the anatase phase break and then reform into the larger crystals of the rutile phase, this processes is known as a reconstructive processes.[4, 65] This can be impacted by the concentration of particle present.[1]

1.4.2 Effects of Synthesis Conditions on Titania Formation and Transition

In 2014, Kumar and Rao completed an extensive review on the synthesis of TiO_2 and the effect various parameters during synthesis has on the ART.[1] The study states that despite the research completed to-date, there has not been a standard method identified for

controlling the TiO_2 phase. This is due to large number of experimental conditions during synthesis *e.g.* method of synthesis, role of solvents and complexing agents, solution pH, titanium precursors, *etc.*[1] Factors which are of importance to this study are the sol-gel synthesis, the impact of aging solutions and the titanium precursor.

Sol-Gel Synthesis

Sol-gel synthesis is one method used to produce TiO_2. It is a inorganic polymerisation reaction which converts the precursor solution into a solid when water is present and results in a metal-oxo-polymer (*i.e.* metal alkoxides or metal salts).[1] When an acid is present the method is a hydrolysis-condensation reaction, the hydrolysis ratio and titanium precursor co-ordinating groups can direct the reaction process.[1, 66-69] Growth in the cross-linked network TiO_2 system is a result of condensation while hydrolysis results in the production of original nuclei or basic unit of TiO_2.[1] The rate at which the sol-gel reaction occurs dictates the resulting phases formed and effects the uniformity of the particles. An amorphous phase and non-uniform particles are found when there is a fast rate of reaction, while a crystalline sample could be formed from a slower rate of reaction.[1] However, the use of precursors with alkoxy groups can result in fine particles with uniform size as they are used to slow the rate of hydrolysis.[1, 70] Large quantity of powders are easily produced during this method.[1]

Aging Effects

Generally, powders formed from the sol-gel preparation are amorphous and require calcination for the formation of TiO_2 phases such as anatase. However, the formation of anatase can be promoted and the crystallinity can be improved by heating or boiling the sol-gel for 12-48 hours.[1] The time a sol-gel is aged for also can have an effect on the physical properties of the gel and the ART temperature.[71] The longer the aging time of the sol-gel the higher the transition temperature will occur at.[1]

Titanium Precursors

One major impacting factor on the morphology and crystalline phase of TiO_2 is the nature of the Ti precursor.[1] Anionic species and proton/hydroxyl concentrations effects how the polynuclear complexes are formed and organised, which impact the polymorph nucleation and growth.[1] Precursors that are commonly used (titanium chlorides, titanium halides, *etc.*) are considered to be very sensitive to moisture (hydrolyse in water or

moisture in air), expensive and corrosive. The use of these during synthesis results in the formation of amorphous TiO_2 and require sintering for the formation of anatase.[1]

1.4.3 Thermodynamics and Kinetics of ART

The ART in TiO_2 includes both kinetic and thermodynamic aspects.[1] During ART, two of the six Ti-O bonds in the anatase octahedral are broken which causes the reorganisation of titanium and oxygen, it also causes the formation of oxygen vacancies.[1, 72] The presence of the oxygen vacancies increases the rate at which the breakage of these bonds occur at and leads to rapid crystalline growth.[1] TiO_2 anatase is metastable and tends to transform into a more thermodynamically stable rutile phase, at fairly high temperatures.[73] At all temperatures and pressures, rutile is the most stable TiO_2 phase.[4] This has been reported after a number of thermodynamic studies have been carried out.[53, 74-77] The results from these studies show that it would take negative pressures in order for anatase to be more stable than rutile.[78] This phase transition from anatase to rutile is a non-reversible process due to the greater thermodynamic stability of the rutile phase over the anatase phase.[6] As stated in Section 1.4.1., there have been various temperatures that have been reported at which the transition occurs.[4] A wide range of parameters can be altered in order to extend the ART to higher temperatures, *i.e.* higher temperatures than transition of pure synthetic TiO_2.[16] However, the general consensus is that in a pure anatase phase TiO_2 powder, the transition happens between 600-700°C.[4]

In 1965, it was reported that the percentage of anatase varied when heated to elevated temperatures, and in some cases it was not present.[4, 60] This was a result of the TiO_2 powders being contaminated with impurities, thus ART was hindered. When Shannon and Pask (1965) studied the transition temperature they analysed the samples with differential thermal analysis (DTA) instead of onsets and/or high calcination temperature.[4, 60] The use of DTA has showed higher transition temperature when compared with the method used for X-ray Diffraction (XRD).[4] The TiO_2 phase transition begins at approximately 600°C, it is very likely that the exotherm maximum is identified later in the phase transition *i.e.* when the rate of the transition is at the highest.[4] The rate of the transition then begins to significantly slow down with the corresponding latent heat when anatase transfers to rutile.[4] The parameters of an experiment can greatly affect the DTA analysis and therefore the curve produced and how these are incorporated, *e.g.* a

slow calcination rate causes the peak to broadening (this results in the onset temperature to lower).[4]

The kinetics of the TiO_2 phase transition was studied by Rao (1961), the conditions for the experiments were on a soak of 24hrs, the use of extremely pure powders and analysis with XRD.[79] Rao reported that the rate reduced with the temperature until it came to a practical limit (610°C ±10°C).[4, 79] After this temperature, the rate of the phase transition became infinitesimally slow. While this research was completed over 5 decades ago, there have been studies since then that support Rao's research.[80-83]

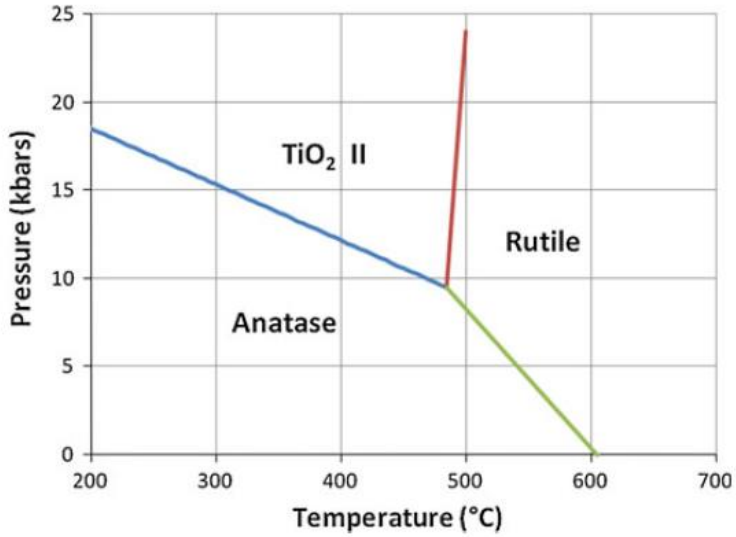

Figure 1.4: Reaction boundaries from transitions between anatase, srilankite (TiO_2 II) and rutile.[4] Reprinted with permission from Hanaor, D. A., & Sorrell, C. C. (2011). Review of the anatase to rutile phase transformation. *Journal of Materials science*, *46*(4), 855-874.

Rutile is the phase of equilibrium for TiO_2, when anatase is present it indicates that equilibrium has not being reached.[4, 53, 75-79, 84, 85] When the pressure and temperature equilibrium approximation was examined by Danchille *et al*. (1968) one main conclusion was made, ART occurs at 605°C at 1 atmospheric pressure (101 kPa), see Figure 1.4.[80] The phase boundaries were later described as the reaction boundaries by Jamieson and Olinger (1969).[78]

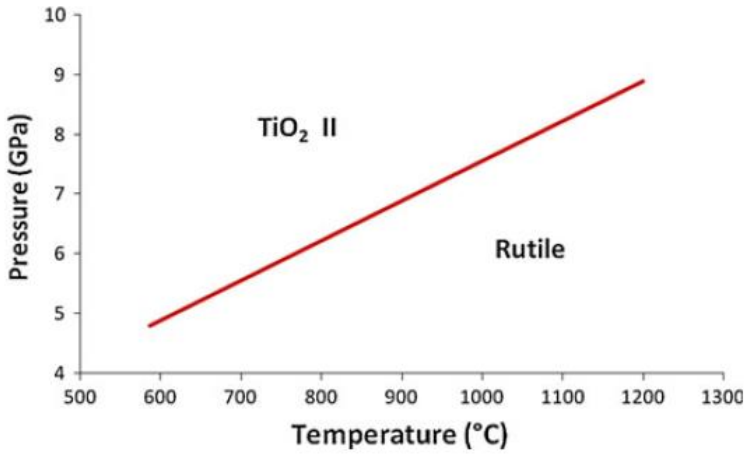

Figure 1.5: Suspected behaviour for the transition of rutile to TiO_2 II.[4] Reprinted with permission from Hanaor, D. A., & Sorrell, C. C. (2011). Review of the anatase to rutile phase transformation. *Journal of Materials science*, *46*(4), 855-874.

All research is in agreement that ART is irreversible.[4] However, there has been some consideration given to the possibility that when high pressures is applied, rutile converts to the α-PbO_2 structure of the TiO_2 II phase (Figure 1.5).[86, 87]

In order for ART to react at significant rate, a vast amount of thermal energy is needed so that the atoms can rearrange themselves.[4] The activation energy (E_a) required for the ART varies from 147-837 kJ/mol.[1, 88-90] Large particle size distribution and variation in morphology results in a high E_a for ART. The thermal energy required is considered to be reached between 600-700°C for bulk TiO_2 samples, when dopants and impurities are not present.[4] The presence of oxygen vacancies in the sublattice significantly affects the TiO_2 phase transition.[4, 81, 91, 92] As the oxygen vacancies increase during the transition, it causes the oxygen sublattice to become less rigid. This increases the ability of the atoms to rearrange for the transition.[4, 60, 93, 94]

1.4.4 Morphological Effects

The grain morphology of the phases has a vital role in the photocatalytic applications of TiO_2.[4] The stability of the TiO_2 phase is largely impacted by the grain size of the initial powder.[1] There have been reports of nanocrystallinity reducing the required temperature for disinfection and improving photocatalytic acitivity.[44, 48, 53, 95] One main goal is to stop grain growth of TiO_2 during calcination, this will give the samples a higher surface area and enhance its performance.[4] The stability of the anatase phase compared to rutile is

dependent on the environment it is present in. For example there is a difference at which size anatase is stable at in water or in a vaccum.[1]

The anatase planes have a lower surface energy in comparison to that with rutile,[44] thus anatase is stable with crystals of very small sizes and large surface areas.[4] When in the presence of brookite, anatase will transform into rutile at a faster rate if it has a larger grain size compared to brookite than if it had a smaller grain size compared to brookite.[1] The grain size and the surface area of anatase compared to brookite determines the order of transition between the three phases and if ABT or brookite-anatase transition (BAT) occurs (see in Scheme 1). If brookite has a grain size which is smaller than critical size than BAT to ART occurs or brookite directly transitions into rutile.[1] When the opposite occurs *i.e.* brookite grain size is larger than critical size than ABT to ART occurs or ART only takes place. However, anatase and brookite both directly transition into rutile when the grain size of anatase and brookite are equal. [1] Changes to the surface energy have a greater effect on the phase transition than changes to the thermodynamic, when crystalline size is below the critical size, this leads to anatase having the lower free energy.[44, 53, 96] As the transition proceeds, there is increasing grain growth in anatase and formation of rutile.[53, 59, 91, 97-101] Anatase grains that are side by side begin to merge together, causing the rutile grains to begin to form until there is no more room for growth.[58, 102] The decrease of surface area and photocatalytic activity is a direct result of this grain growth.[53, 103, 104]

1.5 Dopants/Chemical Modifiers

In order to improve the photocatalytic properties of TiO_2, the majority of research has focused on the effect that dopants have.[4] For a dopant to be considered effective it is required to:

- Reduce the band gap[4, 105, 106]
- To produce a mid-gap state[4, 107, 108]
- Improve the charge carrier separations[4, 53, 109]
- Increase the level of adsorbed species[4, 110]

Dopants, such as Cu^{2+}, Co^{2+}, Fe^{2+}, *etc.*, are known to accelerate the reaction while others, such as SO_4^{2-} and PO_4^{3-} , are known to retard it.[15]

When a substitutional solid solution is formed, the ions from the dopant can be incorporated into the anatase lattice and can have an effect on the oxygen vacancy levels.[4] This can stop the transition from occurring. When interstitial solid solution formation occurs lattice constraint could possibly result in destabilisation or stabilisation, which is dependent on size, valence and content effects.[4] This also has an effect on ART.

1.5.1 Non-Metal Dopants

Nitrogen

Nitrogen (N) has been considered to be relatively simple to incorporate into the TiO_2 matrix because of its atomic size when compared with the atomic size of oxygen, its high stability and its small ionisation energy.[8, 111, 112] One of the first examples of using N doping was in 1986 when Sato added NH_4OH to a TiO_2 sol-gel procedure, which showed visible light activation.[8, 113, 114] Since then there has been extensive research into N-doped TiO_2, the properties of the samples and the effect it has on photocatalysis. When examined with model pollutants (*e.g.* phenols, methylene blue, volatile organic compounds), N-doped TiO_2 as a visible light active photocatalyst has been reported to degrade the pollutants successfully.[8] Doping TiO_2 with N has been reported to cause the transition to occur at elevated temperatures.[4]

A number of methods have been examined for the incorporation of nitrogen into TiO_2, such as sputtering, atomic layer deposition, but the most used method is sol-gel synthesis. This method includes a Ti precursor (*e.g.* titanium tetra-isopropoxide or titanium tetra-chloride) and a N precursor (*e.g.* nitrates, urea or ammonium salts).[8] One pioneering and successful sol-gel method for a visible light active photocatalyst is the use of a surfactant containing N with a Ti precursor, Choi *et al*. (2007) used dodecylammonium chloride as the surfactant.[8, 115] Another method that has been used is synthesising TiO_2 and then doping with N containing chemicals (NH_3, urea, gaseous nitrogen, and ethylamine) at elevated temperatures.[8, 116-118] When this method is used, the atoms from the nitrogen are mainly found on the surface of the TiO_2.

Most of the results of N-doped TiO_2 report that the nitrogen acts as a substitutional element, either on the oxygen lattice sites or the interstitial lattice sites. Determining which has occurred is analysed with XPS by looking at the two binding energies for the nitrogen 1s orbital (N *1s*) at 396eV and 400eV.[8]

Carbon

Using carbon (C) as a dopant has shown favourable results for visible light activity when used with TiO_2.[8, 119, 120] When the C is doped onto the TiO_2 it narrows the band gap to < 3.2eV and improves the use of anatase as a photocatalyst.[4, 8, 85] While nitrogen has been reported to be the most promising non-metal dopant, using carbon has gained interest in recent years.[10] Hanaor and Sorrell (2011) commented on the fact that there is a lack of reported research on the effects Carbon has on the anatase to rutile phase transition.[4] This is due to the oxidation of C at temperatures lower than the transition temperature. They suggest that as C is a reducing agent it would likely cause the sample to transition to rutile at lower temperatures than normal.[4]

One study that used C doped TiO_2 was when Etacteri *et al.* (2013) used it for doping TiO_2 heterojunctions (anatase and brookite).[10, 121] This study showed that the C doped TiO_2 can be used as a photocatalyst that utilises visible light for antibacterial applications.[121]

1.5.2 Metal Dopants

The alteration of titania with transition metals (including Cr, Co, V and Fe) have made it possible to use visible light for photocatalysis.[8, 122-125] However, some transition metals can end up being used as recombination sites, which leads to the reduction of the quantum efficiency.[8] It has been stated that while the band gap energy is decreased when metal is doped on TiO_2, the photocatalytic properties are not significantly improved. This would suggest the transition metals are not being included within the structure of TiO_2 and the ions sit on the surface blocking some of the reaction sites.[8] Cr-doped TiO_2 actually reduces the photocatalytic activity, but when Morikawa *et al.* (2006) co-doped Cr and V onto TiO_2 they reported that there was an increase in photocatalytic activity.[126] There have been a significant number of studies that examined metal doped TiO_2, some of the dopants that have been used to date include Al, Au, Co, Cr, Cu, Fe, Mn, Mo, Ni, Nb, Ru, Pt, V, W and Y.[4, 8] Tables 1 and 2 show example of dopants that have been used to inhibit the transition (Table 1) and promote the transition (Table 2) from anatase to rutile.

Table 1.1: Dopants that are phase transition inhibitors

Element	Chemical used	References
Al	AlOOH, $Al(OC_4H_9)_3$, $AlCl_3$, $Al(NO_3)_3$	4, 59, 99, 100, 127
Au	$HAuCl_4$	4, 128
Fe	$FeCl_2$	4, 129
Mn	$Mn(NO_3)_2$, <1%mol $Mn(CH_3COO)_2$	4, 130, 131
Nb	$NbCl_5$	4, 132
Y	$Y(NO_3)_3$, Y_2O_3	4, 81, 133

Table 1.2: Dopants that are phase transition promoters

Element	Chemical used	References
Co	CoO	4
Cr	$CrCl_3$	4, 132
Cu	CuO	4
Li	LiF	4
Ni	$Ni(NO_3)_2$, $Ni(CH_3COO)_2$	4, 134, 135
V	VO_2, V_2O_5	4, 134, 136

Gold

Li and Li (2001) examined the use of Gold as a TiO_2 dopant photocatalyst for water and wastewater treatment.[137] This research uses concentrations of 0.25%-3.0% Gold ions (Au/Au^{3+}), with tetrachloroauric acid as the source and titanium tetra-isopropoxide (TTIP) as the Ti precursor. All samples were in the anatase phase, with peaks for Au. The 0.5% Au-TiO_2 was reported to show the highest photocatalytic activity. There have also been other studies that have used tetrachloroauric acid as the source of Gold,[138, 139] but they used titanium butoxide as the Ti source instead of TTIP. Buso *et al.* (2007) examined the effect various calcine temperatures (100-500°C) have on phase and photoactivity of Au-TiO_2,[138] while Li *et al.* (2007) studied the sample effects of varying the concentration of Au-TiO_2 (0, 0.1, 0.5, 1, 2 and 5% of mesoporous nanomaterials.[139] Both studies show an improvement in the photocatalytic activity, however Buso *et al.* (2007) found that there were only gold peaks up until 400°C and anatase was detected at 500°C. [138, 139]

Tetrachloroaurate (III) trihydrate has also been used as a source of Gold for the doping of TiO_2.[140, 141] Xu *et al.* (2007) used P25 TiO_2 (previously manufactured by Degussa but now made by Evonik Industries, which contains 75% anatase and 25% rutile), while Rahulan *et al.* (2011) use TTIP as the Ti precursor.[140, 141] Xu *et al.* (2007) use the Au-TiO_2 photocatalyst for eradicating human colon cancer LoVo cells in photodynamic therapy.[140] Of all concentrations (0, 1, 2, 3 and 4%), the 2% Au-TiO_2 proved to be the optimum concentration for increasing the photocatalytic inactivation of tumour cells, when comparing with pure TiO_2.[140] The increase in % Au concentration also inactivated the LoVo cells.[140] These results show promise for future cancer treatment with doped TiO_2.[140] Rahulan *et al.* (2011) also varied the concentration percent (0, 0.1, 0.3, 0.5 and 1.0 mol %) with the samples being at a constant temperature (100°C).[141] This study reported that anatase is detected for all samples, there were no peaks for Gold present when XRD was ran, Au particles were not in high enough concentration for dectection.[141]

Palladium

Potassium tetrachloropalladate (K_2PdCl_4) was doped onto two different sources of TiO_2, commercial TiO_2 (100% anatase) and TTIP.[142] Both contained 0.5 %wt. Pd and were calcined between 300-550°C.[142] The synthesised Pd-TiO_2 (K_2PdCl_4 and TTIP) showed no peaks on XRD until 350°C, at which point the anatase phase formed. Anatase was detected in all samples up until 550°C. The sample with the commercial TiO_2 included, had only anatase at all temperatures.[142] The synthesised sample did show better activity as a photocatalyst over the sample containing commercial TiO_2.[142]

Comparative Studies

Epifani *et al.* (2000) doped different thin films, including TiO_2, with Silver (Ag) or Gold. $AgNO_3$ and $HAuCl_4.3H_2O$ were used as the Ag and Au precursors respectively and titanium tetrabutoxide was used as the source of titanium.[143] There were two separate samples made up in this method, one containing Au-doped TiO_2 and one with Ag- doped TiO_2. These was calcined at various temperatures, Ag films were calcined between 500-800°C and Au films were calcined between 100-700°C.[143] There are Ag peaks shown on the XRD when heated to 500°C, they are more prominent when H_2 is used for the heat treatment after preheating with air at the same temperature. However, when the temperature increases with this method there is a decrease in the Ag peak intensity. The peaks for the remaining temperatures are due to the anatase phase. When the samples have been calcined with H_2 at 600° and 700°C, new peaks are formed, Epifani *et al.*

(2000) state that these are due the presence of Ti_3O_5. There are peaks for Au on the XRD diffractogram between 100-500°C, above 500°C there is detection of the anatase phase.[143]

There have been two studies that examine the effects Silver, Gold or Platinum (Pt) has on TiO_2 transition and its use as a photocatalyst.[144, 145] Longanathan *et al.* (2011) used TTIP as the Ti precursor, $AgOOCCH_2$ (Ag source), $HAuCl_4.4H_2O$ (Au source) and H_2PtCl_6 (Pt source), while Mogyorosi *et al.* (2009) used the standard Degussa P25 TiO_2 (89% anatase and 11% rutile), silver nitrate, hexochloroplatinic acid and gold (III) chloride.[144, 145] Mogyorosi *et al.* (2009) examined the hydrogen production with each of the doped TiO_2 samples, the Pt-doped TiO_2 was reported to be the most favourable results in comparison to the Au-doped TiO_2 and the Ag-doped TiO_2.[145] The report concluded that research can be completed in order to improve the experimental conditions and noble metal loading.[145] Longanathan *et al.* (2011) used a number of concentrations of the dopants (0.05, 0.1, 0.3, 0.5, 0.8 and 1.0 wt.%) for the examination of ART.[144] Anatase was the only phase detected with XRD for the three dopants, with the exception of 1 wt.% Au-TiO_2 which had characteristic peaks for Au presence.[144]

1.6 Photocatalysis

The ability of TiO_2 to act as a photocatalyst was first discovered approximately 90 years ago.[146, 147] However, it did not become an extensively researched area until Fujishima and Honda discovered that TiO_2 electrode could be used to photocatalytically split water in 1972.[146-150] In the decades since this discovery, there has been extensive research in understanding the photocatalytic process and attempting to improve the efficiency of using TiO_2 as a photocatalyst.[148] There also has been a significant number of publications examining the applications photocatalysts, *e.g.* water or air decontamination and self-cleaning surfaces.[146, 151] The reactions for heterogeneous photocatalysis occur at the surface of the semiconductor material.

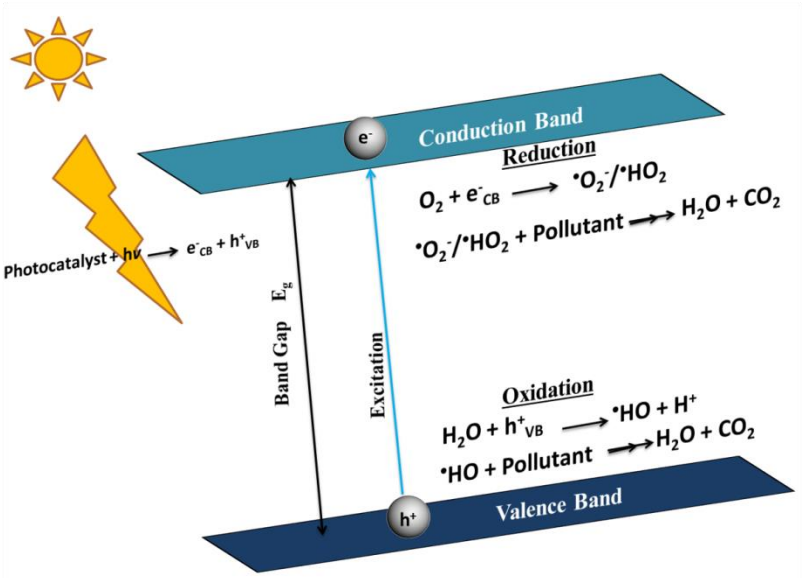

Figure 1.6: Mechanism of Photocatalysis. [Original publication – Appl. Catal. B, 2018, 225, 51-75]

Photocatalysis is initiated by the photocatalyst (*e.g.* semiconductor TiO_2) being bombarded with photons (hν) from UV light (from an artificial source or solar light).[4, 148] These photons cause the electrons (e^-) on the surface photocatalyst to become 'excited' in the VB if the energy of the photons is greater than the band gap, this causes the e^- to go up into the CB, see Figure 1.9.[4, 8, 146] Once the e^- have absorbed to the CB (e^-_{CB}), a positive hole is formed on VB (h^+_{VB}) (eq. 1.1 and Figure 1.6).[8, 9, 152, 153]

$$TiO_2 + h\nu \longrightarrow h^+_{VB} + e^-_{CB} \qquad \text{(eq. 1.1)}$$

The excited electrons that are now in the CB (e^-_{CB}) will react with Oxygen (O_2), which produces superoxide radicals (${}^{\bullet}O_2^-$), or hydroperoxide radicals (${}^{\bullet}HO_2$), see Figure 1.6 and eq. 1.2.[9, 154, 155] These reactive oxygen species are then used for the degradation of pollutants into water (H_2O) and carbon dioxide (CO_2), see Figure 1.9.[156, 157] The superoxide radicals can also be used for secondary degradation steps.[158] While this reaction is occurring, the oxidation of water takes place at the positive hole in the VB (h^+_{VB}).[9] This reaction generates hydroxyl radicals (${}^{\bullet}OH$) and hydrogen ions (H^+), see Figure 1.6 and eq. 1.3.[9] The ${}^{\bullet}OH$ reacts with pollutants present and forms H_2O and CO_2.

$$e^-_{CB} + O_2 \longrightarrow {}^{\bullet}O_2^- \qquad \text{(eq. 1.2)}$$

$$h^+_{VB} + H_2O \longrightarrow {}^{\bullet}OH + H^+ \qquad \text{(eq. 1.3)}$$

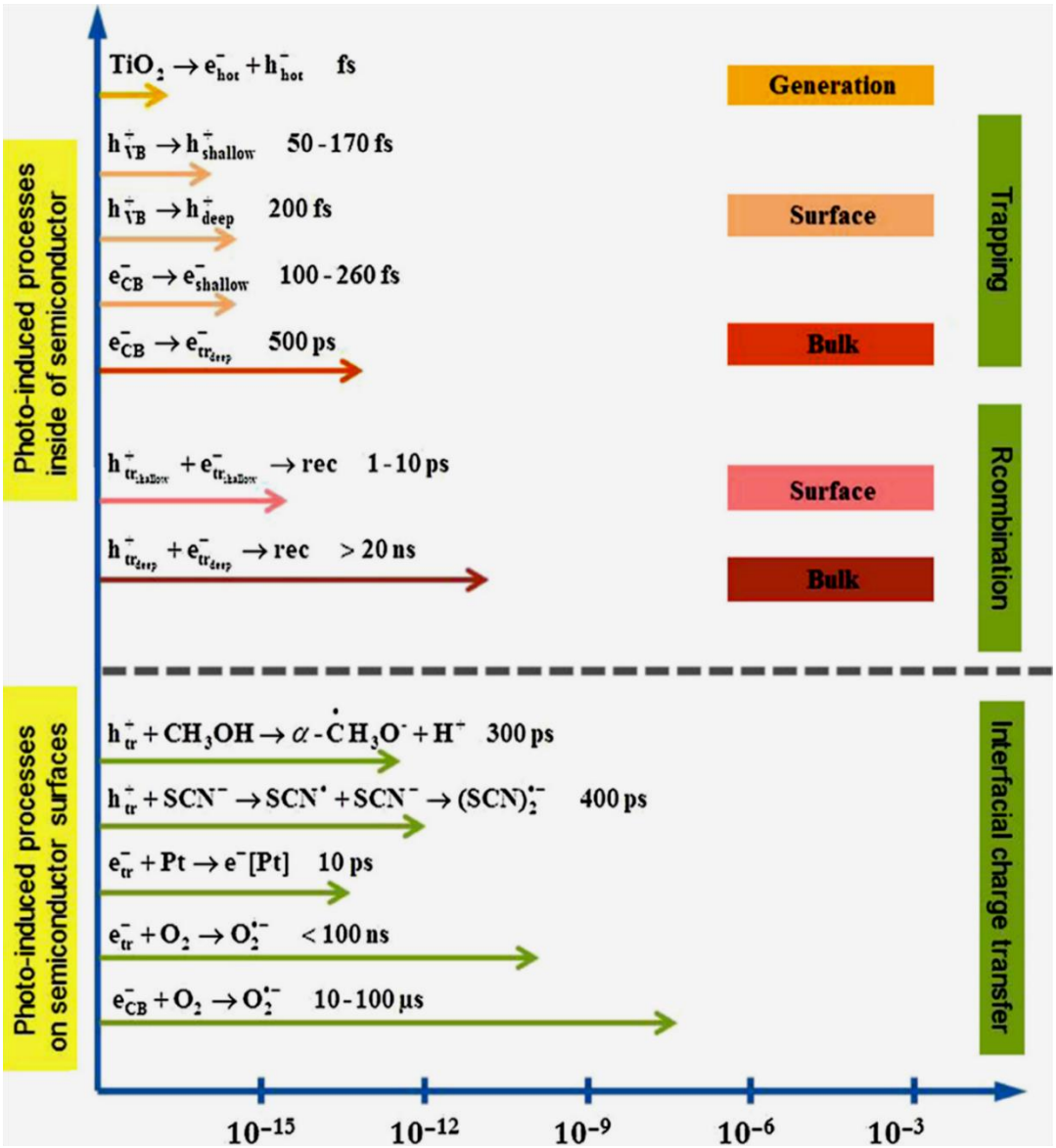

Figure 1.7: Steps of the TiO_2 photocatalysis process.[159] Reprinted with permission from *Chem. Rev*. 2014, 114, 19, 9919-9986. Copyright 2014 American Chemical Society.

While the exact mechanism of photocatalysis may vary slightly depending on the materials used and the pollutants being examined, the technology generally follows a redox reaction of electrons and holes.[159-162] Figure 1.7 shows the possible pathways taken during photocatalysis inside and on the surface of TiO_2. The photocatalysis process begins on the surface of a semiconductor when photons are absorbed.[38, 111, 159, 162-165] The electrons from the VB become 'excited' from these photons to the CB when the energy is higher than that of the band gap. The photocatalytic reaction is shown in Figure 1.6 while Figure 1.7 shows the time scale that this reaction occurs. Spectroscopic analysis, such as transient absorption (TA) spectroscopy, transient diffuse reflectance (TDR)

spectroscopy, and time-resolved microwave conductivity (TRMC) measurements can be used to detect photogenerated charge carriers.[162, 163, 166-177] These instruments use the fact that electron-hole pairs absorb light in the visible and near infrared (IR) regions and free electrons absorbs light in the IR or microwave regions.[162, 167, 178-183]

Serpone *et al.* examined TA analysis for TiO_2 sols that had been 'excited' by 30-ps-width UV laser.[168] Based on the spectra from a 30 ps laser pulse, they concluded the time for trapping electrons and holes should take approx. ≤ 1–10 ps. [168] In 2001, Yang *et al.* examined TiO_2 nanoparticles using femtosecond TA spectroscopy and proposed that hole trapping takes ~50 fs and electron trapping takes ~260 fs. [162, 184] They found that the time from inside the TiO_2 nanoparticle to the surface was 40 times quicker for the hole than the electron. [162, 184] The transient adsorption of TiO_2 nanoporous film between 400-2500 nm was studied by Yoshihara *et al.*[167] They studied a TiO_2 film that had been dipped into N_2-saturated deuterated water that had been 'excited' by low intensity pulse laser. This allowed less than one electron-hole pair could be generated per particle. As a result of this, the study to be performed closed to real photocatalytic conditions. [162, 167] They found that it had a recombination rate is approximately 1 ms.[167] This is a much slower rate than previous studies (10 ns) that used high power laser pulses found.[162, 176, 177, 183, 185] However, this result is similar to those gained from Peiro *et al.* and Yamakata *et al*.[163, 186] Later, Tamaki *et al*. studied nanoporous TiO_2 films for the electron-hole trapping.[187, 188] They found that it took 100 fs to generate trapped electrons-holes that were shallow in depth, while it took 150 fs and 200 fs for deeply trapped electrons and holes, respectively.[187, 188] Tamaki *et al*. stated that it took 100 ps for trapped holes to go from shallow to deep traps and that it took the electrons 500 ps to go from the shallow traps to the deep traps. They concluded that the electrons-holes should be trapped and not free charge carriers.[162, 187, 188]

Yamakata *et al.* used time-resolved infrared absorption to examine the decay of free electrons prompted by water and oxygen environments.[174] They found with P25 TiO_2, the oxygen captured the electrons and there was increase of the decay rate of 10-100 µs, while in less than 2 µs there was a reaction between the water vapour and the holes. [162, 174] Furube *et al.* examined the charge recombination kinetics for Pt/TiO_2 and found that on top of finding the normal charge recombination there was a new decay component (a few ps) when excited at 390 nm. They found that the higher amount of Pt present, the more it

effected the migration of electrons. [174] They determined the migration of the electrons between TiO_2 and Pt caused the increase in the decay process.[162, 174] Iwata *et al.* also examined the decay process with Pt-TiO_2. As with Furube *et al.*, Iwata *et al.* also stated that the electrons are transferring from TiO_2 and Pt and the found the decay rate of 2.3ps.[173] They propose that a small portion of the electrons remain on TiO_2 as there is still signal present after some time (100s of ps).[162, 173]

Fujishima and Zhang proposed three points based on the research examined. Firstly, they speculated that the recombination during photocatalysis is a slow process as a result of efficient charge trapping.[162] Secondly, they speculated that the charge transfer process competes with charge recombination.[162] Finally, they concluded that it can take µs to ms for photocatalysis to occur once the electron-hole pair created. This suggests that under low-intensity UV irradiation (1 mW cm^{-2}, ~1015 photons s^{-1} cm^{-2}), the electron-hole pair is generated and has already gone through reaction or charge recombination before a photon is absorbed by the photocatalyst. [162]

In the last decade or so, the ability to synthetize a photocatalyst that is activated by UV and visible light has gained significant interest.[146] One method that has been examined is using photocatalysts which have smaller band gaps than the band gap of TiO_2, these are discussed in Section 1.6.2.[146]

However, even with an increased interest in developing a new photocatalyst, TiO_2 still remains one of the most researched photocatalyst. Despite all the benefits of using TiO_2 as a photocatalyst there is one major disadvantage. At present, TiO_2 can only utilise the UV light (<390nm) in solar irradiation due to its large band gap (anatase = 3.2 eV). [146] Solar light is made up of only 4% of UV but visible light counts for approximately 42% of solar light.[8, 22] A visible light (400-700nm) active, high temperature (≥1000°C) stable anatase phase is required for many of its applications.[19]

1.6.1 Improvements to Photocatalysis

There a number of ways to improve the rate of photocatalytic activity and producing a TiO_2 photocatalyst that utilises both UV and visible light.

One solution to these problems is the use of a TiO_2 heterojunction photocatalyst. While anatase is commonly considered the most photocatalytically active phase of TiO_2, there

have been studies that have reported that the use of two phases (anatase and brookite or anatase and rutile) as a heterojunction can improve the photocatalytic activity when compared with the use of anatase alone, see Figure 1.8.[8, 53, 54, 103, 189-191] This improvement is due to the effect it has on the charge carrier separation, as it leads to trapping the electrons in the rutile phase and minimises the electron-hole recombination.[65, 192, 193] There have been reports that the electrons are trapped within the lattice while simultaneously the trapping of holes on the surface occurs.[4, 192, 194] The 'excited' state electrons in the CB in brookite can be transferred into the CB of anatase.[121] This is due to the CB of brookite being approx. 0.2 eV higher than the anatase CB.[121] This transfer reduces the rate of electron-hole recombination and improves the visible light photocatalytic activity.[121] Heterojunctions between two different photocatalysts follows the same mechanism shown in Figure 1.8.

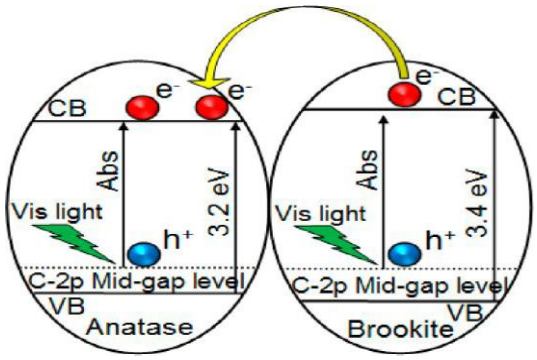

Figure 1.8: Heterojunction photocatalysis with anatase and brookite phase.[121] Reprinted with permission from *ACS Appl. Mater. Interfaces* 2013, 5, 5, 1663-1672. Copyright 2013 American Chemical Society.

Numerous studies use the reference material, P25, which is a mixed phase (anatase and rutile) TiO_2 photocatalyst, for comparison with work being completed.[4, 146] It is considered that the enhanced performance of this material is due to its high specific surface area.[4, 195] The material is generally comprised of 80 wt.% anatase and 20 wt.% rutile.[4] A 70 wt.% anatase and 30 wt.% rutile sample displayed a larger surface area and increased photocatalytic ability when compared with P25, with surface areas being 72 m^2/g and 49 m^2/g respectively.[54] However, caution must be taken when comparing the materials photoactivity based on the ratio of each phase as the method of synthesis has a significant impact on particle size and surface area.[4] The precursor used calcination temperature and pH directly affects the parameters such as surface area, morphology, and phase distribution obtained during sol–gel synthesis.[51, 53, 54, 76, 102, 103, 196-201] A mixed phase

sample with the desired ratio of wt.% can be produced by altering the kinetics of the reaction.[4] However, the effects of each of the following must be comprehended so this can happen: temperature; atmosphere; purity of raw materials; chemical, microstructural and thermal homogeneity during heating; particle and agglomerate size distribution; grain and agglomerate morphology.[4] While P25 is suitable reference for photocatalysis which is activated by UV light, it is not suitable to act as a reference under visible light due its low activity under visible light.[146] As of yet, there is no standard reference material for visible light photoactivity for comparing to novel work.

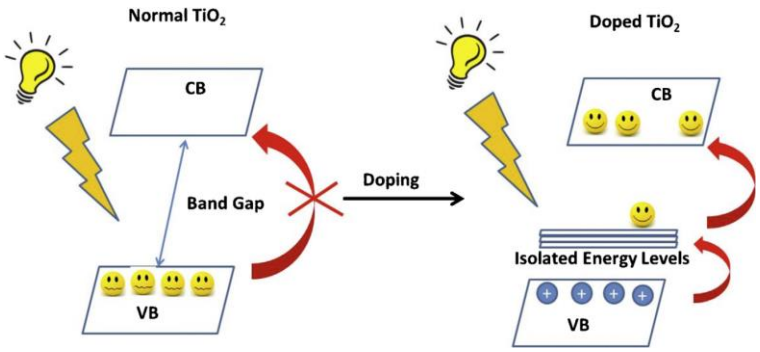

Figure 1.9: General principle of narrowing the band gap with a dopant.[38] Reprinted from *J. Photochem. Photobiol. C,* Vol. 25, Etacheri, *et al.*, Visible-light activation of TiO_2 photocatalysts: Advances in theory and experiments, pp 1-29, Copyright 2015, with permission from Elsevier.

Of course, another method for tailoring the phase mixture of TiO_2 is the use of dopants, chemical modifiers and chemical additives. There have been thousands of compounds that have been 'doped' onto TiO_2 for this purpose.[146, 151] These can be non-metal dopants (such as Carbon,[10, 25, 119-121] Nitrogen,[111, 115-117, 202] Sulphur[14, 192, 203, 204] and Fluorine[24, 122, 205]) or metal dopants (such as Iron,[129, 203] Silver,[7, 206] Chromium[132] and Manganese[130, 131]). When a 'dopant' is used, it can change the samples properties including the structure and could lead to the degradation of the photocatalytic activity. It can also lead to the improvement of photocatalysis by narrowing the band gap between the VB and CB, Figure 1.9.

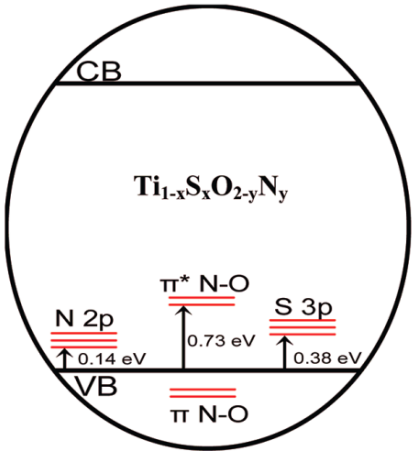

Figure 1.10: Electron Structure of $Ti_{1-x}S_xO_{2-x}N_y$, showing the presence of impurity energy states.[207] Reprinted with permission from *Inorg. Chem.* 2012, 51, 13, 7164-7173. Copyright 2012 American Chemical Society.

The narrowing of the band gap between the VB (O 2*p*) and CB (Ti 3*d*) occurs when dopant is used on TiO_2. The dopant introduces a new occupied orbital between the VB and the CB. [9, 150, 207] An example of this is when nitrogen and sulphur is used as co-dopants (Figure 1.10 and 1.11). The N *2p* orbital of nitrogen is used as a mid-band gap orbital for the electrons in the VB. The electrons now require less energy in order to be excited enough in the mid-band gap orbital to reach the CB. When all the electrons have left the VB, there is a positive hole left in the VB and the reaction occurs as described in Section 1.6. [9, 150, 207] The rate constants calculated for this doped-TiO_2 and control titania both calcined at 600°C, and commercial sample (Degussa P25) are 0.0323, 0.0163, and 0.004 min^{-1}, respectively.[207]

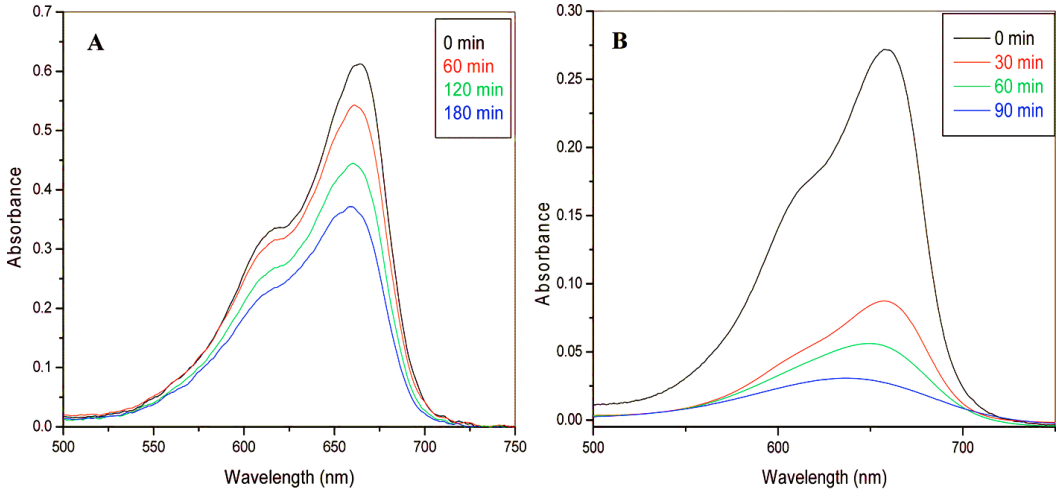

Figure 1.11: UV spectra analysis of visible-light induced organic dye degradation using (A) Degussa P25 and (B) N,S doped TiO_2 sample.[207] Reprinted with permission from *Inorg. Chem.* 2012, 51, 13, 7164-7173. Copyright 2012 American Chemical Society.

1.6.2 Novel Photocatalysts

There has been a growing importance in the investigation of photocatalysts other than TiO_2, for example ZnO, ZnS, ZrO_2, semiconductor-graphene, perovskites, MoS_2, WO_3, CdS and Fe_2O_3.[146, 208-215] These photocatalysts were originally developed for the photocatalytic splitting of water, they are also being used for water/air treatment.[146] Both applications follow the same general method as described Section 1.6. There are a few differences which include the number of electrons transferred, the amount of minimum energy required for the process to be induced and if the process is endothermic or exothermic. Paslernak *et al.* (2013) extensively compares and contrasts the two applications.[216] With the vast amount of studies looking at non TiO_2 photocatalysts, they have been divided into two categories; oxide photocatalysts and non-oxide photocatalysts (see Figure 1.12). One difference between the two is that the oxide photocatalysts VB and CB are affected by changes in the pH, whereas changes in pH in non-oxide photocatalysts has little or no effect on the VB and CB.

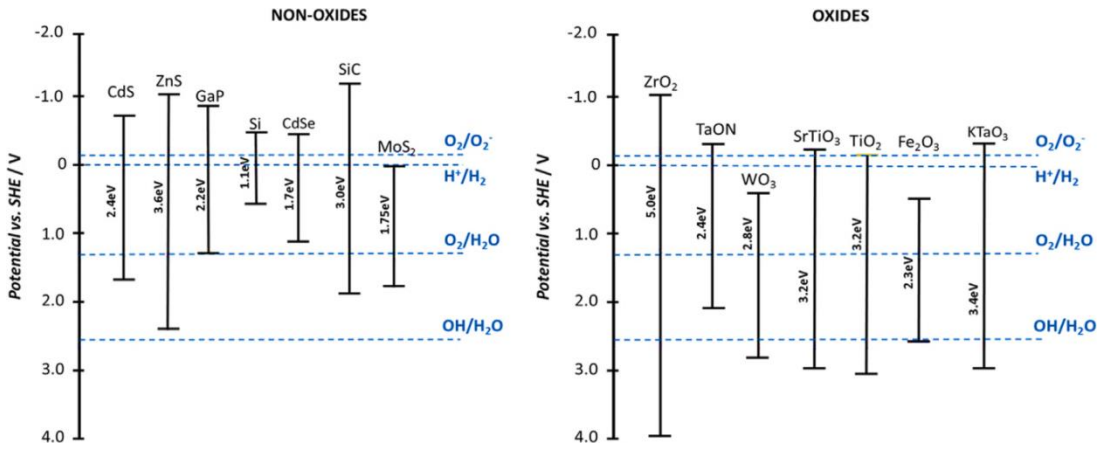

Figure 1.12: The band gaps of non-oxide photocatalysts (left) and oxide photocatalysts (right) at a pH of 7.[146] Reprinted from *Mat. Sci, Semicon. Proc.,* Vol. 42, Shaham-Waldmann, N., & Paz, Y., Away from TiO_2: A critical minireview on the developing of new photocatalysts for degradation of contaminants in water, pp 72-80, Copyright 2016, with permission from Elsevier.

Composites of two different photocatalysts has also recently gained interest.[146] The aim of this is to form heterojunctions between the photocatalysts. These heterojunctions will mean that the energy adsorbed by the first photocatalyst is transferred to the second photocatalyst.[146] This method causes the charge separation to increase and have a significant impact on the rate of degradation.[146, 196]

One example of photocatalyst that has gained significant interest is ZnO, this is because it's inexpensive and has a similar photodegradation mechanism as TiO_2.[217-223] Tian *et* (2012) examined ZnO photodegradation of methylene orange in comparison to Degussa P25 TiO_2 when both were calcined at 600°C. The study showed that the rate of degradation ZnO is significantly higher (4 times) than that of P25.[219] As with TiO_2, there have been a number of studies that have examined 'doped' ZnO photocatalyst.[217, 220-222] Dopants such as graphite-like C_3N_4, Ag, Cr, Al, Sn, Co and reduced graphene oxide (rGO) have been examined with ZnO.[217, 220-222, 224-226] All these studies reported an enhancement in photocatalytic activity when compared with the ZnO control and a stable photocatalyst, for example Wang *et al.* (2011) found that including a graphite-like C_3N_4 dopant improve the UV light photoactivity by 5 times. [217, 220-222, 224-226] Bai *et al*. (2013) found that a ZnO_{1-x}/graphene composite enhanced the UV and the visible light photocatalytic activity, by approximately 1.2 and 4.6 times respectively.[217] There has also been some interest into several other photocatalysts. Cadmium sulphide (CdS) has been examined as a photocatalyst,[227-241] with a number of studies focusing on the

production of hydrogen initiated with visible light.[227, 229, 230, 234, 236] Doped samples include ZnS-CuS-CdS, carbon spheres/CdS, *g*-C_3N_4-Au-CdS, ZnS-WS_2-CdS, C_3N_4-CdS and Pd-Cr_2O_3-CdS.[227-229, 232, 235] There has also been numerous studies into ZnS for applications such as hydrogen production and the degradation of chemicals and dyes (*e.g.* Rhodamine B (Rh B) and metronidazole).[211, 212, 227, 229, 242-250]

1.7 Applications of Photocatalysis

1.7.1 Self-Cleaning Materials

One important application of photocatalysis is the development of self-cleaning surfaces. The self-cleaning surfaces are produced using both photocatalysis and photoinduced hydrophilicity seen by most photocatalysts.[154, 251, 252] As these surfaces can be cleaned by a flow of water there tends to be a lower maintenance cost associated. Self-cleaning surfaces are either considered hydrophilic or hydrophobic.[252] When the contact angle (θ) of the liquid drop on a solid surface is less than 90° the surface is hydrophilic, if the angle is greater than 90° then it is said to be hydrophobic.[252] If $\theta<10°$, the dust/contaminants will be washed off the surface with water flow as the liquid drop spreads out uniformly on the surface.[252] Two factors that have a major impact on this are the porosity and the roughness of the surface.[252-255]

Self-cleaning building materials (*e.g.* tiles and window glass) have been fabricated using TiO_2 thin films.[252] In order to remove pollutants, the photocatalytic TiO_2 films utilizes the UV light from the sun and rain (Figure 1.13).[252, 256]

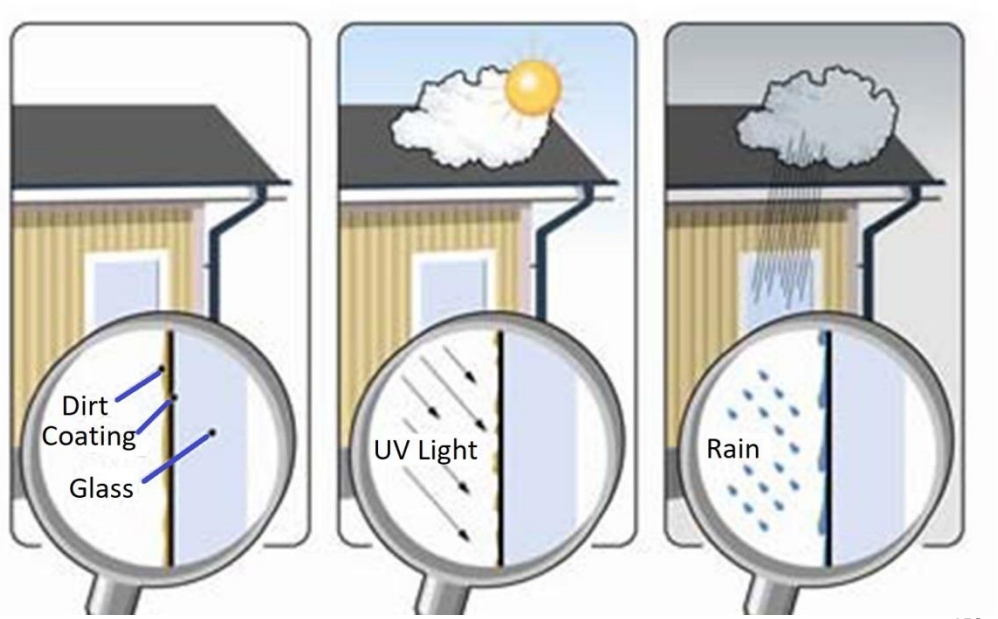

Figure 1.13: Schematic representation of the working principle of self-cleaning glasses.[256] Reprinted from *Sol. Energy Mater Sol. Cells*, Vol. 109, Midtdal & Jelle, Self-cleaning glazing products: A state-of-the-art review and future research pathways, pp 126-141, Copyright 2013, with permission from Elsevier.

1.7.2 Photo-Inactivation of Bacteria

Microbial contamination is a major issue for areas such as in the food industry and in hospitals. One method that has become important for the inactivation of microbes is the use of photocatalysts. [8, 257-260] There has been a vast number of dopants that have been examined specifically for the inactivation of bacteria, some examples include Nitrogen,[261], Nitrogen-Silver,[262, 263] Nitrogen-Copper,[3] Sulfur,[264] Carbon,[121] Nickel,[203] and Copper.[10, 203] Figure 1.14 shows the effect photocatalysis has on bacteria. The photocatalytic mechanism that inactivates bacteria begins with rupturing the cell membrane, this results in the bacteria's internal components to leak from the areas that have been ruptured.[10] The components that have been leaked are oxidised by photocatalytic sites.[10]

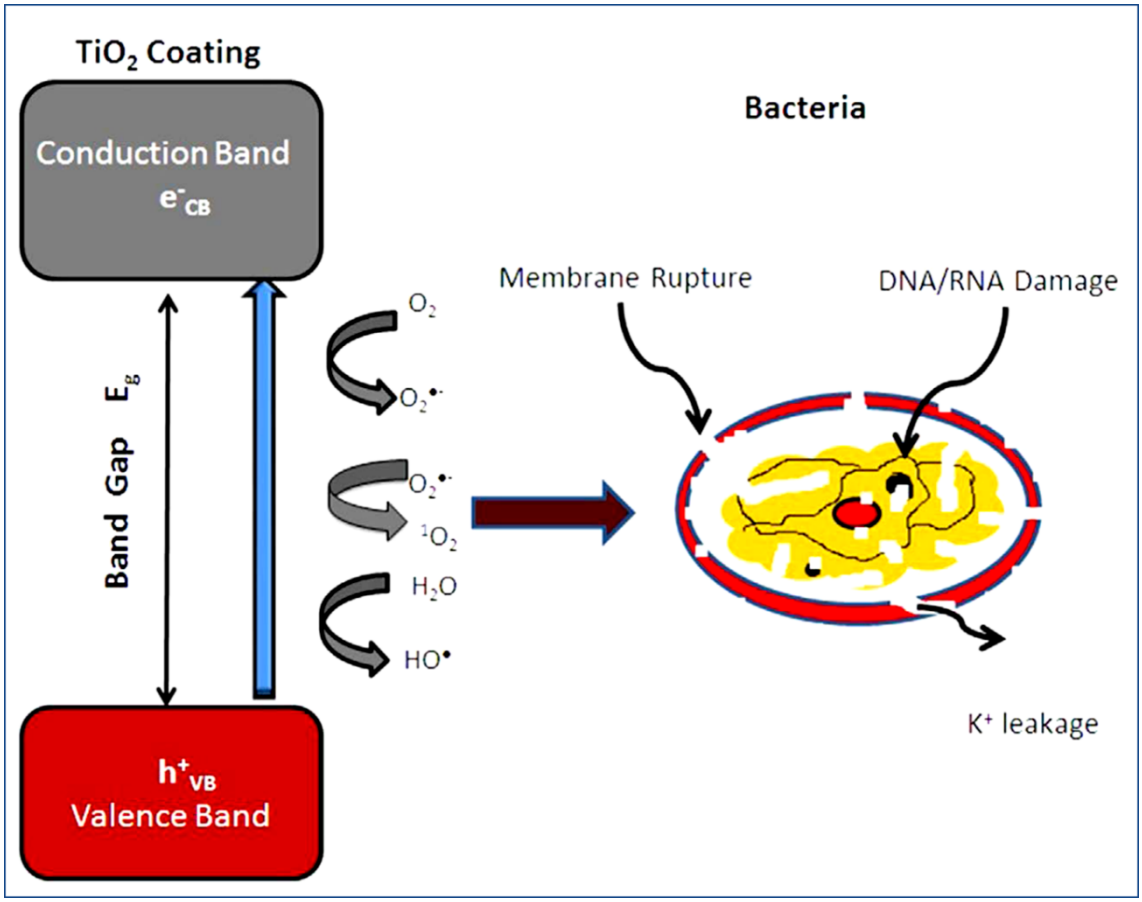

Figure 1.14: Schematic diagram showing the mechanism of antibacterial action of TiO_2.[265] Reprinted with permission from Leyland, N. S., Podporska-Carroll, J., Browne, J., Hinder, S. J., Quilty, B., & Pillai, S. C. (2016). Highly efficient F, Cu doped TiO 2 anti-bacterial visible light active photocatalytic coatings to combat hospital-acquired infections. *Scientific reports*, *6*, 24770.

Pulgarin's research group have completed an extensive study on N-S doped TiO_2 and its effect on photocatalytic inactivation of *E. coli*.[266-269] Their study uses thiourea as a source of N-S for co-doping TiO_2 and for the inactivation of *E. coli*.[266] After calcination at 400°C and 500°C, they were able to determine that varying the temperature resulted in different doping species.[10] The formation of reactive oxygen species (ROS), they concluded, is affected by the nature of the dopant used, the particle size and the surface hydroxylation.[10, 266-269] From the studies it can be suggested that under visible light treatment, *E. coli* is inactivated when superoxide anion radicals ($O_2^{\bullet-}$) and singlet oxygen ($^1O_2$) are formed.[10, 266-269] These are formed from electrons in Nitrogen and Sulfur localised states.[267, 268] These samples were also examined under UV light for ROSs.[269] It was found that under UV light, it was $^{\bullet}OH$ that was involved in the inactivation of *E. coli*. These radicals are formed on the VB holes by the oxidation of water.[10, 266-269]

1.7.3 Photocatalytic Degradation of Organic Effluents

Fresh water resources such as lakes, rivers and ground water are contaminated with a variety of organic, inorganic and microbial pollutants. Organic contaminants include industrial and agricultural chemicals; pharmaceuticals and personal care products.[10] Among these contaminants, pharmaceuticals are of particular concern because they alter the metabolic activity of the living biota and could cause serious biochemical changes.[270-272] More than 200 diverse kinds of pharmaceutical chemicals are reported worldwide in different river systems.[273] Effluent from waste water treatment plants is regarded as the primary source of these pollutants.[270, 274-276] Moreover, the suspended particles and sludge generated in waste water treatment plants (WWTP) are concentrated with contaminants and directly applied in agricultural fields as manures.[270] These facts reveal the inefficiency of conventional water treatment methods those employed in WWTP and the need to opt for advanced water treatment technology such as TiO_2 photocatalysis.

TiO_2 photocatalysis has emerged as a promising water and wastewater treatment technology. For example, UV/TiO_2 photocatalysis was evaluated for the simultaneous degradation of five different contaminants such as 1,4 dioxane, n-nitrosodimethylamine (NDMA), tris-2-chloroethyl phosphate (TCEP), gemfibrozil, and 17β estradiol.[277] Under optimized conditions (pH 5.0 and TiO_2 dosage of 1.5 g L^{-1}) 77% 1,4 dioxane, 92% for NDMA, 45% TCEP, 95% gemfibrozil and 93% 17β estradiol was photodegraded within 30 min. Interestingly, relatively less water soluble compounds (gemfibrozil and 17β estradiol) were degraded faster than the other contaminants examined.[277] Quite different from the usual studies that employ single contaminant to evaluate TiO_2 photocatalysis, Pino *et al.*, studied the simultaneous photodegradation of two phenolic pollutants 4-CP and 2,6-DCP to understand TiO_2 photocatalysis in competitive conditions. The study concluded that apart from active sites on the surface, other parameters such as initial pH, initial concentration, light intensity, the interplay of several parameters related to the surface properties, phenol structure and the adsorption effect of intermediate products also affect the performance of the system.[278] In view of operational feasibility, immobilized TiO_2 is more preferred than TiO_2 suspended in the form of slurry. TiO_2 immobilised on glass substrate was successfully applied for the solar photocatalytic degradation of 15 emerging contaminants (acetaminophen, antipyrine, atrazine, carbamazepine, diclofenac, flumequine, hydroxybiphenyl, ibuprofen, isoproturon, ketorolac, ofloxacin, progesterone, sulfamethoxazole and triclosan) present in simulated

and real Municipal Wastewater Treatment Plant (MWTP) effluents at environmentally relevant concentrations in a pilot compound parabolic collector. Significant (~85%) removal of these contaminants was achieved within 120 min, revealing the potential application of this technology for WWTPs effluents.[279]

1,4-dioxane

The contamination of potable water by 1,4-dioxane, a synthetic cyclic ether, is of growing concern due to its adverse impact on human health. [280-284] This conventional industrial solvent and commonplace chemical processing by-product is typically deposited downstream from industrial effluent,[284, 285] and is currently classified by the U.S. Environmental Protection Agency (EPA) as a probable human carcinogen (Group 2B).[280-284, 286] The physiochemical properties of 1,4-dioxane, such as the organic compound being highly volatile in its pure form but highly water soluble (low vapour pressure and a boiling point of 101°C), tend to create treatment challenges for traditional solvent removal methods and biodegradation.[280, 281, 287-289] The inefficiency of current detoxification methods has necessitated efforts to enhance degradation through a number of technologies, including H_2O_2/O_3 oxidation pre-treatment, advanced biodegradation processes, and photochemical methods.[280, 284, 288-292]

1.8. Objectives of the Current Study

The two main objectives of this research were to examine the impact various dopants had on the ART transition temperature and how this effected the photocatalytic activity of the nanomaterials. The following properties were examined for each dopant;

1. X-ray Diffraction (XRD) was used to determine if the samples were amorphous or crystalline, the phase composition and the crystalline size.
2. Raman Spectroscopy was used as an additional tool in confirming the phase composition all materials.
3. Determination of elements present, chemical/elemental state, quantity of an element and if the dopants were doped on the surface or if they were included within the crystal lattice structure of the TiO_2 materials was completed using X-ray Photoelectron Spectroscopy (XPS) analysis.
4. Where applicable, Fourier Transform Infrared Spectroscopy (FTIR) was used in determining the bonds present in samples. FTIR was also used in confirming the XPS analysis.

5. Brunauer Emmett Teller (BET) analysis used to measure the surface area of samples.
6. Where applicable, Scanning Electron Microscopy with Energy Dispersive X-Ray Analyser (SEM-EDX) was used for imaging of samples.
7. The photocatalytic degradation of 1,4-dioxane was used to determine the photocatalytic activity of various samples. From the results in this testing, it was then possible to determine the impact doping had the TiO_2 photocatalysis and their ability to act as a photocatalyst.
8. The optimum sample for each dopant in improving the transition temperature and photocatalytic activity was determined. Additionally, the sample that showed the highest increase in the transition temperature and photocatalytic activity was concluded.
9. Finally, based on literature and this current research, possible future work was suggested.

This work was completed in collaboration with Dublin Institute of Technology (Ireland), University of Surrey (UK), University of Valladolid (Spain) and Complutense University of Madrid (Spain).

The following information provides a summary of each chapter in this thesis and how each of the above objectives were achieved.

Chapter 2 provides a detailed description of the synthesis process of the three types doped TiO_2 nanomaterials. The methods for characterising the nanomaterials with XRD, Raman Spectroscopy, FTIR, XPS, SEM-EDX and BET were outlined. Finally, the photocatalytic degradation of 1,4-dioxane was discussed, including the methodology analysing the samples taken throughout the experiments.

Chapter 3 discusses the effects of a non-metal dopant had on TiO_2. Benzoic acid (a carbon precursor) was added at various concentrations and the calcined for a final nanomaterial. XRD and Raman spectroscopy determined the phase composition of the nanomaterials while XPS and FTIR indicated the binding/bonding involved. XPS showed that the carbon was doped to the surface of the TiO_2. Additionally, SEM-EDX and BET showed the surface properties of the samples investigated. The photocatalytic activity of the nanomaterials was examined by the photocatalytic degradation of 1,4-dioxane. For both

ART and photocatalysis, the inclusion of benzoic acid showed improvement compared to the control sample.

The impact of tungsten doping to TiO_2 is examined in Chapter 4. As with the previous chapter, XRD and Raman spectroscopy were used for identifying the anatase/rutile phase composition of all samples. These methods showed that in addition to TiO_2, tungsten was present in the form of WO_3. This was further confirmed with XPS. The surface area of the samples was determined using BET. The percent of anatase present at higher temperatures increased as the mol. % of tungsten increased up to 8% W-TiO_2. There was a significant increase in the efficiency of photocatalytic activity for the W-TiO_2, with 3 samples showing 100% removal of 1,4-dioxane. It is suggested that this increased activity is due to a heterojunction between WO_3 and TiO_2 forming.

Chapter 5 examines a second non-metal dopant, boron nitride (BN). Once again XRD and Raman spectroscopy were used for the phase composition of the nanomaterials. It shows that there is an improvement in ART compared to the control, but not above 700°C. XPS determined that the BN is doped onto the surface of the TiO_2, forming a N-B-O-Ti bond. As with benzoic acid and tungsten, BN doping increased that rate at which 1,4-dioxane was removed compared to the control.

The overall conclusions were present in Chapter 6. The optimum sample for ART and photocatalysis for each dopant was concluded. In addition, possible future work which include the photocatalytic splitting of water, the formation of novel heterojunctions and photodynamic therapy were discussed.

.

Chapter 2 - Experimental Methods

2.1 List of Materials

The following reagents were purchased from Sigma-Aldrich and were used without additional purification:

- Titanium Tetraisopropoxide (97%)
- Benzoic Acid (≥99.5%)
- Isopropanol (≥99.5%)
- Tungstic Acid (99%)
- 35% Ammonia Hydroxide solution
- Boron Nitride Powder

1,4-dioxane (>99%) was purchase from Merck. Deionised water was used for all experiments, unless stated otherwise.

2.2 Synthesis of Materials

2.2.1 Benzoic Acid Modified Titania

In a typical experiment for the preparation of the 1:1 TiO_2: benzoic acid modified titania sample, 25mL of titanium isopropoxide (TTIP) was added to 200mL of isopropanol (IPA) (solution A). 10.31g of benzoic acid (BA) was dissolved in 100mL of IPA and this solution was heated until a clear solution was formed (solution B). Solution B was then immediately added to solution A. The mixture was stirred for 5 min and 150mL of deionised water was added, which was then stirred for a further 15 min. This mixture was then aged at room temperature for 30 min. The resulting gel was dried at a temperature of 100°C for 24 h. A similar procedure was applied for the preparation of 1:0, 1:4 and 1:8 TiO_2:BA samples. The powders were calcined at 10°C/min to 500°C, 600°C, 700°C, 800°C, 900°C and 1000°C, the samples were held at the required temperature for 2 hrs.

2.2.2 Tungsten Doped Titania

The quantity of H_2O_4W and TTIP was calculated based on the mol. % of tungsten (W) and TiO_2 incorporated in each sample *e.g.* 2 mol. % W: 98 mol. % TiO_2. In a typical experiment to prepare a 2 mol. % W-TiO_2 powder, 0.566g of H_2O_4W was dissolved in 50mL of 35% ammonia solution which was stirred for 20 min at 50°C. This was added to 32.26mL of TTIP and 200mL IPA and the mixture was stirred for 5 min. 100mL deionised water was added to the solution to form a sol-gel and was stirred for 15 min.

The sol-gel was dried at 100 °C for 24 hrs. The powder was calcined at 500, 600, 700, 800, 900, 950 and 1000°C (the hold time for each temperature was 2 hrs and ramp rate of 10°C/min). This method was used for 0% W, 4% W, 8% W and 16% W, varying the volume of TTIP and weight of H_2O_4W.

2.2.3 Boron Nitride Doped Titania

For the 2 mol. % Sample, 55.4mL of TTIP was added to 200mL of IPA and was stirred for 15 min (solution A). 0.0948g Boron Nitride (BN) was added to 200mL of deionised water, this was stirred for 15 min (solution B). Solution B was added to solution A and this was stirred for 30 min. The resulting sol-gel was dried in the oven at 100 °C for 12 hrs. The resulting powder was annealed at 500°C, 600°C and 700°C, at a ramp rate of 10°C/min and was held for 2hrs. This method was repeated for the 0%, 4%, 8% and 16% Boron Nitride (BN) samples by changing the volume of TTIP and grams of BN (0% - 56.6mL and 0g; 4% - 54.2mL and 0.1897g; 8% - 52.2 mL and 0.3793g; 16% - 47.6mL and 0.7587g).

2.3 Characterisation

2.3.1 X-ray Diffraction (XRD)

All samples were analysed with XRD. The diffractograms were produced using a Siemens D500 X-ray powder diffractometer, using Cu Kα radiation (λ= 0.15418 nm). The diffraction range examined was between 2θ=10°-80°. To determine the fraction of rutile in the samples, the Spurr equation was used (eq. 2.1).[293]

$$F_R = \frac{1}{1+0.8[I_A(101)/I_R(110)]} \qquad (2.1)$$

where F_R is the quantity of rutile in mixed sample and $I_A(101)$ and $I_R(110)$ are the intensities of the main anatase and rutile peaks. The %error from this calculation is ±5%.

XRD data was also used for examining the size of the crystalline structures in each sample, this was determined using the Scherrer equation (eq. 2.2).[294]

$$\Phi = \frac{K\lambda}{\beta \cos\theta} \quad (2.2)$$

where Φ is the crystallite size, K is the shape factor, λ is the wavelength of Cu Kα radiation (0.15418 nm), β is the full line width at the half-maximum height of the main intensity peak and θ is the Bragg angle.

2.3.2 Raman Spectroscopy

For Raman spectroscopy, the Horiba Jobin Yvon LabRAM HR 800 system was used. The grating that was used was 300 gr/mm. The objective lens of 100X was used. The laser line used was a 660nm solid state diode laser standard bandwidth version with double edge filter upgrade and the acquisition time for the data was 3 seconds. The sample was placed onto a microscope slide and was levelled off, and this was placed in the slide holder for analysis.

2.3.3 X-ray Photoelectron Spectroscopy (XPS)

A ThermoFisher Scientific Instruments (East Grinstead, UK) K-Alpha$^+$ spectrometer was employed for XPS analysis of samples. A monochromatic Al Kα X-ray source (hν = 1486.6 eV) with a spot radius of ~400 μm was used to obtain the XPS spectra. A Pass Energy of 200 eV was used for acquiring survey spectra, while a Pass Energy of 50 eV was employed for producing core level spectra with high resolution for all elements. C1s (285 eV) was used as a reference peak to correct for charging effects during acquisition. After accounting for the removal of a non-linear (Shirley) background, the core level spectra were used in calculating the quantitative surface chemical composition. In order to correct for electron energy analyser transmission function and integrate the applicable sensitivity factors the manufacturers software (Avantage) was used.

2.3.4 Fourier Transform Infrared – Attenuated Total Reflection (FTIR-ATR)

FTIR-ATR was used for analysis of samples. A PerkinElmer Spectrum 100 FT-IR spectrometer was used in examining the samples, in a range of 400cm^{-1} to 4000cm^{-1}, a resolution of 4cm^{-1}, and 4 scans per sample.

2.3.5 Brunauer– Emmett–Teller (BET)

In order to determine the surface area of the samples the BET method was used. The samples were first degassed for an hour at 300°C. The adsorption isotherms were acquired at -196.15°C.

2.3.6 Scanning Electron Microscopy with Energy Dispersive X-Ray Analyser

The surface morphology of the samples was analysed using the Siemens TM1000 Scanning Electron Microscopy with Energy Dispersive X-Ray Analyser (SEM-EDX) giving % element composition.

2.3.7 Total Organic Carbon

The following analyses were made according to the standard methods for the examination of water and wastewater (APHA 2005). Total organic carbon (TOC) was measured by the combustion-infrared method using a multi N/C® 3100 TOC/TN analyser (Analytik Jena AG, Jena, Germany), which performed the catalytic combustion on cerium oxide at 850 ºC

2.3.8 Gas Chromatography

1,4-Dioxane was quantified using gas−liquid chromatography (GC) on a 7980A instrument (Agilent Technologies Inc., Palo Alto, CA) equipped with a flame ionization detector. The temperatures of the injector and the detector were 310 °C and 280 °C, respectively. Samples (2 µL) were injected using the pulsed-split mode (split ratio 5:1) and analysed in a TRB-FFAP (Teknokroma, Sant Cugat del Vallès, Spain) fused silica column (30 m x 0.25 mm internal diameter x 0.25 µm film thickness) with He (43 psi) as carrier gas, and the following temperature programme: 80 °C to 240 °C at a 15 °C min^{-1} ramp rate, after a 9 min initial hold. Peaks were identified according to relative retention time figures provided by commercial standards. Quantification was performed according to peak area, corrected with the response factors calculated for each compound using 1-butanol (60 ppm) as internal standard, and the GC-ChemStation software Rev.B.04.02 (96) from Agilent.

2.4 Photocatalytic Degradation of 1,4-dioxane

Photocatalysis testing was conducted using a total volume of 50 ml of synthetic solution, which was comprised of 1,4-dioxane (100 $mg \cdot L^{-1}$) and TiO_2 catalyst (1 $g \cdot L^{-1}$). Every 30 min, a sample was taken, up to a total photocatalytic reaction of 240 minutes. Blank experiments either performed without adding the catalyst, without switching the solar simulator lamp on, or using no metal concentration were performed. All experiments were repeated three times.

The source of the light was a solar simulator supplied by Newport (Irvine, USA) equipped with a Xenon lamp (300 W) with a correction filter (ASTM E490-73a) providing the solar

spectrum under ideal conditions. A total photon flux of $6.8 \cdot 10^{19}$ photon$\cdot s^{-1}$ was calculated to flow inside the photochemical reactor, as described by Liang *et al.* (2011). Light intensity between 200 to 400 nm resulted of 150 W$\cdot m^{-2}$ at 3 cm from the light source on a total surface of 0.0104 cm^{-2}, which was the distance between the sample surface and the lamp. Light intensity was recorded using a radiometer (UV-Elektronik, UV-VIS Radiometer RM-21, Ettlingen, Germany).

2.4.1 Determining % error of degradation plots

All photocatalytic degradation experiments were completed in triplicates. The replicates were completed on separate days across 1-3 weeks. All measurements were made on the same day as the experiment. The average and the standard deviation were calculated in excel and the standard deviation was used for error bars.

Chapter 3 - New Approach of Modifying the Anatase to Rutile Transition Temperature in TiO_2 Photocatalysts

3.1 Introduction

As mentioned in Section 1.1, TiO_2 has recently gained increasing interest due to its ability to act as a photocatalyst.[9] The factors which impact the ability of TiO_2 to act as a photocatalyst are discussed in detail in Chapter 1 and include the phase ratio and purity, particle size, surface area, the type of dopant and the concentration of the dopant.[295] An improvement in the amount of anatase phase present at high temperatures (≥ 1000°C) will be useful for a number of applications.[6, 14]

A high temperature anatase phase can be achieved by using dopants (Section 1.5).[6, 14, 296-298] One of these approaches includes the use of metal oxide doping.[6, 14, 296-298] Al_2O_3, SiO_2 and ZnO are examples metal oxide dopants that have been studied in the past to examine their effect on ART. [6, 19, 297, 298] While this method can be an effective one, there is one major limitation identified to dope TiO_2 samples by using metal oxides. At high temperatures impurities begin to form, for example Al_2TiO_5, which results in decreased photocatalytic activity.[6, 19] Instead, non-metal doping (Section 1.5.1) is examined for increasing the transition temperature.[299, 300] Using carbon as a dopant has shown favourable results for visible light activity when used with TiO_2.[8, 119, 120, 301] When the carbon is doped onto the TiO_2, it narrows the band gap to < 3.2eV and improves the photocatalytic activity in the visible region.[4, 8, 85] While nitrogen has been reported to be the most promising non-metal dopant, using carbon has gained interest in recent years.[10] Hanaor and Sorrell (2011) commented on the fact that there is a lack of reported research on the effects carbon has on the ART.[4] This is due to the oxidation of carbon at temperatures lower than the transition temperature. They suggested that as carbon is a reducing agent, it would likely to cause the sample to transform to rutile at lower temperatures than normal.[4]

The current Chapter examines the study of how the addition of various concentrations of an aromatic acid (benzoic acid) affects ART in TiO_2. XRD and Raman were employed to determine the % anatase and/or the % rutile in the samples. BET and SEM examined the texture and surface morphology of the samples. While FTIR and XPS were used for determining the bonding involved in the samples. The photocatalytic degradation of 1,4-dioxane has also been examined.

3.2 Results and Discussion

3.2.1 Phase Composition of Titania Nanomaterials

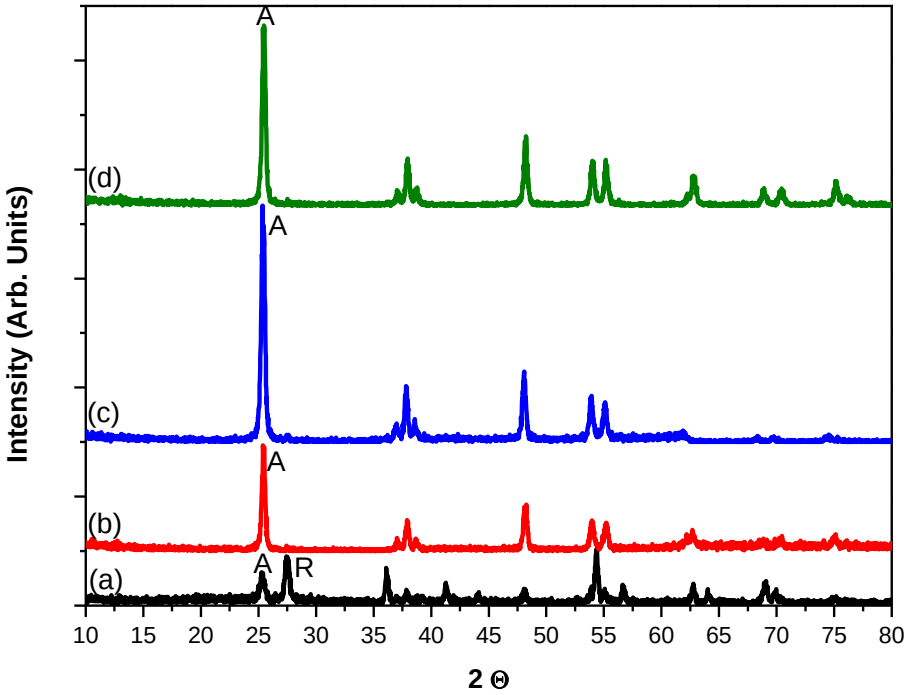

Figure 3.1: XRD of all concentrations that have been calcined at 600 °C. (a) Undoped TiO_2 (b) 1:1 TiO_2:BA (c) 1:4 TiO_2:BA and (d) 1:8 TiO_2:BA. A=anatase and R = rutile.

In order to determine the effect of chemical modification on the phase transition in TiO_2, XRD was employed. In order to determine the fraction of anatase and rutile in a sample, the intensities of the main anatase (101) and rutile (110) peaks were used for the analysis using Spurr equation (eq. 2.1). All diffractograms showed only the presence of TiO_2 peaks and there were no BA peaks (one at approx. 8° and two peaks at approx. 16 and 17°) present for any of the samples.[302] All samples contained 100% anatase phase TiO_2 when calcined at 500°C. At 600°C all samples that have benzoic acid as a chemical additive contain 100% anatase, while the control sample converted to 73% rutile phase (Figure 3.1).

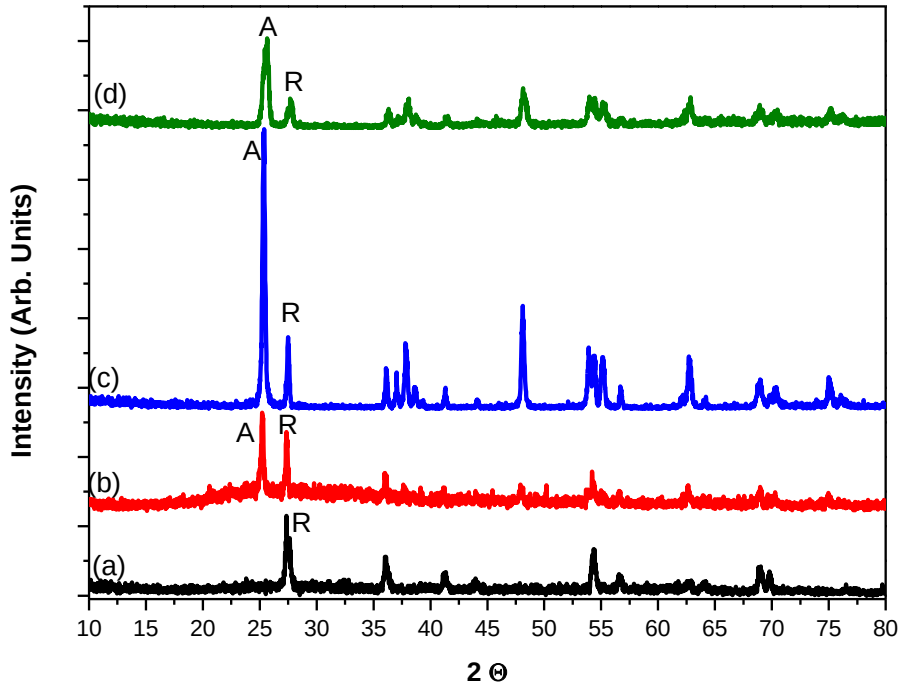

Figure 3.2: XRD of all samples which have been calcined at 700 °C. (a) Undoped TiO_2 (b) 1:1 TiO_2: Benzoic Acid (c) 1:4 TiO_2:BA and (d) 1:8 TiO_2:BA. A=anatase and R = rutile

As already stated in Section 3.1, the ART occurs in pure synthetic TiO_2 between 600-700°C,[16, 21] the control for this study followed this pattern as it was 100% rutile by 700°C. The samples with benzoic acid have a significant increase in the anatase phase at 700 °C when compared with the control, 1:1 has 50% anatase, 1:4 has 76% anatase and 1:8 has 71% (Figure 3.2). By 800°C, the 1:1 sample had transitioned into 100% rutile while the 1:4 and 1:8 samples at the same temperature still had small amounts of anatase present (10% and 7%), Figure 3.3.

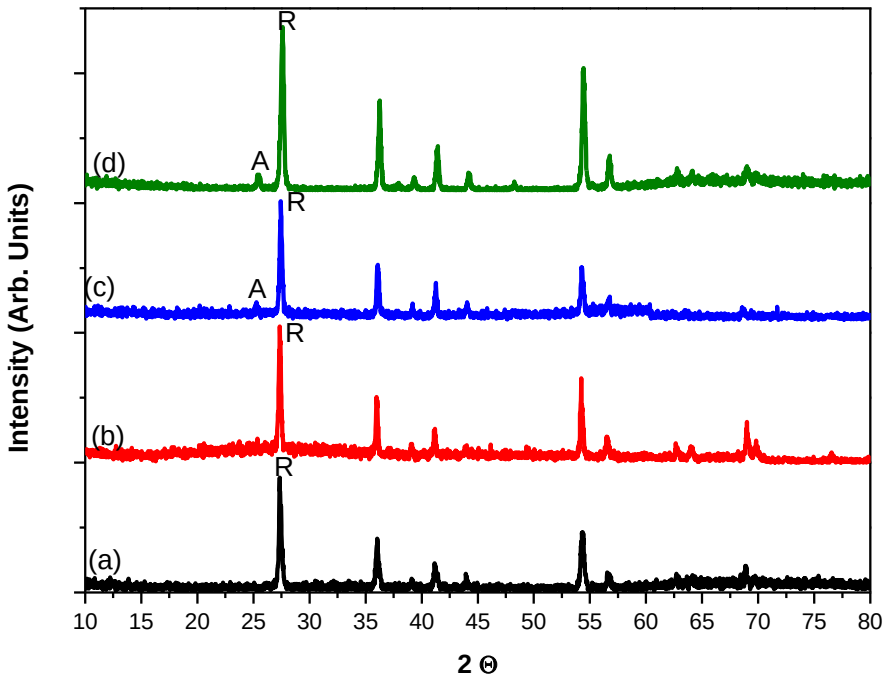

Figure 3.3: XRD of all samples which have been calcined at 800°C. (a) Undoped TiO_2 (b) 1:1 TiO_2: Benzoic Acid (c) 1:4 TiO_2: Benzoic Acid and (d) 1:8 TiO_2: Benzoic Acid. A=anatase and R = rutile

Figure 3.4 shows the % anatase for all samples. Above 900°C, all samples are 100% rutile. The results show that using benzoic acid as a carbon dopant does inhibit the ART, causing it to occur at higher temperatures than normal.

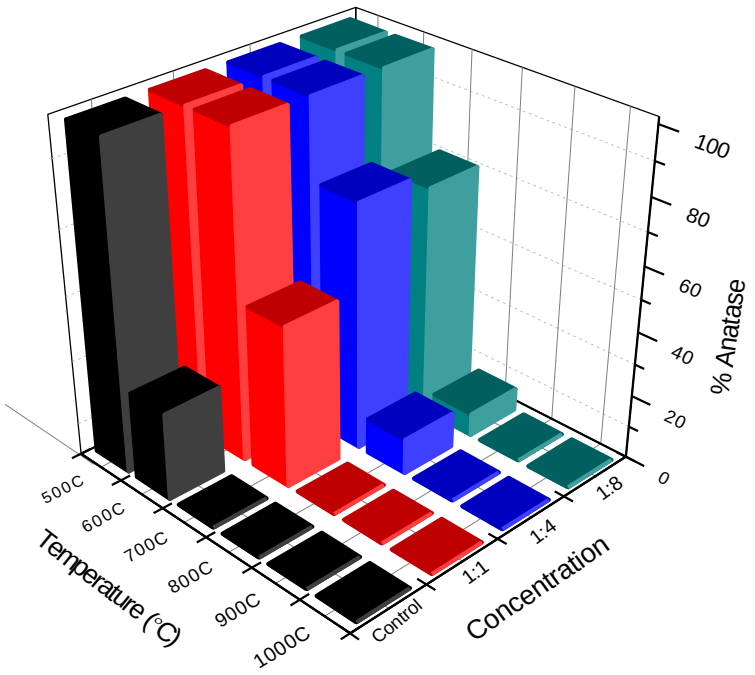

Figure 3.4: Anatase present (in %) in each of the samples at various temperatures.

Raman spectroscopy was employed as a complementary tool for identifying the anatase and/or rutile phase formation at all temperatures. As with XRD, there are characteristic peaks and modes for both phases. [6, 121, 295] The only peaks on the Raman spectra, as with XRD, where those that indicate the presence of the two TiO_2 phases. The active modes for anatase are A_{1g}, $2B_{1g}$ and $3E_g$ at 147, 197, 396, 516 and 638cm^{-1}.[6, 121, 295, 303-305] For rutile they are A_{1g}, B_{1g}, B_{2g} and $3E_g$ at 144, 238, 446, 612 and 827cm^{-1}. [6, 121, 295, 303-305] The results gained from Raman analysis concur with those of XRD analysis. The 1:8 TiO_2: benzoic acid sample calcined at 600°C contains 100% anatase, the characteristic anatase peaks for Raman can be seen in this sample can be seen in Figure 3.5 (a). The 1:8 TiO_2: benzoic acid sample calcined at 900°C contains 100% rutile; the characteristic rutile peaks for Raman can be seen in Figure 3.5 (b). When the sample is a mixed phased sample the Raman peaks for anatase and rutile will be present, see Figure 3.5 (c).

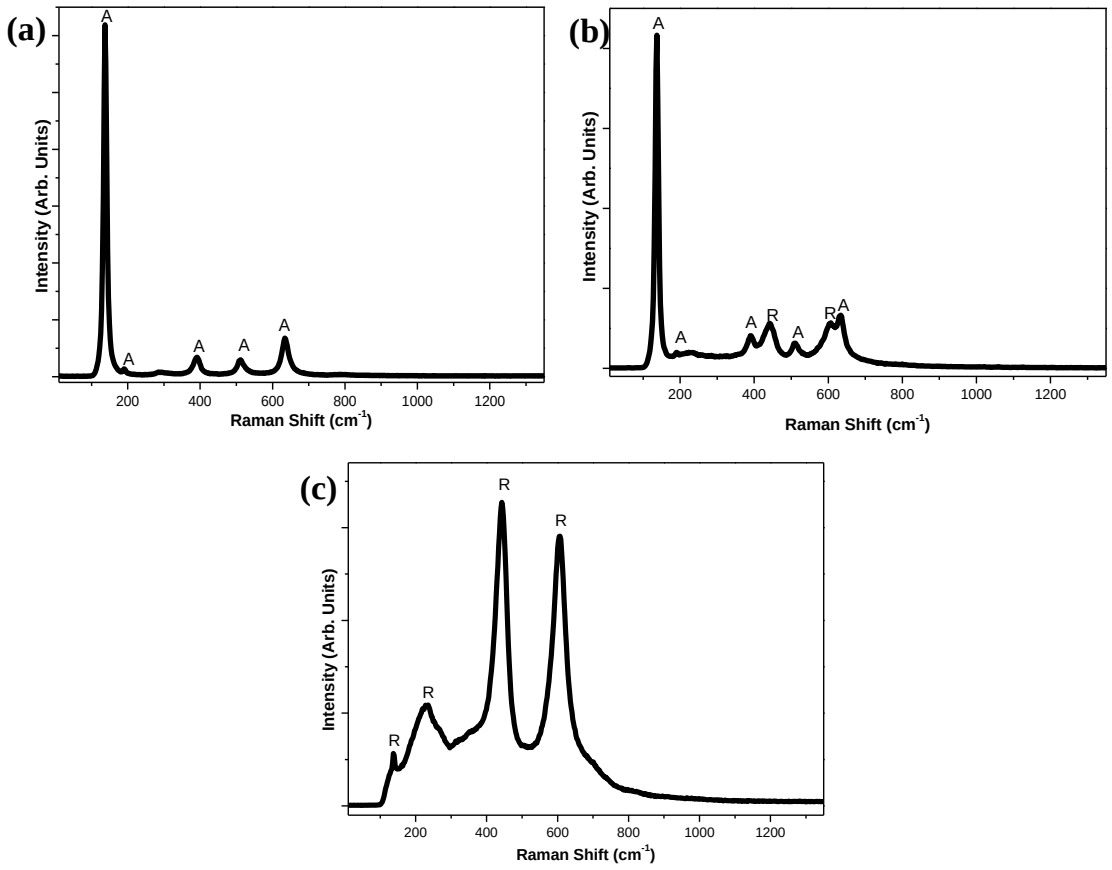

Figure 3.5: Raman spectra of (a) 1:8 TiO_2:BA sample calcined at 600°C, (b) 1:1 TiO_2:BA sample calcined at 700°C and (c) 1:8 TiO_2:BA sample calcined at 900°C

3.2.2 Elemental Surface Composition and Chemical Bonding of Benzoic Acid Doped Titania

XPS was used in order to determine the bonding/binding that was occurring for each sample. It was also employed for examining if the carbon was integrated into the titania structure or if the carbon resided on the titania surface. XPS was employed to determine the impact of precursor modification on the binding energy (eV). XPS analysis was only carried out on samples between 600-800°C.

The eV for C *1s* for all four concentrations at the three temperatures remained unchanged, see Table 3.1. The peak at 285.0 eV is indicative of adventitious carbon (C-C, C=C and/or C-H bonds).[19, 121, 295] The characteristic peak for Ti-C (281.5 eV) was not present, which indicates that the carbon was not doped into the TiO_2 lattice but onto the TiO_2 surface.[6, 121, 306] When Yang *et al.* (2006) examined N-C doped TiO_2, they also found that there was carbon doping into the TiO_2 lattice for the TiO_2 films however in the films containing carbon and nitrogen it is suggest that the carbon is doped in the TiO_2 films.[307] There were also no peaks present for C-O, C=O and carbon bonded to three oxygen, 287, 289 and 291 eV respectively.[120, 121, 150, 308, 309] This could mean that the BA is being burned off, FTIR supports this observation.

Table 3.1: XPS results showing the binding energies (eV) for samples calcined at 600°C, 700°C and 800°C

	Control	**1:1**	**1:4**	**1:8**
C *1s*	600°C – 285.0 700°C – 285.0 800°C – 285.0	600°C – 285.0 700°C – 285.0 800°C – 285.0	600°C – 285.0 700°C – 285.0 800°C – 285.0	600°C – 285.0 700°C – 285.0 800°C – 285.0
O *1s*	600°C – 530.2 700°C – 529.8 800°C – 530.0	600°C – 530.2 700°C – 530.0 800°C – 529.8	600°C – 530.2 700°C – 530.2 800°C – 530.0	600°C – 530.0 700°C – 529.8 800°C – 529.8
Ti *2p*	600°C – 459.0 700°C – 458.8 800°C – 458.6	600°C – 459.0 700°C – 458.8 800°C – 458.6	600°C – 459.0 700°C – 458.8 800°C – 458.8	600°C – 458.8 700°C – 458.6 800°C – 458.6

For all concentrations, there was a slight decrease in binding energy of O *1s* as the temperature increased, there was a similar decrease in the binding energy of all samples for Ti $2p_{3/2}$ (Ti-O),[19] see Figure 3.6 and Table 3.1. The slight decrease in O *1s* binding energy shows that the samples are oxygen rich and as the temperature increases oxygen vacancies begin to form. The slight decrease in the Ti $2p_{3/2}$ binding energy also demonstrates the formation of oxygen vacancies and this leads to the conversion of Ti^{4+}

to Ti^{3+}.[19, 47, 305] In a similar study, Yang *et al.* (2009) co-doped TiO_2 with carbon and nitrogen there was such a significant decrease in Ti *2p* $_{3/2}$ that it lead to the conversion Ti^{4+} to Ti^{3+} to Ti^{2+}.[307] This decrease in the O *1s* and Ti *2p* $_{3/2}$ signifies that anatase is transitioning into rutile. Peaks for Ti *2p* $_{1/2}$ are present in all samples between 458.6-459.0 eV.[301, 307] These peaks donates the presence of Ti the form of TiO_2, i.e. in a tetravalent state.[301, 307]

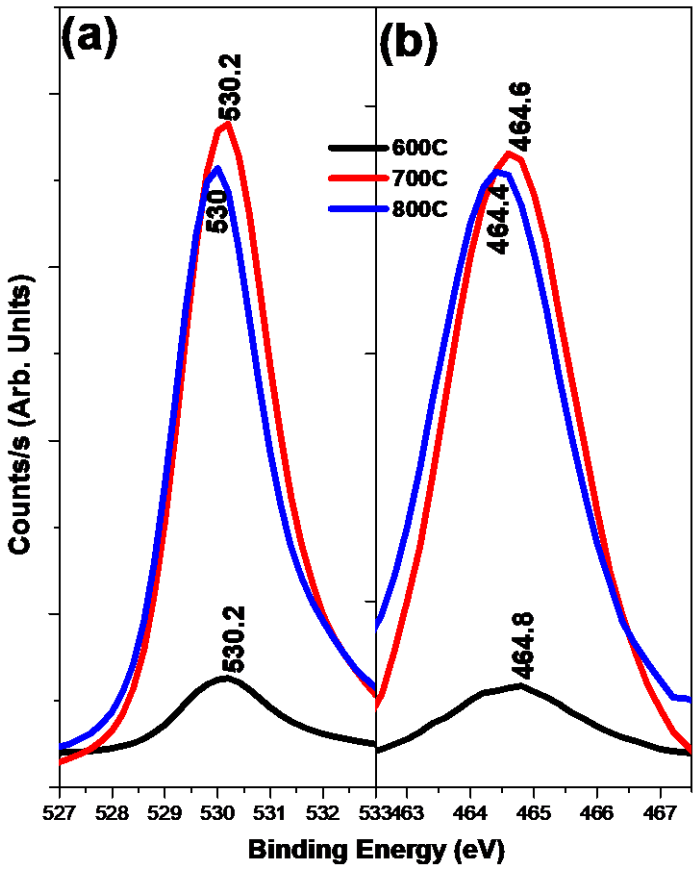

Figure 3.6: XPS of 1:4 TiO_2:BA calcined at 600°C, 700°C and 800°C for (a) O *1s* and (b) Ti *2p*

FTIR-ATR was used in order to examine the various bonds and shifts that are present as a result of the samples (1:1, 1:4 and 1:8) containing benzoic acid ($C_7H_6O_2$). Each concentration was examined when uncalcined, at 500°C and 900°C (see Table 3.2).

The type of binding a carboxylate group displays can be observed with the use of FTIR.[16] The difference between the carboxylate stretches and the asymmetric carboxylate vibrations, $\Delta = \nu_{as}$ (COO-) - ν_s(COO-), is used for identifying the type of binding.[16, 310] The Δ for ionic carboxylate is reported to be 191 cm^{-1}.[311] Bridge coordination relates to when one divalent titanium cation binds to one of the oxygens in the COO^- group, another

to the remaining oxygen. This results in the ionic moiety occurring at the same place as the asymmetric stretch.[16, 310, 312] There are four pairs of electrons in the carboxylate functional group (Figure 3.7) that have the ability to react with the titanium.[16] The lone pair of electrons are pushed apart at an angle of 120°, they are labelled *syn* and *anti*-lone pair of electrons depending on their position, Figure 3.7.

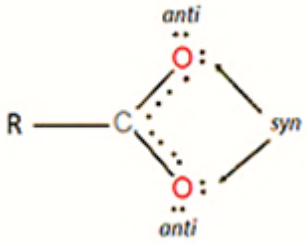

Figure 3.7: Carboxylate (COO^-) functional group. [Original publication - RSC Adv., 2016,6, 95232-95238 - Reproduced by permission of The Royal Society of Chemistry]

Many studies report that when $\Delta(COO^-)_{\text{formate complex}} \leq \Delta(COO^-)_{\text{sodium salt}}$ there is the formation of the bidentate bridging carboxylate.[16, 313-317] Nolan *et al.* (2009) suggested that the Ti centre will interact with the formate group in the bidentate bridging mode, in *syn-syn* or *syn-anti* formation.[16] It is noted that the benzoate group reacts with the Ti centre in the same manner as the formate group. However, due to the bulky nature of the benzene ring and steric hindrance, it is anticipated that *syn-syn* formation (Figure 3.8(a)) will be favoured over the *syn-anti* formation, Figure 3.8(b).

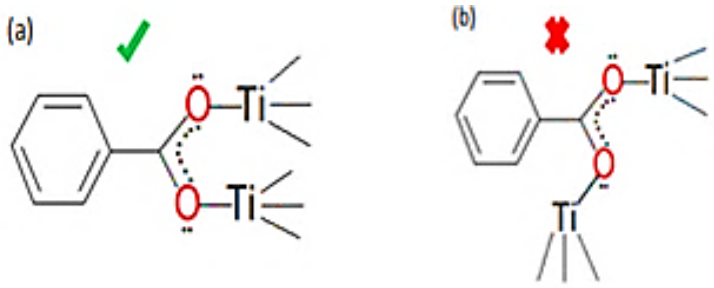

Figure 3.8: Bidentate bridging modes of the benzoate group and TiO_2 (a) *syn-syn and* (b) *syn-anti*. [Original publication - RSC Adv., 2016,6, 95232-95238 - Reproduced by permission of The Royal Society of Chemistry]

When control samples were examined with FTIR-ATR, the only peaks that were present were those for Ti-O-Ti (570-430 cm^{-1}). The peaks for the three concentrations all occurred at similar points: uncalcined materials contained peaks at 515cm^{-1} and 527cm^{-1} with weak

signal and 538cm^{-1} and 547cm^{-1} with very weak signal; 500°C contained peaks of 515cm^{-1}, 526cm^{-1}, 547cm^{-1} and 554cm^{-1} all of very weak signal and the samples at 900°C contained peaks at 515cm^{-1}, 523cm^{-1}, 531cm^{-1} and 546cm^{-1} all of weak signal.[318]

Table 3.2: FTIR results for control, 1:1, 1:4 and 1:8 calcined at 500°C

Sample	Bond	Peak(s) cm^{-1} (strength)
Control	Ti-O-Ti	515, 526, 547, 555 (all very weak)
1:1	Ti-O-Ti C-O $_{symmetric}$	546 (weak) 1417 (weak)
1:4	Ti-O-Ti Benzene ring C-O $_{symmetric}$ C-O $_{asymmetric}$ C=O	564 (very weak) 1125 (weak) 1417 (medium) 1593 (weak) 1600 (weak)
1:8	Ti-O-Ti Benzene ring C-O $_{symmetric}$ Carboxylate Moieties C-O $_{asymmetric}$	530 (weak) 1025 (weak) 1416 (medium) 1538 (weak) 1590, 1690 (weak)

As with the control, when examined with FTIR all 1:1 doped samples contained low Ti-O-Ti peaks, uncalcined at 548cm^{-1}, 500°C at 546cm^{-1} and 900°C at 537cm^{-1}. The uncalcined sample was the only one at 1:1 that a small peak could be observed for a benzene ring, at 1026cm^{-1} and 1071cm^{-1}, the absence of this peak for the calcined sample could mean that the benzene ring had broken into simple hydrocarbon chains. It should be noted that the peak at 1286cm^{-1} in the uncalcined sample indicates a carboxyl group (COOH) and is not present in the other samples. The uncalcined sample contains a medium C-O symmetric stretch (1411cm^{-1}), while 500°C shows a weak C-O symmetric stretch (1417cm^{-1}).[16, 310] This is not present at 900°C. The remaining peaks on the uncalcined spectra, 1515 and 1596cm^{-1} and 1693cm^{-1}, accounting for low asymmetric C-O and C=O stretches, respectively.[16, 310]

All 1:4 samples (Figure 3.9) contained very weak Ti-O-Ti peaks, uncalcined at 559cm^{-1}, 500°C at 564cm^{-1} and 900 °C at 569cm^{-1}. The uncalcined and 500°C samples both showed the presence of benzene ring(s), with a medium peak at 1025cm^{-1} for uncalcined and a weak peak at 1125cm^{-1} for the sample calcined to 500°C. There is also peak at 1289cm^{-1} in the uncalcined sample for a carboxyl group (COOH) and one at 1319cm^{-1} that indicates the presence of C-OH and is not present in the other samples. The uncalcined sample contains a strong C-O symmetric stretch (1403cm^{-1}), while 500°C shows a medium C-O

symmetric stretch (1417cm^{-1}). This is not present at 900°C. There are also peaks that show weak asymmetric C-O (uncalcined-1593 cm^{-1} and 500°C- 1593 cm^{-1}) and C=O (both - 1600cm^{-1}) stretches.

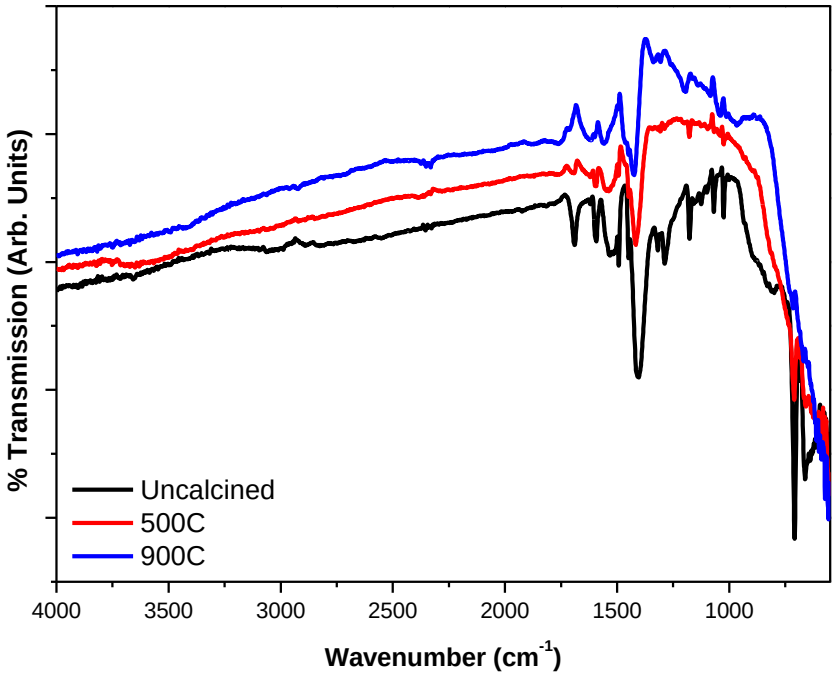

Figure 3.9: FTIR spectra of the 1:4 TiO_2: benzoic acid for uncalcined and calcined at temperatures of 500°C and 900°C

All 1:8 samples contained very weak Ti-O-Ti peaks, uncalcined at 556cm^{-1}, 500°C at 530cm^{-1} and 900°C at 534cm^{-1} (see Figure 3.10). The uncalcined and 500°C samples both showed the presence of benzene ring(s), with a medium peak at 1036cm^{-1} for uncalcined and a weak peak at 1025cm^{-1} for the sample calcined to 500 °C. There is also a peak at 1287cm^{-1} in the uncalcined sample for a carboxyl group (COOH) and one at 1319cm^{-1} that indicates the presence of C-OH and is not present in the other samples. The uncalcined sample contains a strong C-O symmetric stretch (1403cm^{-1}), while 500°C shows a medium C-O symmetric stretch (1416cm^{-1}) and at 900°C a very weak C-O symmetric stretch (1427cm^{-1}). There are vibrations of carboxylate moieties at 500 °C (1538cm^{-1}). There are also peaks that show asymmetric C-O stretches, for uncalcined at 1590cm^{-1} and 1690cm^{-1} (medium) and for 500°C at 1590cm^{-1} and 1690cm^{-1} (weak).

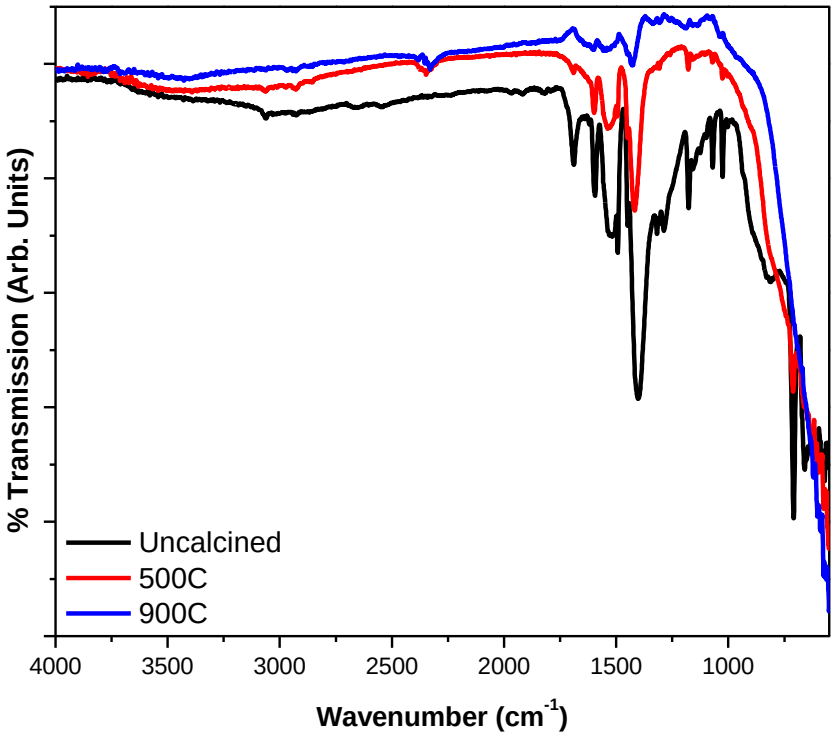

Figure 3.10: FTIR spectra of the 1:8 TiO_2: benzoic acid for uncalcined and calcined at temperatures of 500°C and 900°C

3.2.3 Textural Properties of Benzoic Acid Doped TiO_2

BET analysis was performed in order to determine the surface area and porosity of the sample. The surface area of the samples was 30.7, 15.8, 40.4 and 21.2 m^2/g for the control, 1:1, 1:4 and 1:8, respectively. The pore volume for all samples were very similar varying only by ±1 Å, 20.72 Å (Control), 20.63 Å (1:1), 20.76 Å (1:4) and 20.79 Å (1:8).

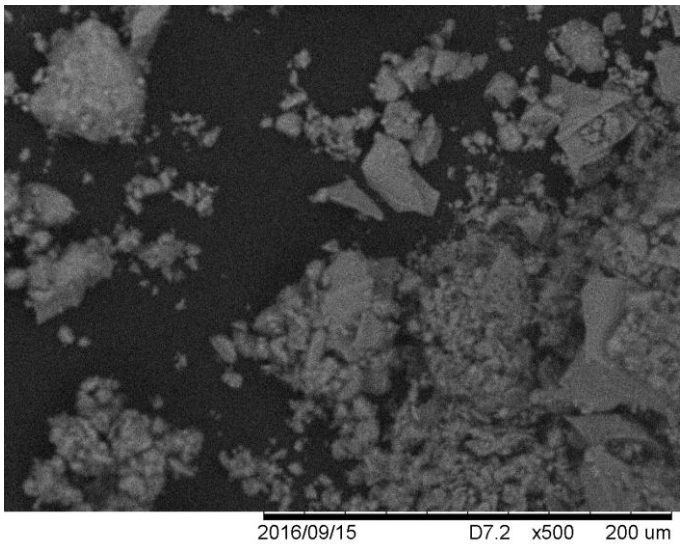

Figure 3.11: SEM of 1:4 TiO_2:BA calcined at 500°C (at X500 magnification).

SEM analysis was employed in order to determine the morphology of each of the sample. These analyses showed that the samples are highly agglomerated, and no specific shapes were identified, see Figure 3.11.

3.2.4 Photocatalytic Degradation of 1,4-Dioxane

The adsorption of 1,4-dioxane onto the doped TiO_2 catalyst surface did not exceed 10% in the dark control experiments, where the catalyst was added without applying solar light. The samples that were examined were the control and 1:4 TiO_2:BA at 500°C and 800°C (Figure 3.11). Photocatalysis degradation performed on 1,4-dioxane under solar light but without the presence of any catalyst (TiO_2 = 0) showed a 15.8% removal of 1,4-dioxane. The control (TiO_2 without BA) and the 1:4 samples at 500°C (both 100% anatase) showed almost full reduction in 1,4-dioxane (97.6% and 97.1% removal, respectively). When the control was calcined at 800°C (100% rutile), it showed only 25.9% removal of 1,4-dioxane. At the same temperature, the 1:4 sample (11% anatase) showed a significant increase in the % removal of 1,4-dioxane, with 70.6% removed (Figure 3.11).

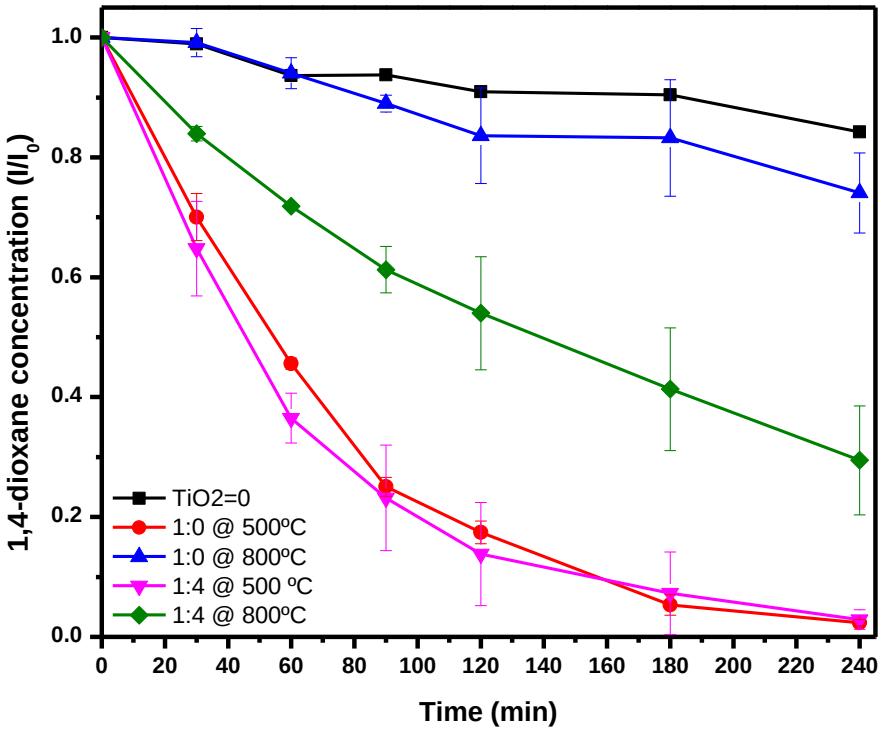

Figure 3.12: Photocatalysis of control (1:0) and 1:4 TiO_2: Benzoic acid

3.2.5 Discussion of Results

From XRD and Raman spectroscopy analysis it was shown that modifying TiO_2 with benzoic acid increased the ART temperature. Nolan *et al.* (2009) found that increasing the amount of water causes the resulting sol to become less acidic during the hydrolysis

of TTIP.[16, 319-321] This minimised the chelation effect, which weakened gel network and consequently lowers the transition temperature.[16, 319-322] It has also been noted by Kung *et al.* (1996) that the size and number of branches within the gel network directly effects the porosity of the gel.[322] This then has an impact on resulting material's surface area, porosity and thermal stability during calcination.[322] The current study kept the volume of water constant and the addition of increasing amounts benzoic acid caused the sol to become increasingly acidic. It can be concluded that the increase in acidity causes the chelation effect to increase, thus strengthening the gel network and causing the ART to occur at elevated temperatures.[16] FTIR showed the presence of the characteristic bonds for benzoic acid (C-O, C=O, COOH, benzene) to various degree depending on the concentration of doped BA (1:1, 1:4, or 1:8) and the calcination temperature (uncalcined, 500 to 1000°C). FTIR analysis, along with XPS, revealed that the carbon was on the TiO_2 surface. This is indicated by the fact only the peaks for Ti-O-Ti are present on the FTIR spectra. The 1:4 sample proved to be the optimum sample for all analysis.

3.3 Conclusions

The current investigation examined the effect that chemically modifying TiO_2 with benzoic acid (at various concentrations) had on the anatase to transition temperature, using XRD and Raman spectroscopy. Whether the carbon was included in the titania structure or if the carbon sat on the surface of the titania was examined with FTIR and XPS. There were large amounts of anatase present at 700°C in the 1:1, 1:4 and 1:8 doped samples (50, 76, 71% anatase). There was also anatase present in 1:4 and 1:8 at 800°C, 11% and 7% respectively. These results were confirmed when the samples were analysed with Raman spectroscopy. This is an increase on the ART temperature; rutile is normally formed fully at 700°C. With the use of XPS and FTIR it was determined that the carbon was present on the surface on the TiO_2. The presence of benzoic acid showed to increase the photocatalytic activity.

Chapter 4 - Nanocomposites of TiO_2 and WO_3 for the Effective Photocatalytic Decomposition of 1,4-dioxane

4.1 Introduction

Due to the improved charge-carrier mobility and enhanced surface hydroxyl sites, the anatase polymorph is generally considered the most photocatalytically active TiO_2 phase.[300] The two of the key challenges faced in TiO_2 research, which are mentioned previously in Section 1.1 and Section 3.1, is the improved temperature stability and enhanced photocatalytic activity of the anatase phase.[8, 299, 300, 323-336] The alteration of TiO_2 with transition metals (including Cr, Co, V and Fe) have made it possible to synthesize visible light active photocatalysts.[8, 122-125] In contrast to this, some transition metals can end up being used as recombination sites which leads to the reduction of the quantum efficiency.[8]

Due to the similar CB levels of both tungsten trioxide (WO_3) and TiO_2 (2.8 eV and 3.2 eV respectively), heterostructure formation of the photocatalysts can reduce recombination of the photogenerated electron-hole pair. In addition, the presence of WO_3 increases the surface acidity of TiO_2, facilitating increased adsorption of HO^- or H_2O molecules and thus the increased production of •OH radicals.[337-340] Consequently, there has been an upsurge in interest surrounding the use of tungsten (W) inclusion on the TiO_2 surface or within its matrix structure. Many studies investigated various concentrations of tungsten while others explored the effect of temperature. For example, Liu *et al.* (2016), Couselo *et al.* (2008) and Sathasivam *et al.* (2015) investigated the role of tungsten concentration of doped TiO_2 at one temperature (0-1%, 0-6% and 0-20% W-TiO_2 respectively).[341-343] Azadi *et al.* (2017) examined the effects of 0.5-4.5 wt.% W doping on TiO_2 calcined between 300-700°C, on the photocatalytic treatment of landfill leachate.[344] However, in the latter reports a maximum contaminant removal was induced by relatively low tungsten loading and a calcination temperature of <500°C. Ioannidoa *et al.* (2017) examined the effect of 1-6 wt. % W-P25 TiO_2 calcined between 600-900°C on the photocatalytic degradation of antibiotic sulfamethoxazole.[345] Due to the use of P25 TiO_2 there was no significant change in the phase % between 600-800°C, while at 900°C there was a 20% reduction in the anatase phase.[345] This study did however show a 50% increased rate of degradation with 4% W-P25 when compared to pristine P25.[345] In a study recently published, Uallah *et al.* (2018) examined four different concentrations of W-doped TiO_2 (0, 2, 4 and 6 mol. % W) at different temperatures (250°C, 500°C, 750°C

and 1000°C) for the degradation of Congo red dye.[346] The doped samples retained 100% anatase phase up to 750°C.[346] The 6 mol.% W-TiO_2 extended photocatalytic activity into the visible light spectrum.[346] When the photocatalyst was examined under UV light the photocatalytic activity was similar. However, when the two materials were illuminated with visible light, the 6 mol. % W-TiO_2 showed photocatalytic activity 10 times higher than that of P25.[346] Interestingly, the findings reported within suggest increased tungsten doping and elevated calcination temperatures could result in superior photocatalytic performance.

This Chapter therefore focused on the development of a high temperature-stable, anatase rich TiO_2 nanocomposites *via* WO_3 incorporation. Calcination temperature and anatase-rutile phase content influence the final photocatalytic properties of TiO_2. Consequently, the W doped TiO_2 catalyst was prepared *via* sol-gel processing, a systematic study of the modified material properties was examined by varying W concentrations (0-16 mo. % W-TiO_2) and calcination temperature (500-1000°C). The physiochemical properties of undoped and W doped TiO_2 catalysts were evaluated using XRD, Raman spectroscopy and XPS. Furthermore, 1,4-dioxane was selected as the target contaminant to examine the photocatalytic activities of the non-doped and W doped, high temperature stable TiO_2 catalysts.

4.2 Results and Discussion

The dispersion of W on the surface of TiO_2, or W^{6+} substitution of the Ti^{4+} lattice could improve the photocatalytic activity of TiO_2 through various modes of action. WO_3 possesses a +0.4 V CB and VB at +3.1 V, a slightly lower CB than TiO_2.[347] Consequently, WO_3 acts as an electron acceptor; photo-generated electrons on the TiO_2 CB may transfer to the WO_3 CB, favouring charge carrier separation, also reducing the recombination of the electron-hole pairs.[348, 349] Moreover, the presence of WO_3, which is considered about 15 times more acidic than TiO_2, increases the Lewis surface acidity of TiO_2 catalysts. Consequently, WO_3/TiO_2 particles have a higher adsorption affinity for the reactant molecules.[338, 349, 350] Furthermore, the tungstate phase hinders the anatase-to-rutile phase transformation.[351]

4.2.1 Crystalline Structure of W Doped TiO_2 Photocatalysts

Crystalline phase formation of the undoped and W doped catalysts, as a result of calcination temperature, has been examined using powder XRD and Raman spectroscopy.

Figures 4.1, 4.2 and 4.3 show the diffraction spectra for all samples when calcined at various temperatures, while Figure 4.4 shows the % anatase present in all samples analysed.

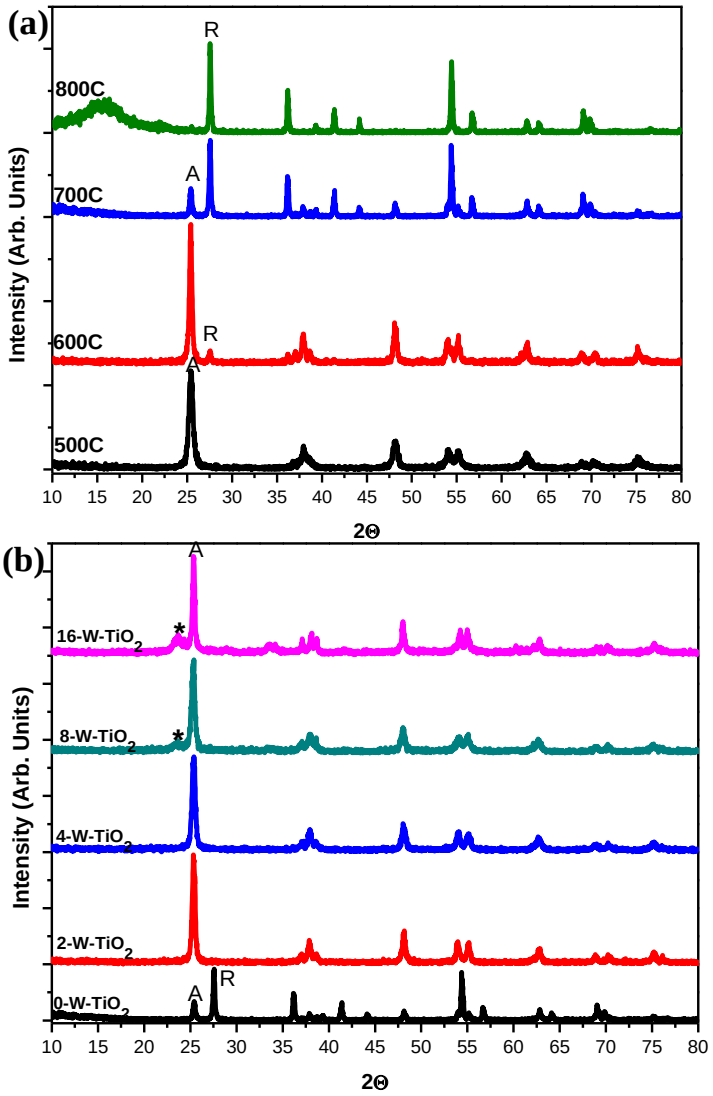

Figure 4.1: XRD spectra of (a) 0% W-TiO_2 at various temperatures and (b) doped W-TiO_2 samples calcined at 700°C. Where A = anatase; R = rutile; * = WO_3

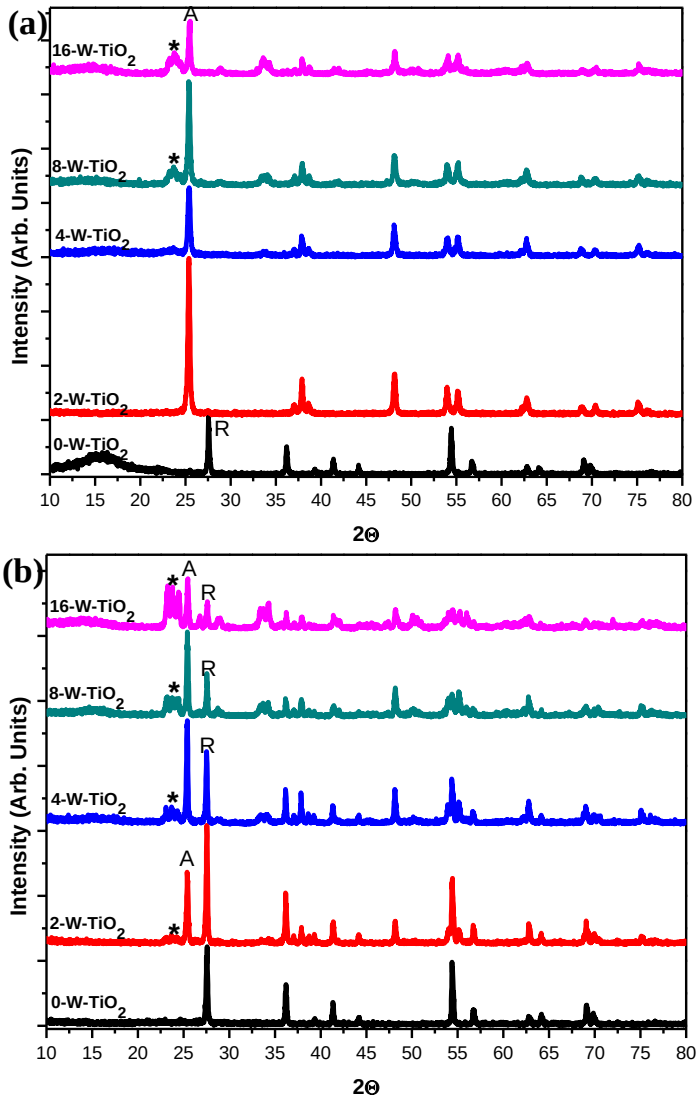

Figure 4.2: XRD spectra of W doped TiO_2 calcined at (a) 800°C and (b) 900°C. Where A = anatase; R = rutile; * = WO_3

All photocatalysts retained 100% anatase up to 500°C calcination temperature. The 0% W-TiO_2 catalysts exhibited 89.3 and 22.9% anatase content at 600°C and 700°C, respectively (Figure 4.1 (a)), converting to 100% rutile at 800°C. In contrast, TiO_2 catalysts doped with tungsten were 100% anatase up to 800°C (Figures 4.2 (a) and 4.4). However, at 900°C the rutile phase appeared within the XRD spectra of all W-TiO_2 photocatalysts, indicative of mixed phase samples (32.7, 53.4, 61.0 and 59.2% anatase for 2%, 4%, 8% and 16% W-TiO_2 respectively) (Figure 4.2 (b)).

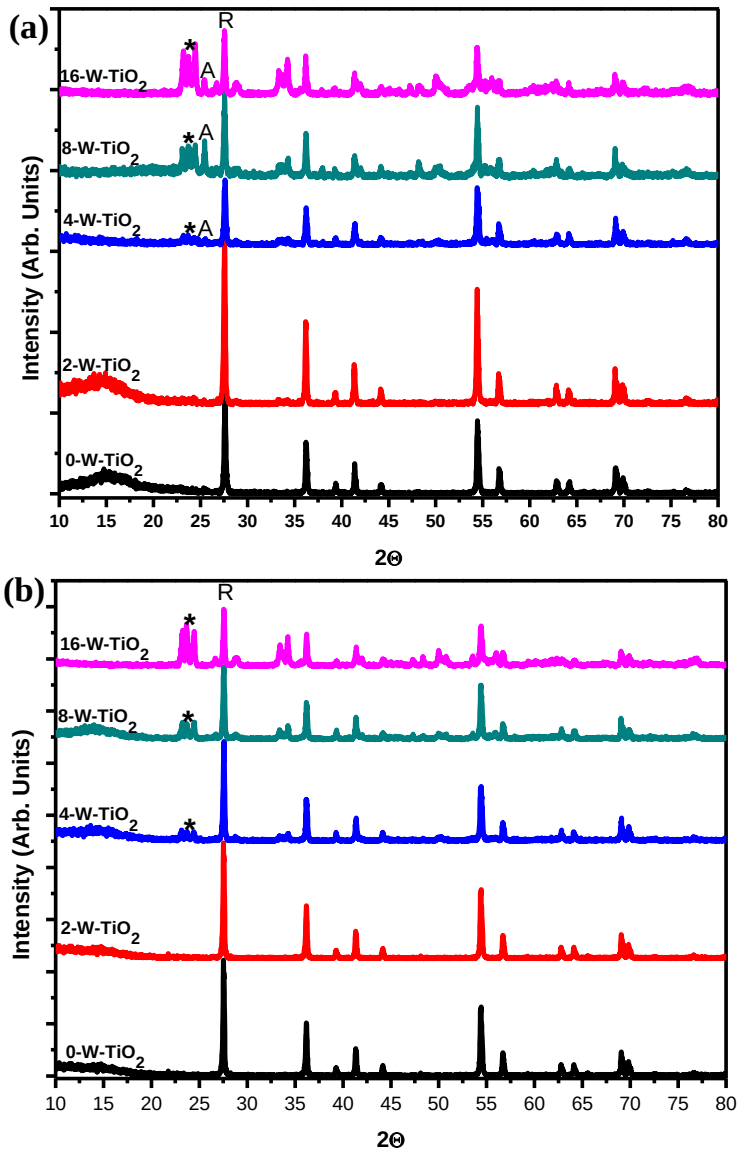

Figure 4.3: XRD spectra of W doped TiO_2 calcined at (a) 950°C and (b) 1000°C. Where A = anatase; R = rutile; * = WO_3.

As processing temperatures surpassed 900°C, the relative intensity of the rutile 110 peak with respect to the anatase 101 peak increased. Figure 4.3 (a) shows all samples at 950°C; the 2% W-TiO_2 sample had become 100% while the 4%, 8% and 16% W-TiO_2 samples remained mixed phased samples (7.7%, 26.0% and 16.8% anatase, respectively). At 1000°C, W doped TiO_2 photocatalysts were designated 100% rutile (Figures 4.3 (b) and 4.4).

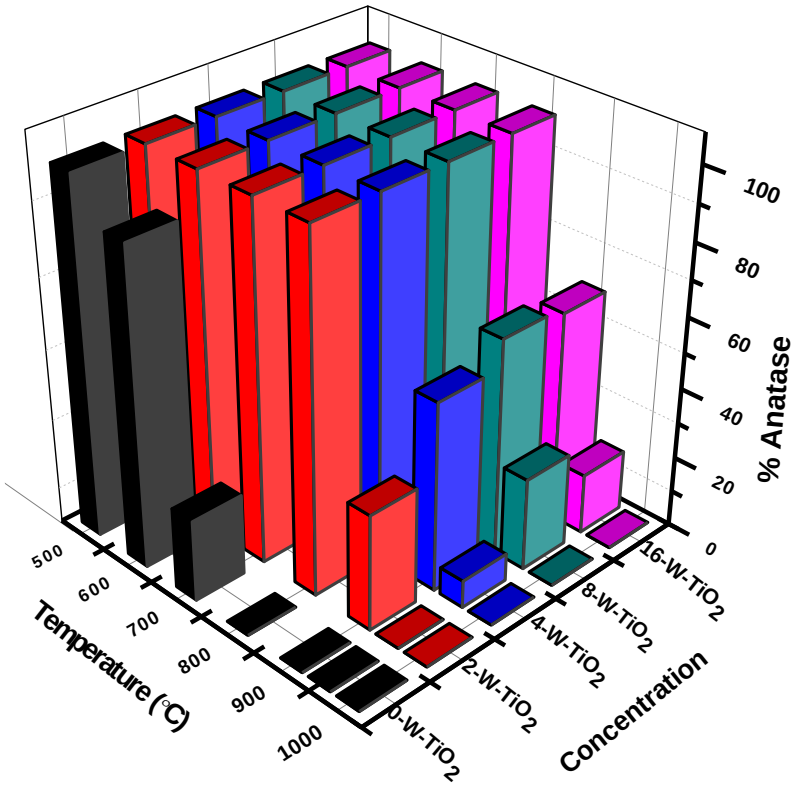

Figure 4.4: % anatase present in all photocatalysts calcined at 500, 600, 700, 800, 900, 950 and 1000°C

In addition to characteristic anatase and rutile TiO_2 peaks, XRD spectra of W doped catalysts calcined at 700°C and beyond also exhibited the presence of monoclinic WO_3.[347, 352-359] The main characteristic peaks for monoclinic WO_3 is a distinct triple peak between 23-25°, as well as peaks between 33.5-34.5° and ~50-56°.[347, 354] Bamwenda and Arakawa (2001) reported that monoclinic WO_3 is most stable at room temperature and at temperatures from 900°C becomes under-stoichiometric WO_x (x = 0.9-1) which denotes the formation of W suboxides [ICDD Card 46-1096, ICDD Card 20-1324, ICDD Card32-1395, ICDD Card 43-1035, ICDD Card 50-388].[347] However, results of the current study show crystalline WO_3 initially forms at 700 °C for 8% and 16% W-TiO_2, 800°C for 4% W-TiO_2 and 900°C for 2% W-TiO_2 (Figures 4.1(a), 4.2 and 4.3).

Thermal processing influences the characteristics and activities of TiO_2 photocatalysts significantly, however, calcination temperature also dictates WO_3 phase composition and crystallinity. Like TiO_2, WO_3 occurs naturally in a variety of phases; δ-WO_3 (triclinic), γ-WO_3 (monoclinic), β-WO_3 (orthorhombic) and α-WO_3 (tetragonal). [360] Upon annealing, these phases transform in the following order: δ-WO_3 (triclinic, −40 to 17°C) → γ-WO_3

(monoclinic, 17–320°C) → β-WO_3 (orthorhombic, 320–720°C) → α-WO_3 (tetragonal, >720°C). [360] The presence of TiO_2 delays crystallization of WO_3 and hinders the transformation of γ-WO_3 (monoclinic) into β-WO_3 (orthorhombic). [360-362]

Table 4.1: Crystalline size (nm) of all W-TiO_2 samples calcined at 500, 600, 700, 800, 900, 950 and 1000°C

Sample	Crystalline Size (nm)	
	Anatase	**Rutile**
0% W-TiO_2 500°C	13.83	-
0% W-TiO_2 600°C	21.04	-
0% W-TiO_2 700°C	26.65	33.02
0% W-TiO_2 800°C	-	34.99
0% W-TiO_2 900°C	-	34.54
0% W-TiO_2 950°C	-	35.23
0% W-TiO_2 1000°C	-	41.40
2% W-TiO_2 500°C	11.01	-
2% W-TiO_2 600°C	15.95	-
2% W-TiO_2 700°C	20.59	-
2% W-TiO_2 800°C	27.17	-
2% W-TiO_2 900°C	32.66	36.85
2%W-TiO_2 950°C	-	36.41
2% W-TiO_2 1000°C	-	39.46
4% W-TiO_2 500°C	11.91	-
4% W-TiO_2 600°C	13.52	-
4% W-TiO_2 700°C	17.98	-
4% W-TiO_2 800°C	24.33	-
4% W-TiO_2 900°C	39.86	39.23
4% W-TiO_2 950°C	-	30.16
4% W-TiO_2 1000°C	-	38.89
8% W-TiO_2 500°C	11.05	-
8% W-TiO_2 600°C	13.46	-
8% W-TiO_2 700°C	16.81	-
8% W-TiO_2 800°C	26.42	-
8% W-TiO_2 900°C	35.18	39.84
8% W-TiO_2 950°C	32.08	32.90
8% W-TiO_2 1000°C	-	36.02
16% W-TiO_2 500°C	12.03	-
16% W-TiO_2 600°C	18.00	-
16% W-TiO_2 700°C	25.41	-
16% W-TiO_2 800°C	26.94	-
16% W-TiO_2 900°C	31.94	34.00
16% W-TiO_2 950°C	-	36.43
16% W-TiO_2 1000°C	-	37.35

XRD analysis also provided an insight into variation within lateral crystallite dimensions due to dopant loading and calcination temperature. Crystallite dimensions were determined using Scherrer equation (eq. 2.2). For the control sample, the crystalline size

increases with increase in calcination temperature. However, this is not the case with the 8-W-TiO_2 sample for which the crystalline size increases up to 900°C but decreases in size above this temperature. The crystallite sizes of 0%, 2%, 4%, 8% and 16% W-TiO_2 photocatalysts are presented in Table 4.1.

Further phase confirmation, by Raman spectroscopy is presented in Figure 4.5. The active modes for anatase are *A1g*, *2B1g* and *3Eg* positioned at 147, 197, 396, 516 and 638 cm^{-1}, respectively.[6, 121, 295, 303-305] The *A1g*, *B1g*, *B2g* and *3Eg* rutile modes resonate at 144, 238, 446, 612 and 827 cm^{-1}, respectively.[6, 121, 295, 303-305] The only peaks identified within the 0% W-TiO_2 and 2% W-TiO_2 catalysts were those for anatase and/or rutile. The spectra of all remaining W doped TiO_2 catalysts (4%, 8% and 16% W-TiO_2), verify the presence of TiO_2 and WO_3, [6, 347, 352] the monoclinic WO_3 peaks occur at approximately 134, 271, 326, 715 and 806 cm^{-1} (Figure 4.5)[352, 363, 364]

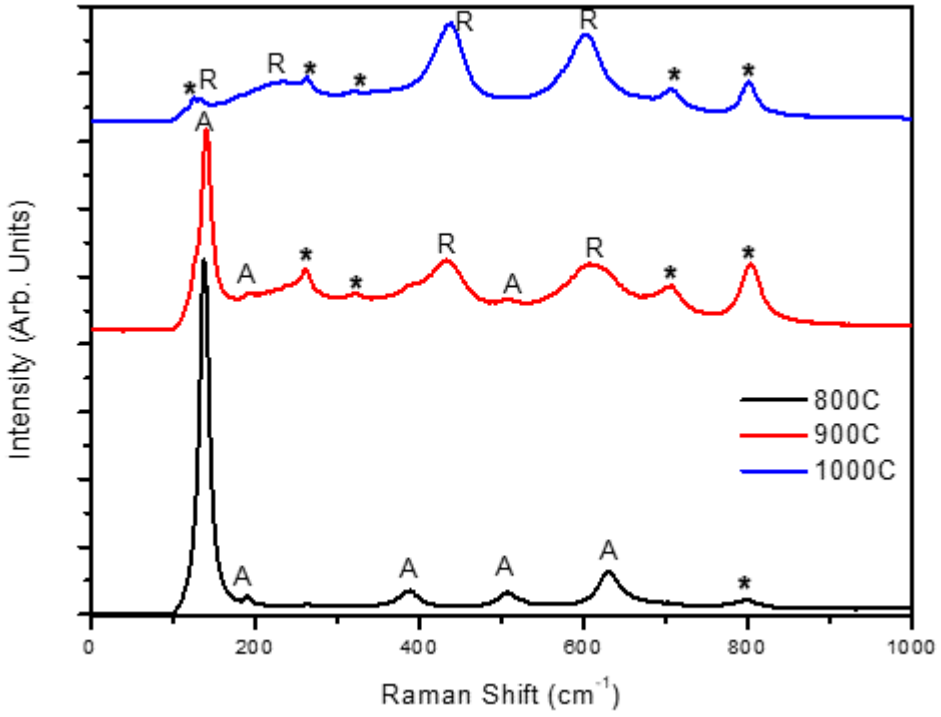

Figure 4.5: Raman spectra of 8% W-TiO_2 photocatalysts calcined at 800°C, 900°C and 1000°C, respectively. A = anatase; R = rutile; * = WO_3

4.2.2 Textural Properties of W Doped TiO_2 Photocatalysts

BET was performed to determine what effect the doping with tungsten had on the surface area of TiO_2. From the results in Table 4.2 it can be seen that 0% W-TiO_2 had a surface of 24.34 m^2/g when calcined at 500°C (100% anatase), 3.43 m^2/g at 800°C (100% rutile) and 1.69 m^2/g at 900°C (100% rutile). W-TiO_2 samples exhibited increased surface area

when compared to TiO_2 without W. When calcined at 500 °C the surface area varies from 33.40-56.02 m^2/g, with 8% W-TiO_2 having the highest surface area. When the 2%, 4%, 8% and 16% W-TiO_2 samples were calcined at 800°C and 900°C there is little variation in the surface area, there is a difference of 1.76 m^2/g and 0.76 m^2/g respectively.

Table 4.2: Surface area (m^2/g) of 0% W-TiO_2, 2% W-TiO_2, 4% W-TiO_2, 8% W-TiO_2 and 16% W-TiO_2 calcined at 500°C, 800°C and 900°C

	0% W-TiO_2	2% W-TiO_2,	4% W-TiO_2	8% W-TiO_2	16% W-TiO_2
500°C	24.34	33.40	49.24	56.02	52.44
800°C	3.43	12.31	12.96	12.26	11.20
900°C	1.69	5.78	5.05	5.09	5.02

4.2.3 Surface Chemical Composition of W Doped TiO_2 Photocatalysts

XPS measurements were completed in order to determine the oxidation state and surface chemical composition of the undoped and W doped TiO_2 catalysts. The Ti *2p*, O *1s* and W *4f* spectra of the 0% W-TiO_2 and 8% W-TiO_2 doped TiO_2 catalysts, calcined at 500°C, 800°C, 900°C and 1000°C, respectively, are presented in Figures 4.6 and 4.7. The Ti *2p* core level spectrum of undoped TiO_2 (Figure 4.6) presents two predominant, symmetrical peaks, assigned to Ti $2p_{3/2}$ and Ti $2p_{1/2}$, of Ti^{4+} octahedral oxygen coordination states at 464.7 and 458.9 eV, respectively.[365]

The binding energies of the undoped catalyst Ti *2p* excitation were not impacted by calcination temperature. A trend toward higher binding energies (465.0 and 459.2 eV, respectively) is witnessed upon addition of W. This upward shift is attributed to the formation of WO-Ti linkage. W^{6+} and Ti^{4+} have ionic radii of 0.06 nm and 0.0605 nm, respectively. Accordingly, W^{6+} is easily introduced into the TiO_2 lattice, substituting Ti^{4+}.[349, 366]

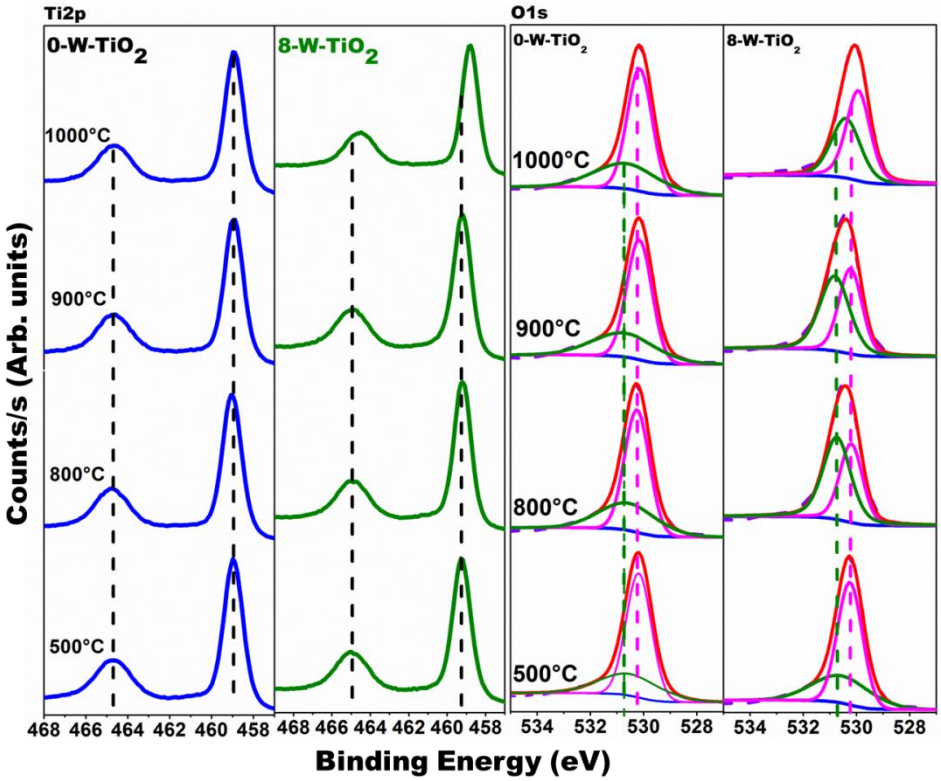

Figure 4.6: Ti2p, and O1s XPS spectra of 0% W-TiO_2 and 8% W-TiO_2 photocatalysts calcined at 800, 900 and 1000 °C, respectively

However, in the case of the doped catalyst, at calcination temperature of 1000°C, the binding energy of Ti *2p* decreased, shifting from 459.2 eV to 458.8 eV. This shift to lower energy signifies an increase in oxygen deficient species due to lowering of a valence state and reduction of Ti^{4+} to Ti^{3+}. [19, 47, 305, 367] Loss of lattice oxygen at a higher temperature decreases electron density and partially reduces Ti^{4+} to Ti^{3+}.[19] The Ti is only partially reduced due to Ti^{4+} being favoured as it is more stable than Ti^{3+}. Furthermore, this slight shift to lower binding energy is also due to the lattice contraction in rutile TiO_2. [368, 369] Lattice distortions are influenced by the presence, nature and degree of intrinsic defects created during diverse growth and processing conditions. As the TiO_2 crystallite phase transforms from anatase to rutile, anatase crystallites grow in size and begin to sinter causing lattice stress and thus contraction.[16]

The O *1s* region of the undoped TiO_2 catalyst constituted a main band peaking at 530.2 eV, ascribed to lattice oxygen bound to Ti, and a weak shoulder at 530.7 eV, attributed to surface hydroxyl species.[349, 370] The O *1s* binding energies of the undoped catalysts were also invariable at higher calcination temperatures. The O *1s* region of 8% W-TiO_2 doped TiO_2 calcined at 500°C was also composed of a distinct peak at 530.2 eV

and a shoulder of less intensity at 530.7 eV assigned to lattice oxygen and hydroxyl species, respectively.[371, 372]

As calcination temperature increased in the range of 500 to 800°C, the O *1s* contribution arising from hydroxyl species was reduced, due to tungsten-induced surface hydration reduction.[349] Meanwhile, the O *1s* peak is shared by W-O and Ti-O to form W-O-Ti linkage.[373] Oxygen vacancies are also illustrated in O *1s* core level measurements (Figure 4.6). The evolution of oxygen vacancies is revealed by a decrease in O1s binding energies in the 8-W-TiO_2 catalyst from 530.8, 530.2 eV to 530.4, 529.9 eV, upon increase in calcination temperature from 800 to 1000°C, denoting the phase transformation from anatase to rutile. [19, 47, 305] This negative shift in binding energy also indicates the formation of tungsten suboxides such as WO_2.[374]

The most prominent peaks of the tungsten XPS spectrum result from electronic excitations of the W *4f* orbital. The W4f spectrum can be deconvoluted into a doublet with pronounced peaks assigned to W $4f_{7/2}$ (36.0 eV) and W $4f_{5/2}$ (37.9 eV), respectively, which are associated with the W^{6+} state of WO_3. The binding energies of this doublet also fall within the same spectral region as Ti3p excitations, often averting precise measurement (Figure 4.7).[375-377] Furthermore, a W *5p* peak, inadvertently accompanies W *4f* excitations due to similarities in binding energy.[378]

The binding energies within W *4f* spin orbital did not vary greatly as a result of calcination temperature. However, as calcination temperature increased in the range from 800 to 1000°C, the binding energies of W $4f_{7/2}$ and W $4f_{5/2}$ decreased from 36.0 eV and 37.9 eV, respectively to 35.6 eV and 37.6 eV. This down shift in energy occurs similar to the one observed for Ti *2p*. As explained in Section 3.2.2, an increase in calcination temperature creates oxygen deficiencies within the W-TiO_2 nanomaterials.[379]

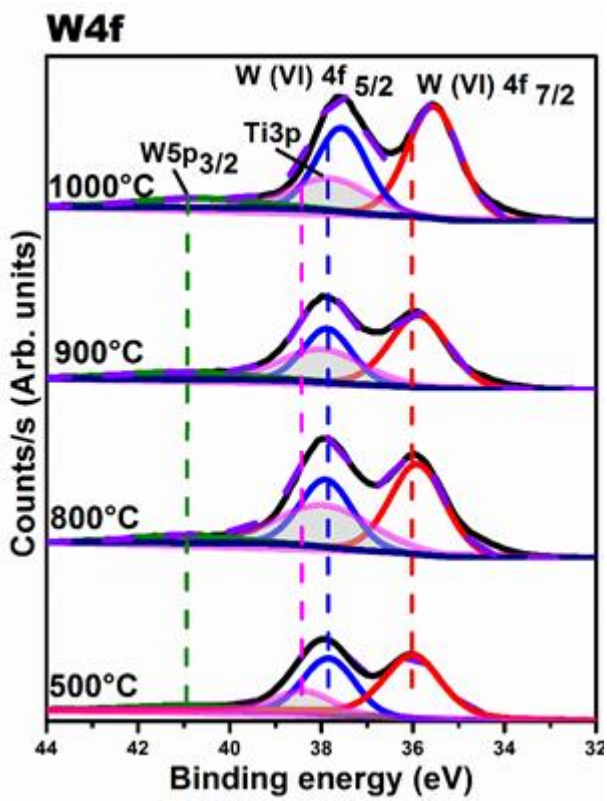

Figure 4.7: W *4f* XPS spectrum of 8% W-TiO_2 photocatalysts calcined at 500, 800, 900 and 1000°C, respectively. Showing W *5p* $_{3/2}$ (green), Ti *3p* (pink), W *4f* $_{5/2}$ (blue) and W *4f* $_{7/2}$ (red).

4.2.4 Photocatalytic Activity of W-TiO_2 Materials

Synthetic water contaminated with 1,4-dioxane was treated under solar light in the presence of the undoped and W doped TiO_2 photocatalysts in order to demonstrate the photocatalytic activity of the semiconducting complexes. The solar stimulated photocatalytic degradation of 1,4-dioxane is illustrated in Figure 4.8.

The degradation of 1,4 dioxane using undoped and W-TiO_2 photocatalysts was also performed in the absence of light. Under dark conditions, in either the presence or absence of the undoped and W doped TiO_2 catalysts, there was no significant degradation of 1,4-dioxane. The experiments under dark conditions showed less than 3% of 1,4-dioxane removal. UV irradiation alone however, successfully reduced 1,4-dioxane by ~10%. The addition of catalysts to contaminated water, under solar irradiation, enhanced pollutant degradation. However, the efficiency decreased once there was a reduction in % anatase. Furthermore, presence of W also enhanced photocatalytic activity.

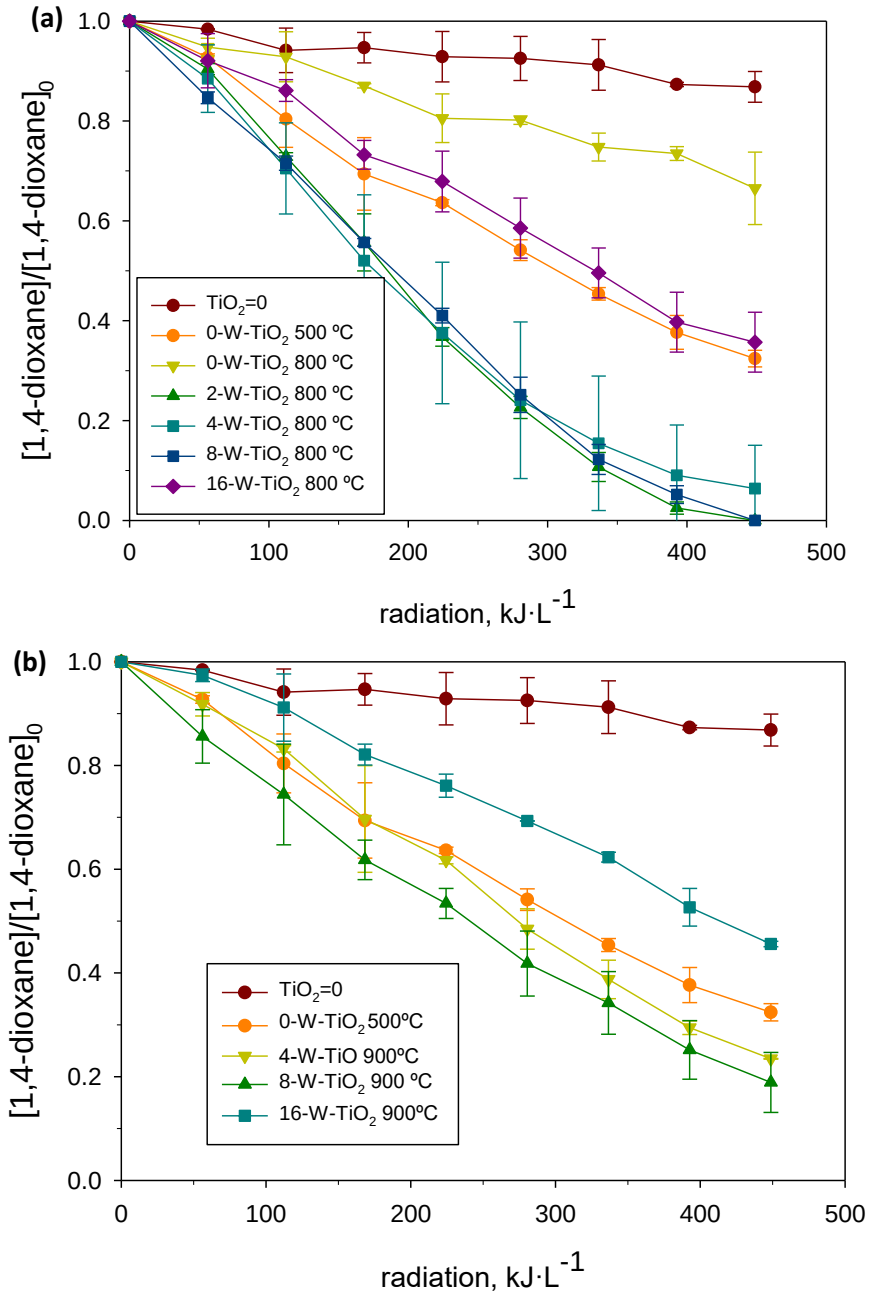

Figure 4.8: Degradation of 1,4-dioxane by W-TiO_2 solar photocatalysis calcined at (a) 800°C and (b) 900°C compared to undoped TiO_2.

The 0% W-TiO_2 catalysts calcined at 500°C removed ~70% of 1,4-dioxane from contaminated water in the presence of UV light. The anatase rich (100%) 2%, 4% and 8% W-TiO_2 catalysts calcined at 800 ºC completely removed 1,4 dioxane from the contaminated water source. As the tungsten loading increased to 16% W-TiO_2 (calcined at 800ºC), although 100% anatase phase was retained, only 70% of 1,4-dioxane was removed, a similar degradation efficiency to that of undoped TiO_2 catalysts, calcined at

500ºC. These findings indicate that the photocatalytic degradation of 1,4-dioxane is dominated by a high-stability anatase phase and tungsten loading, rather than the adsorptive surface properties of the undoped or W-TiO_2 catalysts as it was described above the dark experiments showed less than 3% of 1,4-dioxane adsorption.

Results show no differences in photocatalytic activity at doping level between 2%, 4% and 8% W-TiO_2 although there is a 30% decrease in degradation efficiency at 16-W-TiO_2 for a similar surface area (<10% reduction; Table 4.2). Despite published studies focusing on the degradation of different contaminants and in different conditions, all of them show an improvement in photocatalytic activity of TiO_2 up till the optimum W concentration and a decrease in the efficiency at higher W dosages. For example, Azadi *et al*. (2017) [69] observed that the optimum wt. % of W for the treatment of landfill leachate was 2.5 wt. % W-TiO2 calcined at 500ºC. They stated that an increased W loading may obstruct some surface reaction sites for photocatalytic activity, limiting the rate of the reaction.[11] Similarly, Song *et al.* (2016) [80] observed optimum photocatalytic performance by doping TiO_2 with 2% W and calcining at 550ºC while the degradation efficiency of methylene blue dye decreased as the amount of W increased up to 8% W. On the other hand, Gong *et al*. (2011) [71] obtained the highest degradation at 5% W in a TiO_2 film under visible light treating dodecyl-benzenesulfonate. These facts show that the optimum maybe influenced by the intrinsic properties of the removed contaminant.

As Couselo *et al.* (2008) described W may improve the activity of TiO_2 photocatalysts and may allow maintaining the surface area during the thermal treatment.[342] The surface area was quite similar in all W doped samples, only slightly lower in the 16% W-TiO_2 and higher than in the non-doped samples (Table 4.2). The optimum concentration of W does not only depend on the calcination temperature, but also on the preparation method of the catalyst, and on the use of the catalyst in the photocatalytic treatment [12, 380, 381].

Although there is increased activity shown up until 8% W-TiO_2 and a reduction is seen at 16-W-TiO_2, there is a lower % removal achieved at 900ºC compared to at 800ºC (Figure 4.8(b)). This is likely due to lower % of the anatase phase being present at 900ºC (Figure 4.4). As with catalysts synthesized at calcination temperature of 800ºC, there is a significant decrease in efficiency for 16-W-TiO_2 when compared with lower W-TiO_2 concentrations. There is also an associated reduction in 1,4-dioxane degradation

efficiency due to the decrease of anatase phase at higher temperatures (Figures 4.4 and 4.8).

4.2.5 Degradation of 1,4-dioxane and Reaction Intermediate Decomposition

Formic acid was found to be the main by-product formed during the degradation of 1,4-dioxane. In fact, it was continuously produced during the whole oxidation treatment. In addition, traces of methoxyacetic and glycolic acids were only detected at the end of the process (Figure 4.9). Oxalic and acetic acids were not found in the analysis. Similar results were described in previous studies of the degradation of 1,4 dioxane by photocatalysis.[280, 281, 382, 383] 1,4-dioxane is presumably adsorbed on the catalyst[383] and the attack of •OH generates the hydroxylation of 1,4-dioxane producing 1,4-dioxan-α-oxyl radical.[280, 281, 382] The •OH may attack the different α-C positions of the molecule producing different radicals being the precursor of further oxidation products and the following ring opening reactions (see Figure 4.10).[280, 281, 382, 383] The following intermediates could be desorbed or adsorbed on the catalyst [383] to be subsequently oxidized by •OH and the different radicals produced during the oxidation.

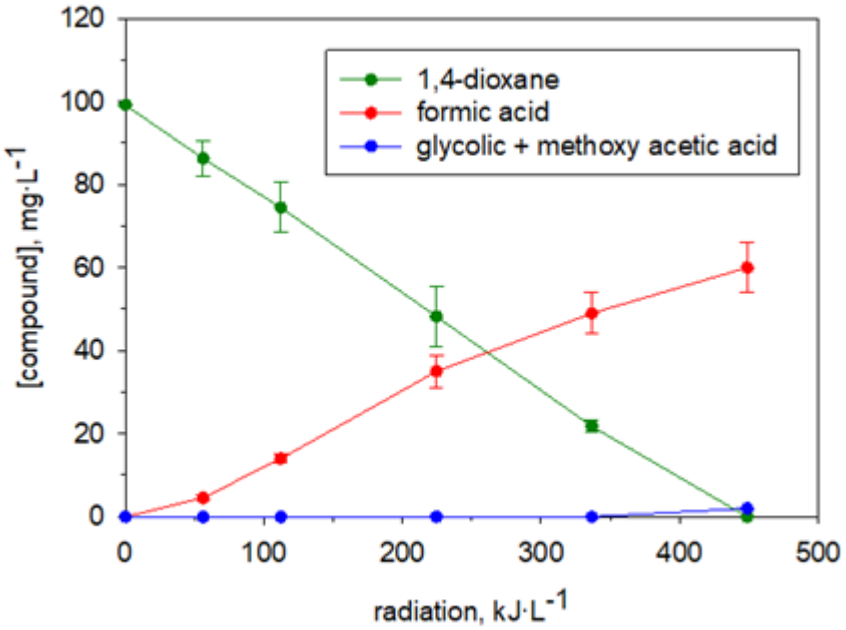

Figure 4.9: Degradation of 1,4-dioxane and production of formic acid and methoxy acetic acid during its photocatalytic treatment using W-TiO_2 (2% W-TiO_2 at 800°C).

The oxidation of different 1,4-dioxane-oxyl radicals could follow two main routes (Figure 4.10): (A) by ΔC-C splitting at the α-C position; and (B) by H abstraction from the α′-C position followed by fragmentation. In route A, the oxidative ring mechanism by the alkyl

peroxyl radical produces 1,2 ethanediol diformate (EDF), 1,2 ethanediol monoformate (EMF), and formaldehyde,[384] which is further oxidized to formic acid; therefore explaining the high concentrations of this compound found during the analysis.[385] In addition, glycolic acid may have been produced from EDF and EMF,[382, 383, 386] however in this study it was only present in very low concentrations (Figure 4.9). Although further oxidation can lead to the formation of oxalic acid,[280, 281] the latter was not found present during analysis. In route B, the oxidation of the C-centred radical produced formaldehyde and formic acid.[280, 281, 382] This could explain the high measured concentrations of these compounds and the continuous production of formic acid. The subsequent production of methoxyacetic acid and acetic acid was not supported due to low concentrations of these acids in the reaction solution as measured in this study. As a result, the mechanism based on the production of methoxyacetaldehyde may be considered negligible.[280, 281]

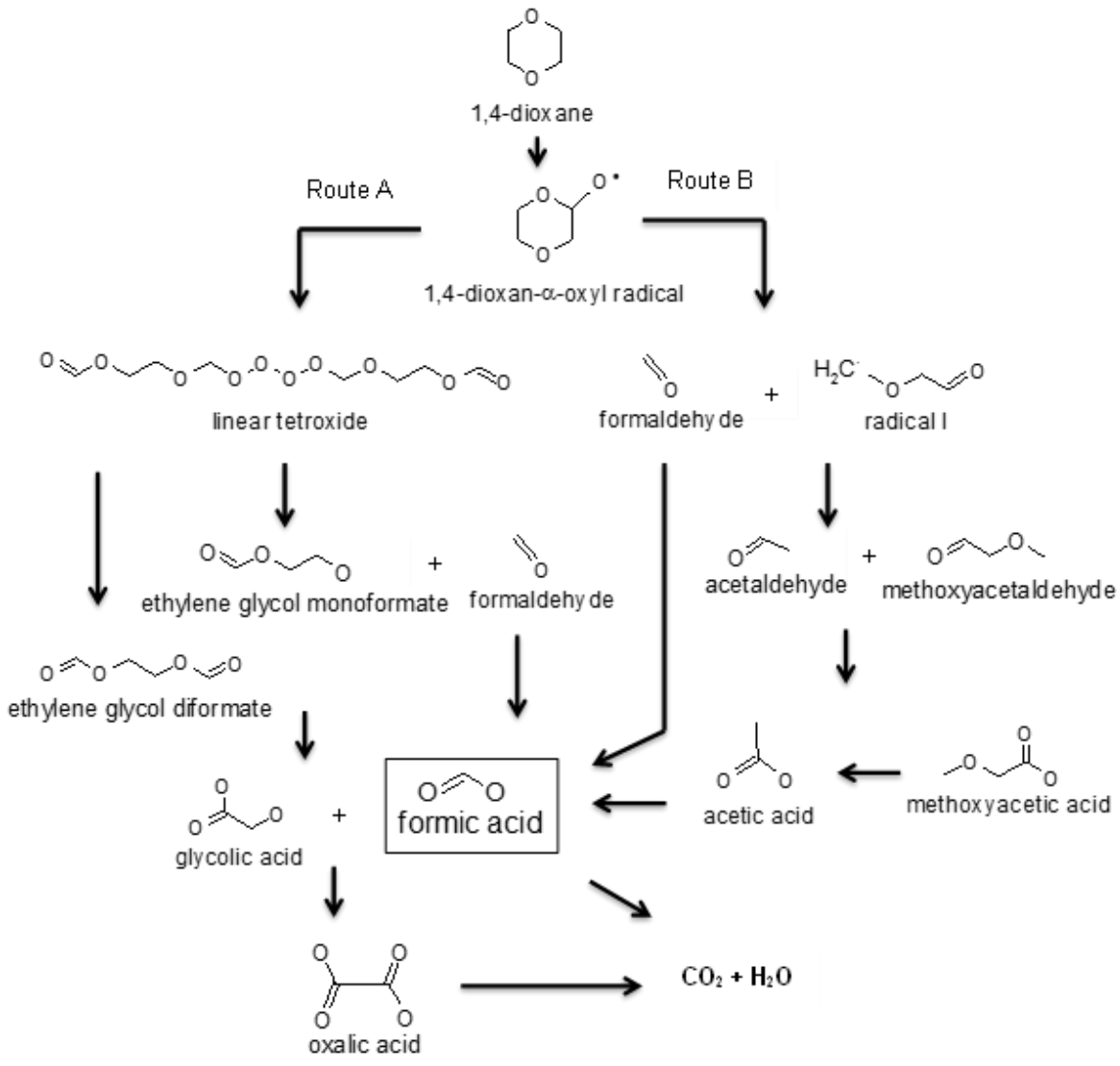

Figure 4.10: Degradation routes of 1,4-dioxane treated by AOPs**.**

4.2.6 Discussion of Results

The addition of tungsten to the TiO_2 matrix delayed ART temperature but TiO_2 also deferred the phase transition of WO_3. Bamwenda and Arakawa (2001),[347] concluded that monoclinic WO_3 is stable from room temperature and tungsten suboxides such as understoichiometric WO_x (x = 0.9-1) form from 900°C. There are no W peaks present in the Raman spectra for 2% W-TiO_2 despite being present in XRD, which is observed as a single peak of low intensity rather than the characteristic triplicate peak, normally between 24-25°. This is likely due to WO_3 only being present at low concentrations. XPS measurements further confirmed doping of TiO_2 with WO_3. W-TiO_2 catalysts calcined at 500°C exhibited an O *1s* trend similar to undoped materials calcined at a range of temperatures, suggesting that tungsten was present as surface species. As the calcination temperature was further elevated to 800°C the O *1s* peak assigned to WO_3 grew in intensity, indicating substitution of Ti^{4+} with W^{6+}, demonstrating incorporation of tungsten oxide species within the TiO_2 lattice. The particle size of all samples was also examined using XRD; this showed that the use of tungsten as dopant changed the particle size of TiO_2. It should be noted that 0% W-TiO_2 had a particle size of 13.33 nm at 500°C and 41.30 nm at 1000°C while the particle size of the W-TiO_2 ranged from 11.01-12.03 nm at 500°C to 37.35-39.46 nm at 1000°C. The inclusion of tungsten increases the surface area of TiO_2 when compared with the control (0% W-TiO_2). The surface area for 0-W-TiO_2 was ~24.3 m^2/g while surface area for the doped samples ranged between ~33.4-56.0 m^2/g. There was very little variation of surface area in the doped samples when calcined at 800°C and 900°C.

In line with improved temperature stability, the 2%, 4% and 8% W-TiO_2 catalysts also demonstrated enhanced photocatalytic removal of 1,4-dioxane. These materials when calcined at 800°C showed complete removal of 1,4-dioxane. When calcined at 900°C, only 4% W-TiO_2 and 8% W-TiO_2 had a higher % removal than that of 0% W-TiO_2 at 500°C, with 8% W-TiO_2 at 900°C having the larger % of 1,4-dioxane removed. From these results, it can be concluded that 8% W-TiO_2 is also the optimum for photocatalysis. The by-products of 1,4-dioxane were also monitored during the photocatalytic reactions. This study observed that formic acid was the main by-product throughout the reaction; this was in line with previous studies. Methoxyacetic acid and glycolic acid were also detected, though these were only found in traces amounts.

Inhibition of ART in TiO_2 and the observation of enhanced photocatalytic efficiency due to W doping can be attributed to the structure-preserving effects of the acidic semiconductor catalyst, preserving a full anatase composition up to calcination at 800°C. Highly crystalline materials with high intrinsic photoactivity would thus be obtained. [387, 388] Theoretically, 3.2 mol. % of WO_3 is required to cover the surface of P25. [337] The formation of WO_3 microcrystals has however been observed at W/Ti ratio ≥8% [389], yet other reports fail to confirm the presence of a WO_3 phases up to 20 wt. %. [390] Previous findings such as these have implied that the nature of tungsten precursor and extent of tungsten loading determine the possibility of monolayer coverage and lattice doping. However, realizations of the current study suggest that calcination temperature rather than precursor parameters dictate W-TiO_2 interactions and the doped catalysts capability to enhance photocatalytic response.[362, 389, 391] Additionally, tungsten doping also reduces anatase particle dimensions (Table 4.1), which generally enhances the photocatalytic degradation rate when expressed per unit mass of catalyst. [349]

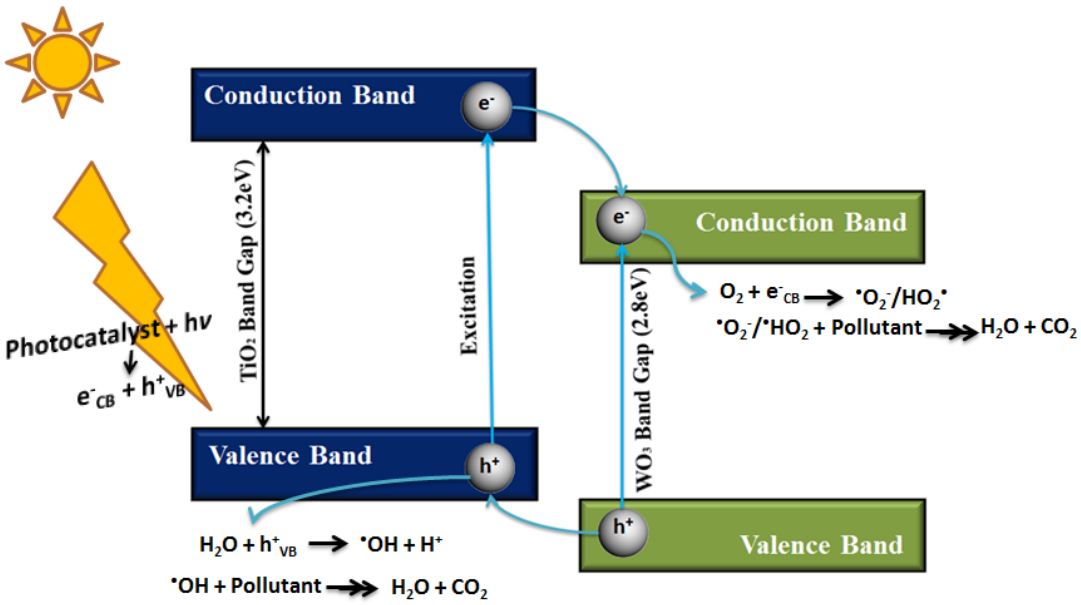

Figure 4.11: The proposed photocatalytic mechanism between the nanocomposites of TiO_2 and WO_3.[349]

The increased photocatalytic degradation of 1,4-dioxane could also be attributed to the WO_3 acting as a heterojunction with TiO_2; this occurs due to the transfer of 'excited' electrons in TiO_2 to WO_3. [349, 392] The band gap of TiO_2 is 3.2 eV and WO_3 is 2.8 eV, as a result the CB and VB of WO_3 sit lower than those of TiO_2. [392, 393] The photocatalytic mechanism between TiO_2 and WO_3 is shown in Figure 4.11,[394, 395] which shows that the

'excited' electrons in the CB of TiO_2 are transferred to the CB of WO_3. In contrast, the photogenerated holes transfer from the VB of WO_3 to the VB of TiO_2. This causes a resulting increase in the separation charge efficiency and the resulting increased photocatalytic degradation of 1,4-dioxane.[394]

4.3 Conclusions

The current study showed that there was a significant improvement in the transition temperature of TiO_2 when tungsten is included as a dopant. There was 22.9% anatase in 0% W-TiO_2 at 700°C and 100% rutile at 800°C. All W-TiO_2 samples remained 100% up to a temperature as high as 800°C. The optimum sample in regard to anatase phase present (8% W-TiO_2) contained 26% anatase at 950°C. The 2% W-TiO_2 sample was 100% rutile at 950°C while the remaining doped samples were not 100% rutile until 1000°C. XRD and Raman also showed the presence of WO_3 peaks.

Photocatalytic studies showed a 100% removal of 1,4-dioxane for 2%, 4% and 8% W-TiO_2 at 800°C. For 4% W-TiO_2 and 8% W-TiO_2 at 900°C, there was approximately 70-80% removal of 1,4-dioxane with 8-W-TiO_2 showing a slightly higher rate of removal than 4% W-TiO_2. From the BET surface area results it can be concluded that the surface area is not the most critical factor in the photocatalytic activity for these materials for the range of surface areas obtained. There is also a significant difference in % removal for 16% W-TiO_2 at 900°C when compared to 4% W-TiO_2 and 8%W-TiO_2 at 900°C.

Due to its highest % anatase content at 950°C and highest % removal of 1,4-dioxane achieved at 900°C, 8% W-TiO_2 is considered the optimum sample for both photocatalysis and phase transition temperature. The % anatase present in the samples impacts the photocatalytic activity; the difference can be seen when comparing the 4% W-TiO_2 and 8% W-TiO_2 samples at 800°C (both 100% anatase) and 900°C (both mixed phases). The tungsten concentration present in the samples is also an impacting factor on photocatalytic activity; the difference can be seen when comparing the 2%, 4%, 8% and 16% W-TiO_2 samples calcined at 800°C.

The major degradation product was identified as formic acid. However, traces of methoxyacetic and glycolic acids were also identified. The enhanced photocatalytic activity for the degradation of 1,4-dioxane is attributed to the formation of nanocomposites of WO_3 with TiO_2.

Chapter 5 - Increased Photocatalytic Degradation of 1,4-dioxane with Boron Nitride Doped TiO_2

5.1 Introduction

As mentioned in Section 1.1 and 1.4, there has been research into chemically modifying/doping TiO_2 for the past 50 years to improve its ART and photocatalytic activity. [129, 203, 336, 396-399] These include non-metal dopants (such as carbon in Chapter 3) and metal dopants (such as tungsten in Chapter 4). As mentioned in Section 3.1, impurities can form at elevated temperatures when doping with metals which can reduce ART and photocatalysis. As a result, many studies focus on non-metal doping of TiO_2.[299, 300]

Boron nitride (BN) doping of TiO_2 has also been examined as a method of anion doping in recent years.[400-404] For example Fu *et al.* used the ball milling method to prepare hexagonal-BN (*h*BN)/TiO_2 composites and examined the photodegradation of rhodamine B and methylene blue.[403] The study examined the effect of various wt. % doping and ball milling times. They found that the optimum sample was 0.5 wt. % *h*BN which had been milled for 30 min. This photocatalyst showed a 15 times higher rate of removal for Rh B and an increase of a factor of 8 in the removal of methylene blue.[403] Lui *et al.* (2017), who examined porous BN/TiO_2 hybrid nanosheets for photocatalytic degradation of Rhodamine B and phenol under simulated solar and visible light.[401] The study found that 38 wt.% porous BN/TiO_2 hybrid nanosheets exhibited visible light photodegradation of both phenol and Rh B.[401] In the same year, Singh *et al.* (2017) examined an ice bath method to synthesis BN-TiO_2 photocatalyst with a large pore size and surface area.[405] The study found the BN doped TiO_2 showed a 79% removal of methylene blue after 200min under visible light, while bare TiO_2 removed on 32% of the methylene blue. They stated that BN doped TiO_2 could be used for practical environmental purification.[405] However, to date there has yet to be a comprehensive systematic study on the effect of various concentrations of BN calcined at numerous temperatures has on ART and photocatalytic activity of TiO_2.

The aim of this investigation was to examine the impact that BN doping has on ART and the photocatalytic activity of TiO_2. BN was doped at five different concentrations (0% BN- TiO_2, 2% BN- TiO_2, 4% BN- TiO_2, 8% BN- TiO_2 and 16% BN-TiO_2) and were calcined at 500°C, 600°C, 650°C and 700°C. They were characterised using XRD, Raman

Spectroscopy and XPS. The ability of the samples to act as a photocatalyst was determined by examining the photodegradation of 1,4-dioxane.

5.2 Results and Discussion

5.2.1 Phase Composition of Titania and BN Doped Nanomaterials

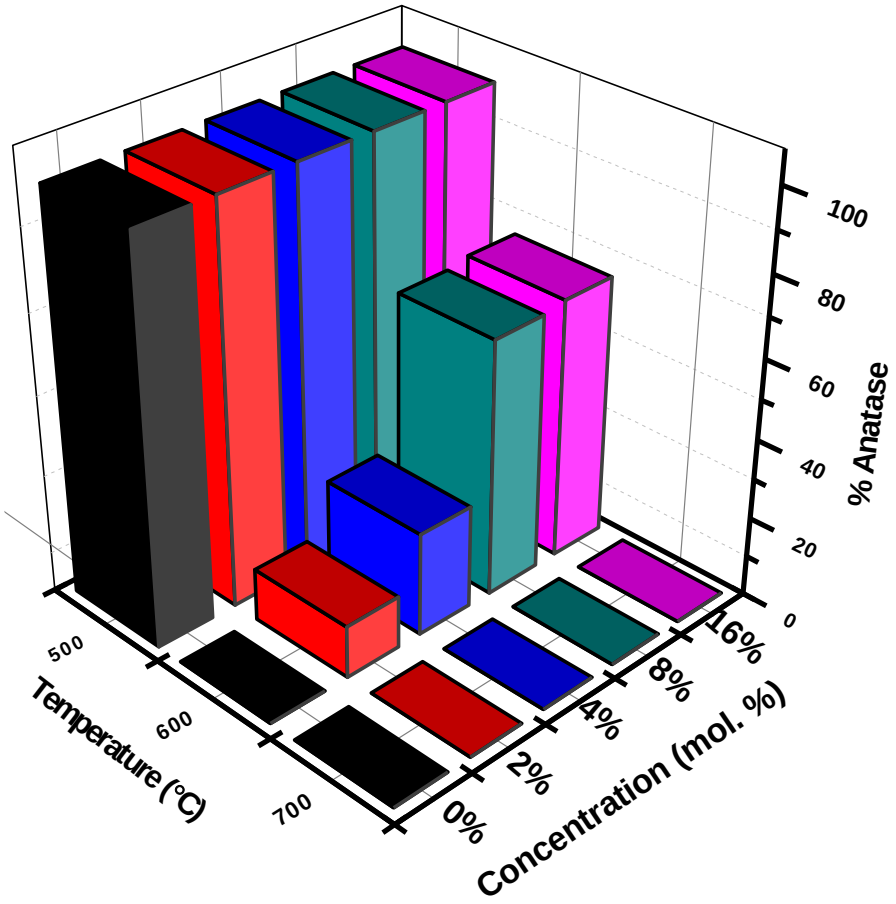

Figure 5.1: Anatase present (in %) of 0%, 2%, 4%, 8% and 16% BN-TiO_2 calcined at 500-700°C.

XRD was used in the determination of the phase of each sample and for this the impact on the transition temperature can also be concluded. The main anatase (25°) and rutile (27°) peaks were used with Spurr equation (eq. 2.1) when examining mixed samples to denote the % of anatase/rutile present (Figure 5.1 and 5.2). Additionally, Figure 5.2 the presence of bulk boron nitride peaks, with the peak at 26° indicating the graphite-like *h*BN structure.[406-409] All samples were 100% anatase when calcined up to 500°C. At 600°C, 0% BN-TiO_2 had converted into 100% rutile, while the all doped samples remained mixed phased samples (2%, 4%, 8% and 16% BN contained 13.2%, 25.9%, 64.4% and 65.5% anatase respectively). All samples consisted of 100% rutile phase when calcined at 650°C and 700°C (Figure 5.1).

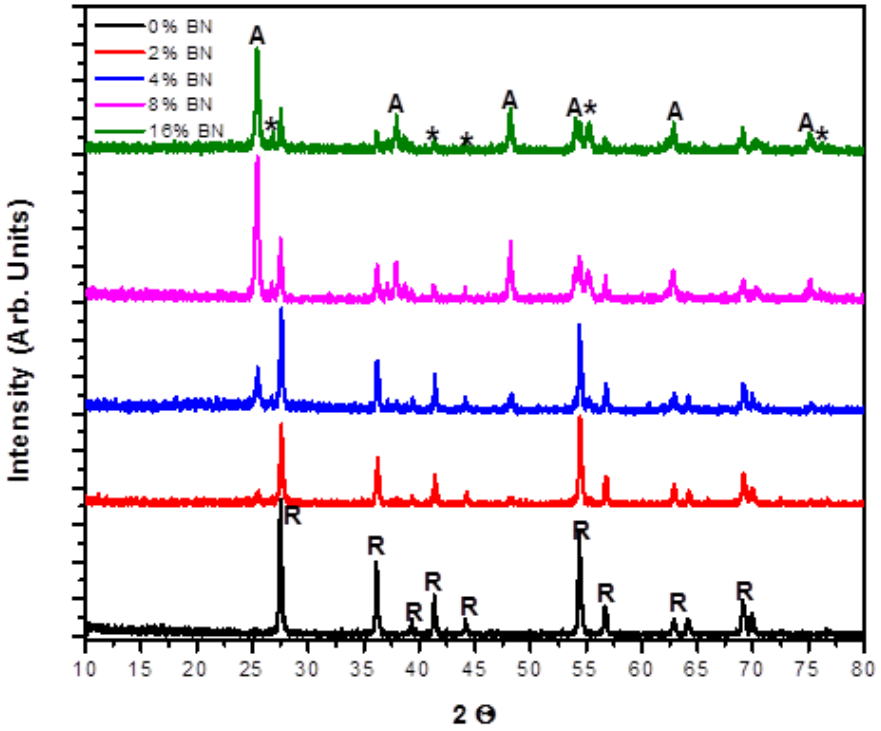

Figure 5.2: XRD of all BN-TiO_2 samples calcined at 600°C. Where A = anatase; R = rutile and * = BN.

In addition to phase composition, XRD was also used to determine the particle size of all samples. The crystalline size of all samples examined is tabulated in Table 5.1, there is some variation across all temperatures and doping concentrations.

Table 5.1: Crystalline size (nm) of all BN-TiO_2 samples calcined at 500, 600, 650 and 700°C. Where 'A' is indicative of the anatase phase and 'R' indicates the rutile phase.

	0% BN	**2% BN**	**4% BN**	**8% BN**	**16% BN**
500°C	9.60 (A)	10.86 (A)	9.28 (A)	9.09 (A)	10.57 (A)
600°C	29.48 (R)	21.20 (A) 24.67 (R)	16.28 (A) 28.46 (R)	22.08 (A) 30.82 (R)	21.78 (A) 29.29 (R)
650°C	33.97 (R)	22.20 (R)	27.05 (R)	27.21 (R)	31.63 (R)
700°C	31.61 (R)	27.07 (R)	30.53 (R)	33.89 (R)	32.17 (R)

When the samples were calcined at 500°C, the smallest particle size was 9.09nm which is seen from 8% BN while 2% BN showed the largest particle size at this temperature (10.86nm.) The 4% BN sample showed the lowest anatase particle size and 2% BN displayed the lowest rutile particle size when calcined at 650°C, 16.28nm and 24.67nm respectively. Once calcined at 650°C and 700°C, 2% BN showed the lowest particle size.

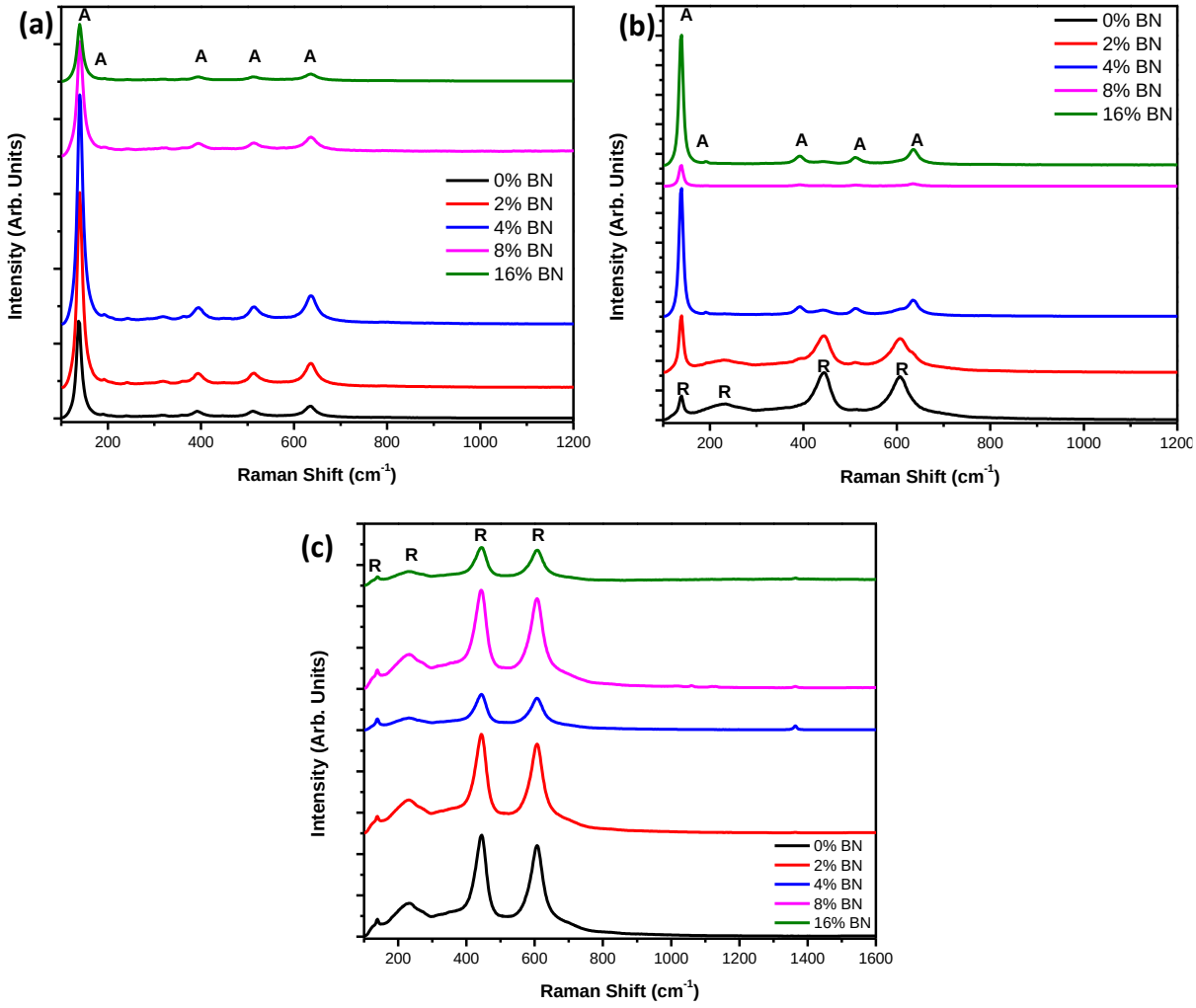

Figure 5.3: Raman spectra for all samples calcined at (a) 500°C, (b) 600°C and (c) 700°C. Where A = anatase and R = rutile.

Raman spectroscopy was used as a complementary tool to XRD and confirmed the phase composition of the titania samples. Figure 5.3 (a) shows peaks at 147, 197, 396, 516 and 638 cm^{-1} which relate to the *A1g, 2B1g* and *3Eg* active modes and are indicative of the anatase phase.[6, 121, 295, 303-305] Spectra showing the presence of anatase and rutile peaks are indicative of mixed phased samples. The intensity of theses peaks is dependent on the % of each phases present, this can be seen in Figure 5.3 (b). Figure 5.3 (c) shows peaks at 144, 238, 446, 612 and 827 cm-1 which relate to the *A1g*, *B1g*, *B2g* and *3Eg* active modes and indicates the presence of the rutile phase.[6, 121, 295, 303-305] Very low intensity BN peaks can also be seen in Figure 5.3 (c).

5.2.2 Surface Chemical/Elemental Composition of Nanomaterials

XPS analysis was completed to determine the chemical composition and oxidation states of elements that were found on or close to the surface of the undoped and BN-doped TiO_2

calcined at 500°C, 600°C and 700°C. The elements found present in the samples were Carbon, Boron, Nitrogen, Oxygen and Titanium; the atomic (at.) % varied depending on the samples (see Table 5.2). Analysis of the spectra for 0% BN-TiO_2 showed the presence of N *1s* peaks, however these N *1s* peaks are considered as contamination as the atomic % for all three samples is under 0.41% (Table 5.2). The 0% and 16% BN-TiO_2 spectra and data were used as examples for deconvoluted peaks.

Table 5.2: XPS results showing the at. % for all samples calcined at 500°C, 600°C and 700°C

	Temp.	**0% BN**	**2% BN**	**4% BN**	**8% BN**	**16% BN**
B1s	500°C	N/A	2.51%	3.47%	9.84%	20.77%
	600°C		3.56%	4.51%	13.10%	19.32%
	700°C		3.94%	6.23%	14.61%	26.98%
C1s	500°C	7.33%	6.87%	7.47%	8.02%	7.18%
	600°C	11.80%	13.02%	10.97%	11.88%	9.96%
	700°C	14.24%	8.69%	12.85%	10.64%	10.35%
N1s	500°C	0.41%	2.51%	2.96%	8.16%	17.29%
	600°C	0.40%	2.75%	3.54%	10.75%	15.66%
	700°C	0.20%	2.58%	3.77%	10.81%	20.91%
Ti2p	500°C	31.02%	29.50%	28.69%	24.34%	18.03%
	600°C	28.96%	26.74%	26.93%	21.04%	18.22%
	700°C	28.25%	27.87%	24.80%	20.34%	12.31%
O1s	500°C	61.23%	58.42%	57.41%	49.31%	36.85%
	600°C	58.83%	53.94%	54.93%	43.23%	36.85%
	700°C	57.30%	56.92%	52.80%	43.60%	29.46%

As it can be seen in Table 5.2, the at. % of B *1s* and N *1s* increases in the doped samples as the concentration of BN increases. However, the at. % of boron remains higher than nitrogen in all doped samples. In contrast, the at. % of Ti *2p* and O *1s* present decreases as the concentration of BN increases. The amount of carbon present various throughout all twelve samples, from 6.87-14.24 at. %.

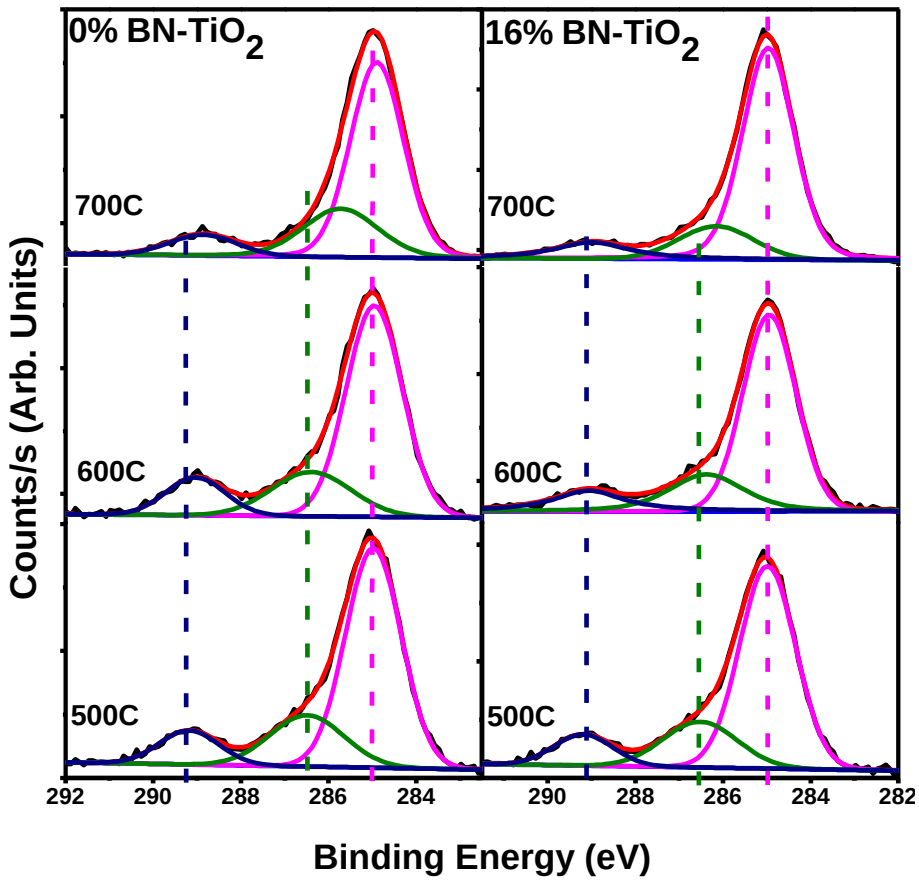

Figure 5.4: Deconvoluted XPS spectra of C *1s* for 0% and 16% BN-TiO_2 calcined at 500°C, 600°C and 700°C.

C *1s* peaks were present in all samples at all temperatures. The eV for all C *1s* peaks remained largely unchanged. Peaks at ~285 eV and ~288-289 eV were initially seen (Figure 5.4). However, after deconvolution of the spectra showed a third peak at ~286 eV (Figure 5.4). The peaks at 285-286 eV are attributed to adventitious carbon (C-C, C=C and/or C-H bonds) which can arise due to contamination during synthesis/calcination and/or the standard used for XPS analysis.[19, 121, 295] There were also C *1s* peaks present for binding with oxygen, these peaks fall between 287 and 289 eV, which are for C-O and C=O respectively.[120, 121, 150, 308, 309] These peaks can also be considered due to surface contamination. This can be confirmed by the lack of the characteristic peak for Ti-C (281.5 eV) being absent.[6, 121, 306] Any surface of samples exposed to the atmosphere will contain contamination from air, including carbon. As XPS is a surface analysis method, there will always be a C *1s* peak present. Additionally, the C *1s* peak is used as a charge correction reference for energy calibration purposes. These account for C *1s* peaks found in the BN-TiO_2 samples.

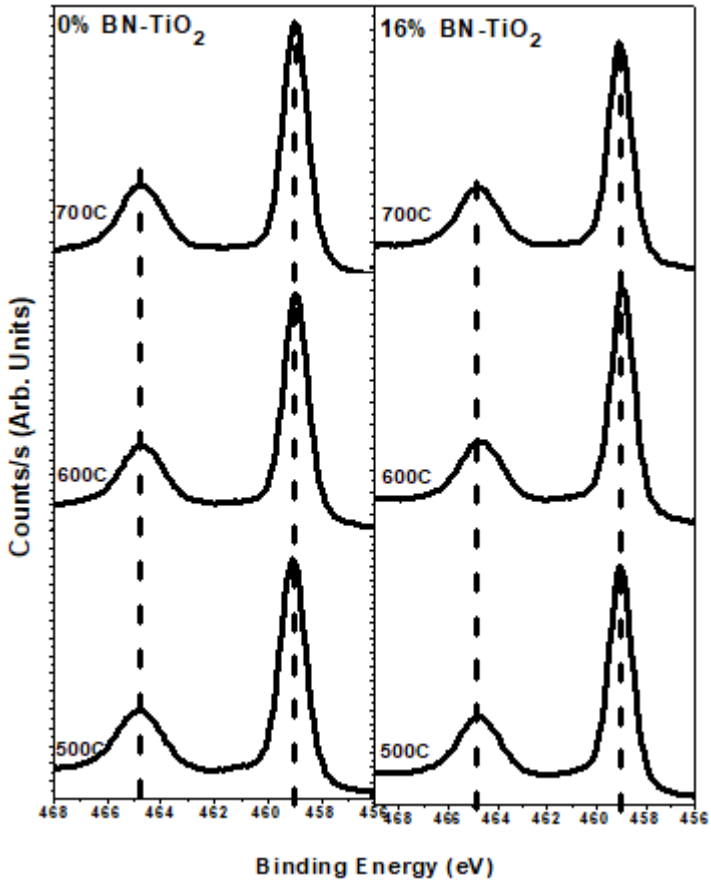

Figure 5.5: XPS spectra of Ti *2p* for 0% and 16% BN-TiO_2 calcined at 500°C, 600°C and 700°C

There is a very slight decrease in the O *1s* and Ti *2p* $_{3/2}$ (Ti-O) as the temperature increases (Figures 5.5 and 5.6). This decrease in the O *1s* shows that the samples are oxygen rich and the formation of oxygen vacancies has begun when the temperature increases.[19] The minor decrease in the Ti *2p* $_{3/2}$ peaks further confirms that the oxygen vacancies have begun to form.[19] A change in the Ti *2p* $_{3/2}$ peak can also determine the conversion of Ti^{4+} to Ti^{3+}, however the peaks in Figure 5.5 only shows a 0.2 eV indicating that Ti^{4+} has not fully converted to Ti^{3+}.[19] This incomplete conversion is due to Ti^{4+} being favoured as it is more stable than Ti^{3+}. The changes in the O *1s* and Ti *2p* $_{3/2}$ is consistent with the transformation of anatase to the rutile phase. Additionally, there is also Ti *2p* $_{1/2}$ peaks (458.98-459.08 eV) present in all samples.[47, 301, 305, 307] The Ti *2p* $_{1/2}$ peaks indicates Ti in a tetravalent state.[301, 307]

The second dominant peak in the deconvoluted O *1s* spectra is at 531.48-531.97 eV (Figure 5.6). As seen in Figure 5.6, these peaks in size as the temperature increases from 500°C-700°C for the 16% BN-TiO_2. These peaks can be indicative of the O-Ti bond within TiO_2 or of O-H binding.[405]

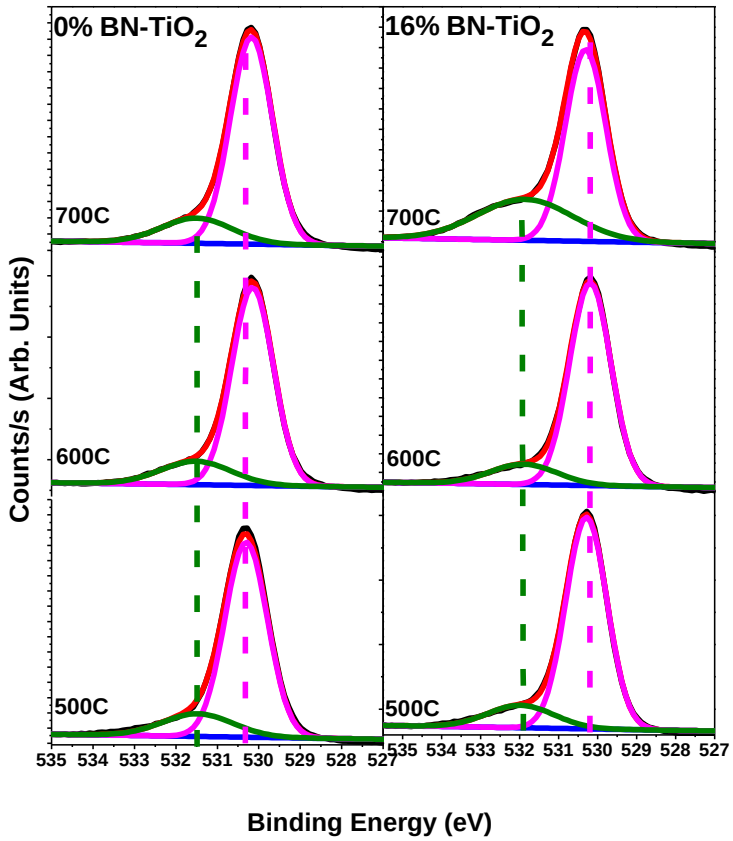

Figure 5.6: Deconvoluted XPS spectra of O *1s* for 0% and 16% BN-TiO_2 calcined at 500°C, 600°C and 700°C

The doped samples (2%-16% BN-TiO_2) also contained B *1s* and N *1s* peaks, the spectra for 16% BN-TiO_2 can be seen in Figure 5.7. The deconvoluted B *1s* spectra (Figure 5.7) shows the presence of two peaks, the first at 190.68-190.78 eV and second at 191.36-191.83 eV. The more dominant peaks at ~190 eV show the presence of elemental boron when examining boron doped TiO_2.[410] The second peak at ~191 eV has a significantly lower counts/s and indicates the presence of doping with B^{3+} ions in interstitial modes.[410] Liu *et al.* (2017) suggests that this peak could also be a result of "*edge/interfacial boron dangling bonds*" which are linked with -OH.[401] It is important to note that the XPS analysis does not show the presence of Ti-B bonds (187 eV) or boron being incorporated into TiO_2 and its environment (Ti-B-O at 192 eV).[411] Finally, the N *1s* peaks that are present in the 16% BN-TiO_2 range from 398.28-398.48 eV, which relate to the B-N bonding and refer to the trigonal units of BN layers (BN3 and NB3).[401] The peak at 396 eV which indicates N-Ti-N environment and is suggestive of lattice bonding is not present in this study.[300]

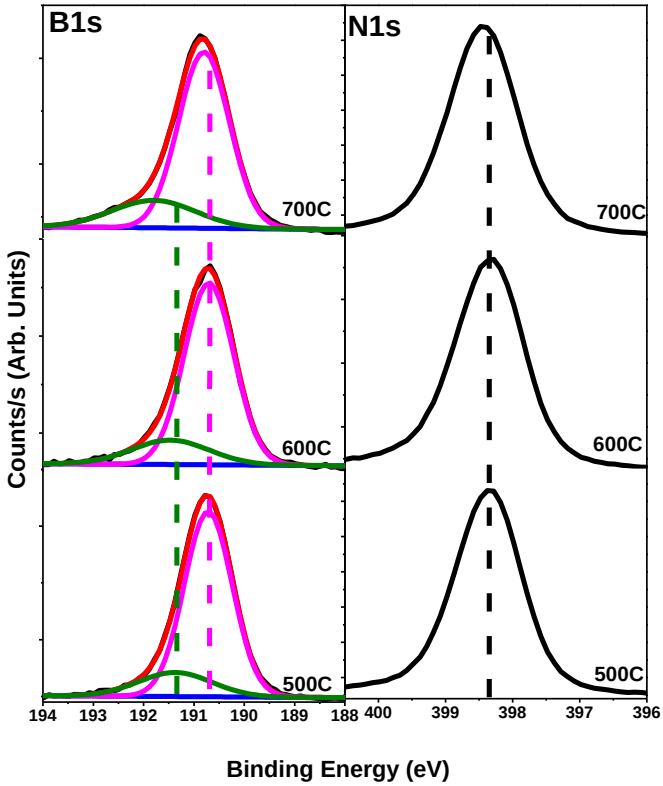

Figure 5.7: Deconvoluted XPS spectra of B *1s* for 16% BN-TiO_2 calcined at 500°C, 600°C and 700°C; and XPS spectra of N *1s* for 16% BN-TiO_2 calcined at 500°C, 600°C and 700°C.

5.2.3 Photocatalytic Degradation of 1,4-dioxane

The photocatalytic activity of 16% BN-TiO_2 materials was determined by examining the photodegradation of 1,4-dioxane and was compared to 0% BN-TiO_2. The reduction of 1,4-dioxane under solar light without any photocatalyst present (TiO_2 = 0) was also examined, this showed 15.8% removal (Figure 5.8). At 500°C and 700°C, the 16% BN-TiO_2 photocatalyts showed a removal rate of 86.3% and 73.4%, repectively (Figure 5.8). However, the undoped TiO_2 calcined at 500°C (100% anatase) showed only 60.5% removal (Figure 5.8), while the sample showed a 17.9% removal of 1,4-dioxane when calcined at 700°C (100% rutile). Therefore, the 16% BN-TiO_2 at given temperatures showed improvements in the photocatalytic activity compared the 0% BN samples.

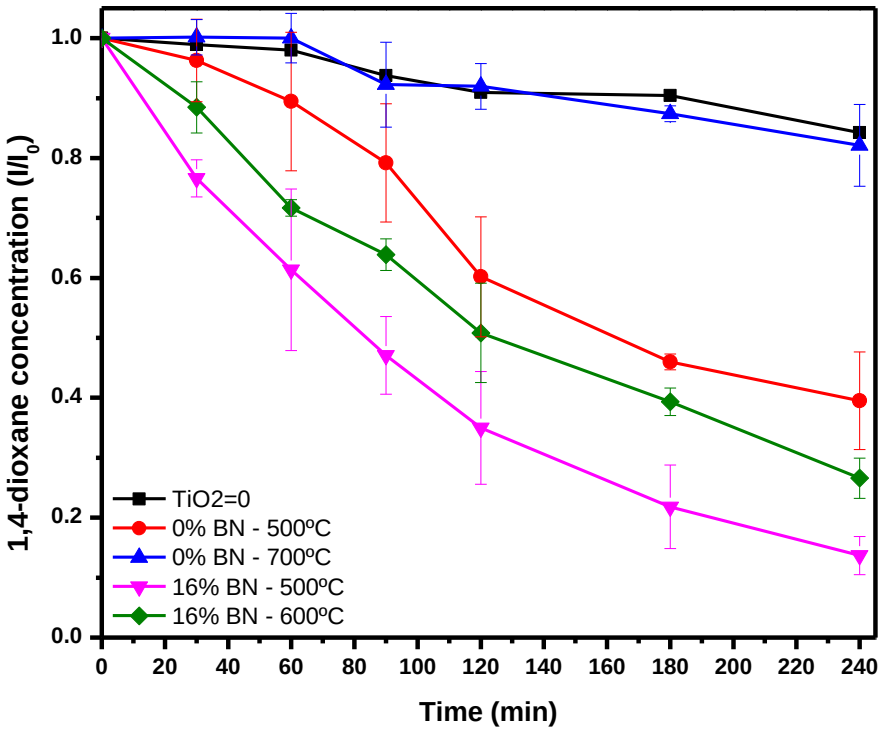

Figure 5.8: Photocatalysis of 1,4-dioxane with undoped and BN doped titania.

5.2.4 Discussion of Results

Traditionally ART is considered to occur between 600-700°C. The inclusion of BN did not bring the transition temperature above this range. However, when the doped samples were compared with the control (0% BN) some improvement could be seen. The control is 100% rutile from 600°C, while the doped samples were mixed phased sample at this temperature and only converted to 100% rutile at 650°C. In addition to TiO_2 peaks, XRD also showed the presence of hexagonal BN. This structure was determined based on its characteristic peak at 26°, which the other structures do not have. XRD was also used in calculating the particle size of the nanomaterials. The particle size increased as the temperature increased, which occurs due to the formation of rutile. Raman spectroscopy further confirmed the TiO_2 phase composition, very small BN peaks could also be seen in some of the Raman spectra. Due to Ti-B or Ti-B-O not being present in the XPS analysis, it can be concluded that the BN doped on the surface of the TiO_2 and it has not been doped within the TiO_2 crystal lattice structure. The photocatalytic activity of the 0% and 16% BN-TiO_2 were evaluated by examining the photocatalytic oxidation of 1,4-dioxane. The 16% BN-TiO_2 at 500°C and 700°C both showed a significant improvement compared to the 0% BN-TiO_2 at 500°C. When comparing the two samples at 700°C a substantial difference in the % removal can be seen (Figure 5.8).

XRD showed that the boron nitride present is in the hexagonal sheets, which are stacked on top of each other to form a layered structure. This layered structure is similar to the structure found in graphite (Figure 5.9).

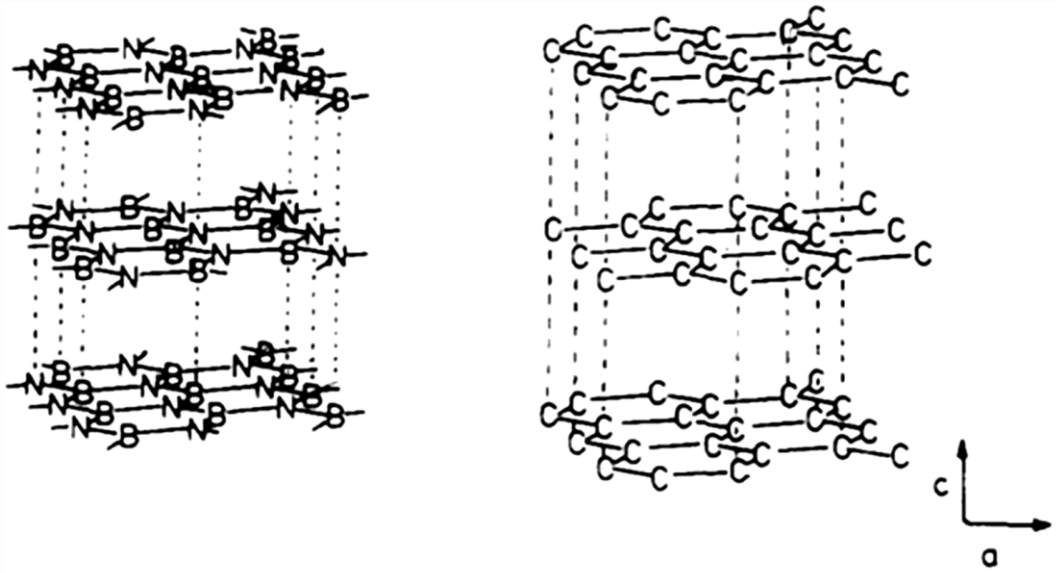

Figure 5.9: Comparison of graphite and graphite-like *h*BN.[412] Reprinted with permission from *Chem. Rev.* 1990, 90, 1, 73-91. Copyright 1990 American Chemical Society.

Lui *et al.* (2017) and Singh *et al.* (2017) propose that the TiO_2 nanoparticles are bonded onto the *h*BN sheets and suggest that this is done *via* a B-O-Ti bond.[401, 405] Sheng e*t al.* further confirmed this during their examination of the BN-TiO_2 nanocomposites for the photocatalytic degradation of Rh B and Methylene Blue (MB).[413] Figure 5.10 shows the proposed photocatalytic mechanism that occurs between *h*BN and TiO_2. The photogenerated electrons transfer across the B-O-Ti bond from the TiO_2 CB to BN, seen in Figure 5.10.[401, 405] The electrons are not in a fixed position within the π-π conjugate system of BN.[405] As a result of this, there is a slower rate of recombination of the electron-hole pair. This results in an increased rate of photocatalysis for TiO_2.[405]

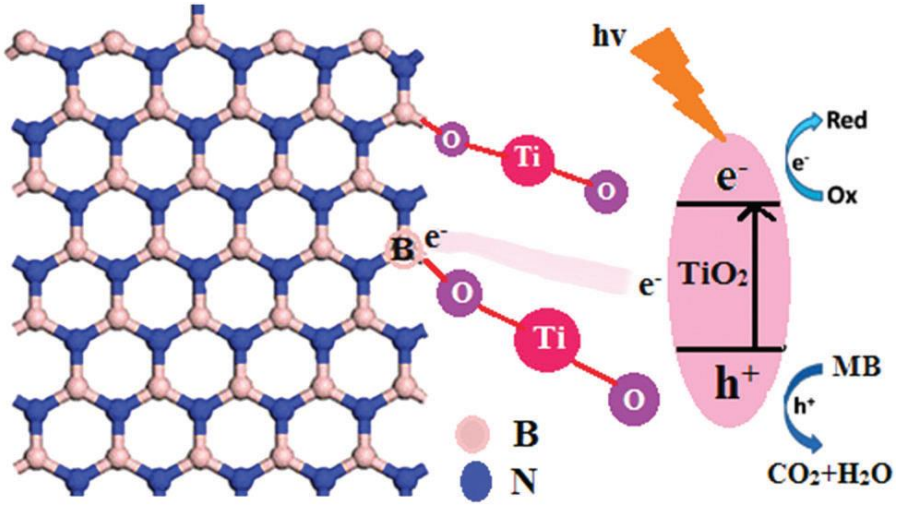

Figure 5.10: Proposed photocatalytic mechanism of BN-TiO_2 nanocomposites.[405] *New J. Chem.*, 2017,41, 11640-11646 - Reproduced by permission of The Royal Society of Chemistry

Li *et al.* (2016) examined nano-graphite doping of TiO_2. This composite was used to fabricate a photoelectrode and its ability to photodegrade phenol.[414] Figure 5.11 shows the schematic diagram of photocatalytic mechanism for the composites. Similar to the mechanism suggested in Figure 5.10, the TiO_2 is incorporated onto the graphite sheets and the transfer of electron occurs *via* a Ti-O-C bond.[414] The diagram of the mechanism in the study by Li *et al.* (2016) shows that the TiO_2 is included onto all layers of the graphite and not just the top layer (Figure 5.11).[414] Due to the similarities in the graphite and graphite-like *h*BN structures (Figure 5.9), it can be suggested that TiO_2 could also be included onto all layers of the graphite-like *h*BN and not just the top layer.

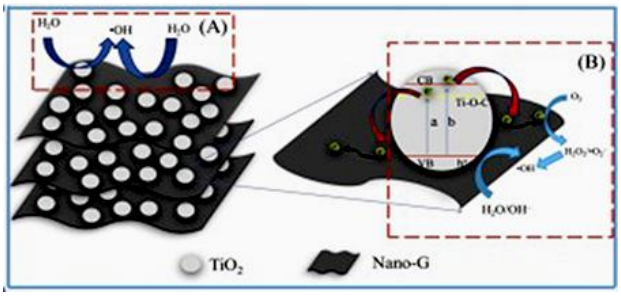

Figure 5.11: Photocatalytic mechanism of nano-graphite and TiO_2 composite. Where (A) shows the electrocatalytic activity and (B) shows photocatalytic activity.[414] Reprinted from *J. Hazard Mater.*, Vol. 315, Dong *et al.*, Preparation and characterization of Nano-graphite/TiO_2 composite photoelectrode for photoelectrocatalytic degradation of hazardous pollutant, pp 1-10, Copyright 2016, with permission from Elsevier.

5.3 Conclusions

The current Chapter showed that, the BN doped TiO_2 samples exhibited an improvement in the % anatase present at 600°C compared to 0% BN-TiO_2. From 600°C, 0% BN-TiO_2 had transition into 100% rutile while all doped samples comprised of both anatase and rutile phases. The optimum sample in regard to anatase phase present (16% BN-TiO_2) contained 65.5% at 600°C. XPS determined that the BN was doped onto the surface of the TiO_2. When examining the photocatalytic degradation 1,4-dioxane, 16% BN-TiO_2 at 500°C (100% anatase) showed over a 25% improvement in the removal rate compared to 0% BN-TiO_2 (86.3% and 60.5% removal respectively). In conclusion, the inclusion of BN increases the transition temperature and photocatalytic activity in comparison to bare TiO_2.

Chapter 6 – Conclusions and Future Work

6.1 Overall Conclusions

The transition temperature between the two main TiO_2 phases (anatase and rutile) occurs when in pure synthetic form between 600-700°C. Chemical modifiers, dopants, additives or impurities can be used to alter the surface and structure of TiO_2, leading to an increased or decreased transition temperature. Additionally, the use of this additives, dopants, *etc.* can also be used to improve the photocatalytic activity of TiO_2. TiO_2 has a large band gap of 3.2 eV (anatase), as a result it only absorbs light from the UV spectrum. The use of 'dopants' or chemical modifiers into the TiO_2 structure or onto its surface can increase the number of active sites and increase the rate of reaction for photocatalysis. The chemical modifiers/dopants can also alter TiO_2 the band gap by the induction of mid-band gap levels between the VB and CB. This change in band gap may lead to samples being both UV and visible light active.

A number of chemical modifiers and dopants were examined throughout this degree to determine the effect they had on the on the TiO_2 lattice structure and surface, the impact on the ART temperature and the degradation of 1,4-dioxane. The current report has discussed in extensive detail the use of 3 chemical modifiers/dopants.

Chapter 3 examines the use of carbon doping TiO_2. Benzoic Acid (a carbon precursor) was used as a TiO_2 chemical modifier. The BA increased the ART temperature, as there was anatase present in 1:4 and 1:8 (TTIP: BA) with 11% and 7% respectively, at 800°C. The presence of BA also increased the photodegradation of 1,4-dioxane when compared with the control (1:0). The second non-metal dopant examined within is BN (Chapter 5). Unlike BA, BN does not show a significant improvement in the transition temperature. The control sample (0% BN) is 100% rutile at 600°C, while all doped samples are mixed phased at this temperature. All samples have transition completely into rutile by 700°C. As with BA, the inclusion of BN improved the photocatalytic activity of TiO_2 when compared to the control. However, BN doping does not show as much of a reduction of 1,4-dioxane that is seen by 1:4 (TTIP: BA) at 800°C.

In addition to theses two dopants, one metal dopant was examined. The W dopant displayed an improvement in ART when compare to the sample set control, 0% W-TiO_2 transitioned to 100% rutile at 800°C. The presence of tungsten increased the transition

temperture to a significantly higher temperature (26% anatase at 950°C). The optimum mol. % for W, in regards to ART, was 8% W-TiO_2. When examining the photocatalytic activity, tungsten showed an increased photocatalytic degradation of 1,4-dioxane when compared to the control. There was ~70% removal of 1,4-dioxane with 0% W-TiO_2 at 500°C (100% anatase), however there was a 100% removal for 2% W-TiO_2, 4% W-TiO_2 and 8% W-TiO_2 at 800°C (all 100% anatase).When the doped samples calcined at 900°C were examined for the removal of 1,4-dioxane, 8% W-TiO_2 showed the highest % removal.

Out of the three dopants/additives discussed throughout this thesis, tungsten showed the most significant improvement in both the transition temperature and the photocatalytic degradation of 1,4-dioxane.

6.2 Future Work

6.2.1 Hydrogen Production

All three photocatalysts prepared and analysed throughout this thesis showed an improvement in the removal of 1,4-dioxane in water (water remediation) when compared to only solar light treatment. Additionally, BA, W and BN also showed various degrees of improvement compared to the control (0%) in each sample set. As stated in Section 6.1, W doping demonstrated the ability to remove 100% of 1,4-dioxane. It is, therefore, worthwhile to consider other environmental applications for these tungsten doped samples. Water remediation is an important environmental application.[415] However, photocatalytic hydrogen production is also considered of significant importance and has been subjected to extensive research since Fujishima and Honda's water splitting study in 1972.[147, 212, 229, 230, 234, 235, 246-248, 336, 416-421] The photocatalytic splitting of water (hydrogen production) has been examined as a clean fuel (clean energy) source due to the low cost involved, abundance of water (seawater) and light (solar light) and it being a sustainable energy carrier.[248]

It was noted in a review by Ismail and Bahnemann (2014), that there had yet to be a photocatalyst produced that had the required band gap and stability that were needed for water splitting and it's practical application.[422] As a result, research into this area has continued.

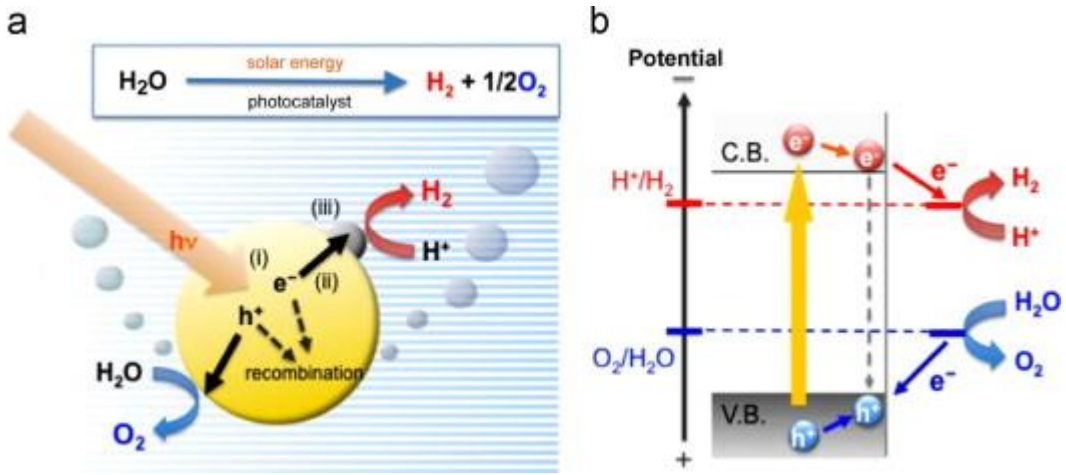

Figure 6.1: Illustration of photocatalytic splitting of water.[422] Reprinted from *Sol. Energy Mater. Sol. Cells.*, Vol. 128, Ismail & Bahnemann., Preparation and characterization of Nano-graphite/TiO_2 composite photoelectrode for photoelectrocatalytic degradation of hazardous pollutant, pp 85-101, Copyright 2014, with permission from Elsevier.

The use of a semiconductor for photocatalytic water splitting into H_2 and O_2 (Figure 6.1) involves three main steps, Figure 6.1 (a) shows the schematic diagram of this.[422] The three steps are: [422-424]

i. The formation of electron-hole pairs which are a result of the photons absorbed from a light source.
ii. The migration of these species after charge separation has occurred.
iii. The reaction of the charge carriers on the surface of the semiconductor with surrounding compounds/liquids (in this case H_2O). It is important to note that not all electron-hole pairs are involved with this reaction, some may undergo recombination immediately.

In order to cause the formation of H_2 and O_2 from water, the CB must sit higher (and therefore show higher negative potential values) than reduction potential of water and the VB must sit lower (and be more positive) than the oxidation potential of water (seen in Figure 6.1 (b)).[422] Additional, in order to undergo photoirradiation of the photocatalyst used must have the ability to be stable in aqueous solutions.[422]

The use of multiple semiconductors for synthesising nanocomposites or heterojunctions can increase the rate at which hydrogen production occurs.[425, 426] This can be due to the transfer of electrons between the CBs of all semiconductors involved which leads to the reduction in the recombination rate.[426] Additionally, the improvement in photocatalysis

could be a result of one of the semiconductors having a narrow enough band gap to absorb visible light.[425] For example, the composite of TiO_2 and WO_3 may show increased activity due to WO_3 having a narrow band gap and absorbing in the visible light region.[425] There have been a number of studies that examined the impact of W (or WO_3) doped titania had on the photocatalytic production of hydrogen compared to bare titania.[427-429]

6.2.2 Novel Photocatalyst - Heterojunctions

As discussed in detail in Sections 1.5.1 and 1.5.2, heterojunctions form when two semiconductors are present and there is a difference in the band gap size. There are two ways a heterojunction can form: (i) between two phases of one semiconductor *e.g.* anatase-brookite TiO_2 heterojunction (Section 1.5.1) and (ii) between multiple semiconductors *e.g.* WO_3-TiO_2 and Pd-Cr_2O_3-CdS (Section 1.5.2). While Section 1.5.2 mentioned several different photocatalysts used for heterojunctions, it primarily focused on cadmium sulphide and/or zinc-based materials. However, there is a continuously growing list of photocatalysts that have now been examined for heterojunctions.

In 2017, Low *et al.* (2017) completed an extensive review on heterojunction photocatalysts. The review included a summary of the heterojunctions examined to date and compared aspects such as fundamental design and synthesis, characterisation and their applications.[430] However, despite the research accomplished to date, a considerable amount of work is still needed before heterojunction photocatalysts can be applied for practical purposes and scaled up for commercialisation applications.[430] Low *et al.* (2017) concluded the review by making the following suggestions in regards to the future work that is required in this field of study: [430]

1. Significant research is needed into controlling physiochemical properties (*e.g.* morphology, contact interface, crystallisation) of the heterojunction materials.[430]
2. Examination of the transferring of electrons and holes between the two photocatalysts.[430] This includes identifying the direct pathway the electron–hole pairs migrate.
3. Further emphases on theoretical methods (calculations and modelling) is crucial in gaining a complete comprehension of the mechanism and charge-migration kinetics.[430]
4. The investigation into novel approaches and new photocatalysts for the purposes of the development of heterojunction materials should continue. The aim is to

produce a heterojunction photocatalyst that has the desired properties, including it being cost-effective, visible-light active and having the necessary bandgap.[430]

6.2.3 Photodynamic Therapy of Cancer

According to the Irish Cancer Society, the rate of cancer occurrence is increasing and the rate of cancer diagnoses in Ireland is expected to increase to 1 in 2 people by 2020.[431] This is on par with projected cancer rates of other countries, including the UK.[431] As a result of the global increase in cancer incidence, it has become imperative that a novel and effective method for killing cancer is delevelop.[140] One method that has gained traction for cancer treatment over the last few decades is photodynamic therapy (PDT).[140, 432-435] PDT has a number of significant benefits compared to the more established cancer treatments (*i.e.* surgery, chemotherapy, radiotherapy), as it specifically targets the cancerous cells, promotes healing in the tissue/cells in the areas surrounding the tumour, it is non-invasive and can result in an improved quality of life for patients.[432] PDT has been used effectively in both clinical research and applications, though advances are still required.[432-434] PDT uses a photosensitizer (PS) that is non-toxic and added to the tumour cells (Figure 6.2).[432, 436] This photosensitizer is activated using focused laser light which leads to the production of cytotoxic ROS.[432, 436]

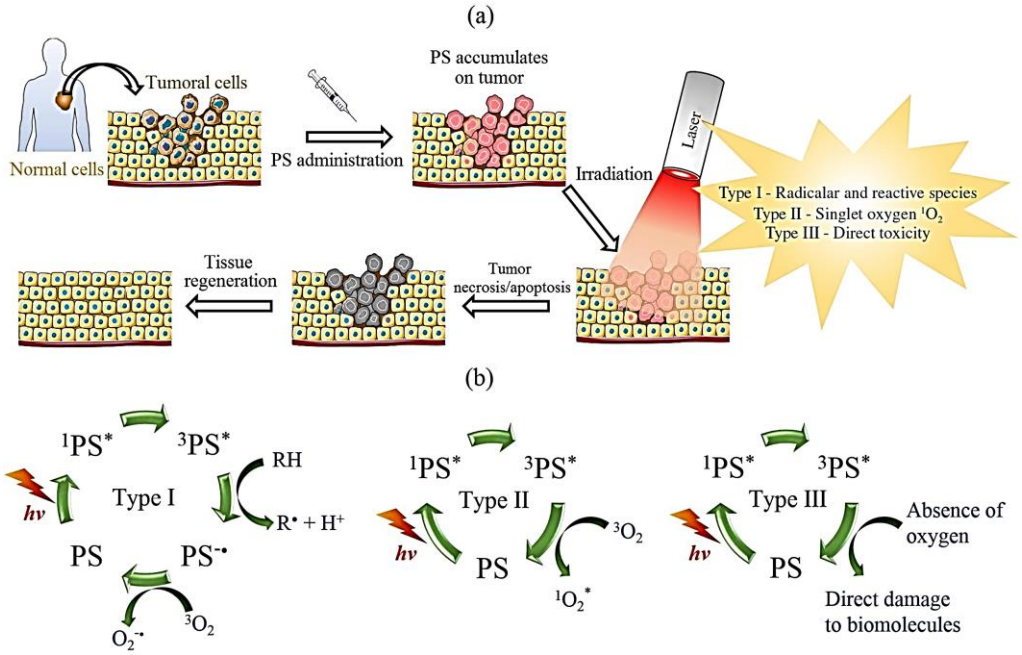

Figure 6.2: (a) Scheme diagram of photodynamic therapy (b) the three possible mechanisms of the ROS.[436] Reprinted from *J. Braz. Chem. Soc.*, Vol. 26, No. 12, 2448-2470, 2015.

To conclude, the recommendations for future work suggested have been made based on the literature. The ability of a nanomaterial to have high photocatalytic activity for several applications would be extremely beneficial for scaling up for industrial applications and it may also be more cost-effective. For this reason, it has been suggested that the tungsten doped samples be examined for hydrogen production. Using a semiconductor as a dopant can cause the formation heterojunctions, the electrons are transferred from the first semiconductor (photocatalyst) to the second which stops recombination and improves photocatalysis. There have been numerous studies on using a semiconductor to dope TiO_2, it is therefore important to examine novel combinations of semiconductors for heterojunction formation. The second recommendation of this work is to research and develop a novel heterojunction photocatalyst. The third and final recommendation is to examine the emerging area of photodynamic therapy. With cancer affecting an increasing number of people worldwide it is important to continue to develop new ways of treatment. Photodynamic therapy has been used to date. However, in order to treat tissue deeper in the body a significant amount of work is required.

References

1. Rao, K. K.; Kumar, G., Polymorphic phase transition among the titania crystal structures in solution based approach: From precursor chemistry to nucleation process. *Nanoscale* **2014**, *6* (20), 11574-11632.
2. Thamaphat, K.; Limsuwan, P.; Ngotawornchai, B., Phase characterization of TiO_2 powder by XRD and TEM. *Kasetsart J.(Nat. Sci.)* **2008,** *42* (5), 357-361.
3. Fisher, M. B.; Keane, D. A.; Fernandez-Ibanez, P.; Colreavy, J.; Hinder, S. J.; McGuigan, K. G.; Pillai, S. C., Nitrogen and copper doped solar light active TiO_2 photocatalysts for water decontamination. *Applied Catalysis B: Environmental* **2013,** *130*, 8-13.
4. Hanaor, D. A.; Sorrell, C. C., Review of the anatase to rutile phase transformation. *Journal of Materials science* **2011,** *46* (4), 855-874.
5. Okasha, A.; Gomaa, F.; Elhaes, H.; Morsy, M.; El-Khodary, S.; Fakhry, A.; Ibrahim, M., Spectroscopic analyses of the photocatalytic behavior of nano-titanium dioxide. *Spectrochimica Acta Part A: Molecular and Biomolecular Spectroscopy* **2015,** *136*, 504-509.
6. Pillai, S. C.; Periyat, P.; George, R.; McCormack, D. E.; Seery, M. K.; Hayden, H.; Colreavy, J.; Corr, D.; Hinder, S. J., Synthesis of high-temperature stable anatase TiO_2 photocatalyst. *The Journal of Physical Chemistry C* **2007,** *111* (4), 1605-1611.
7. Nolan, N. T.; Seery, M. K.; Hinder, S. J.; Healy, L. F.; Pillai, S. C., A systematic study of the effect of silver on the chelation of formic acid to a titanium precursor and the resulting effect on the anatase to rutile transformation of TiO_2. *The Journal of Physical Chemistry C* **2010,** *114* (30), 13026-13034.
8. Pelaez, M.; Nolan, N. T.; Pillai, S. C.; Seery, M. K.; Falaras, P.; Kontos, A. G.; Dunlop, P. S.; Hamilton, J. W.; Byrne, J. A.; O'Shea, K., A review on the visible light active titanium dioxide photocatalysts for environmental applications. *Applied Catalysis B: Environmental* **2012,** *125*, 331-349.
9. Banerjee, S.; Pillai, S. C.; Falaras, P.; O'Shea, K. E.; Byrne, J. A.; Dionysiou, D. D., New Insights into the Mechanism of Visible Light Photocatalysis. *The Journal of Physical Chemistry Letters* **2014,** *5* (15), 2543-2554.
10. Fagan, R.; McCormack, D. E.; Dionysiou, D. D.; Pillai, S. C., A review of solar and visible light active TiO_2 photocatalysis for treating bacteria, cyanotoxins and contaminants of emerging concern. *Materials Science in Semiconductor Processing* **2015,** *42*, 2-14**.** .
11. Hu, Y.; Tsai, H. L.; Huang, C. L., Effect of brookite phase on the anatase–rutile transition in titania nanoparticles. *Journal of the European Ceramic Society* **2003,** *23* (5), 691-696.
12. Carp, O.; Huisman, C. L.; Reller, A., Photoinduced reactivity of titanium dioxide. *Progress in Solid State Chemistry* **2004,** *32* (1), 33-177.
13. de Farias, R. F.; Silva, C. C.; Restivo, T. A., Thermal study of the anatase-rutile structural transitions in sol-gel synthesized titanium dioxide powders. *Journal of the Serbian Chemical Society* **2005,** *70* (4), 675-679.
14. Periyat, P.; Pillai, S. C.; McCormack, D. E.; Colreavy, J.; Hinder, S. J., Improved high-temperature stability and sun-light-driven photocatalytic activity of sulfur-doped anatase TiO_2. *The Journal of Physical Chemistry C* **2008,** *112* (20), 7644-7652.
15. Heald, E. F.; Weiss, C. W., Kinetics and Mechanism of Anatase/Rutile Transformation, as Catalyzed by Ferric Oxide and Reducing Conditions. *American Mineralogist* **1972,** *57* (1-2), 10.
16. Nolan, N. T.; Seery, M. K.; Pillai, S. C., Spectroscopic Investigation of the Anatase-to-Rutile Transformation of Sol− Gel-Synthesized TiO_2 Photocatalysts. *The Journal of Physical Chemistry C* **2009,** *113* (36), 16151-16157.
17. Byun, C.; Jang, J. W.; Kim, I. T.; Hong, K. S.; Lee, B. W., Anatase-to-rutile transition of titania thin films prepared by MOCVD. *Materials Research Bulletin* **1997,** *32* (4), 431-440.
18. Markowska-Szczupak, A.; Ulfig, K.; Morawski, A., The application of titanium dioxide for deactivation of bioparticulates: an overview. *Catalysis Today* **2011,** *169* (1), 249-257.
19. Etacheri, V.; Seery, M. K.; Hinder, S. J.; Pillai, S. C., Oxygen Rich Titania: A Dopant Free, High Temperature Stable, and Visible-Light Active Anatase Photocatalyst. *Advanced Functional Materials* **2011,** *21* (19), 3744-3752.

20. Gopal, M.; Chan, W. M.; De Jonghe, L., Room temperature synthesis of crystalline metal oxides. *Journal of Materials Science* **1997,** *32* (22), 6001-6008.
21. Seery, M. K.; George, R.; Floris, P.; Pillai, S. C., Silver doped titanium dioxide nanomaterials for enhanced visible light photocatalysis. *Journal of Photochemistry and Photobiology A: Chemistry* **2007,** *189* (2), 258-263.
22. Hamilton, J.; Byrne, T.; Dunlop, P.; Dionysiou, D. D.; Pelaez, M.; O'Shea, K. E.; Synnott, D.; Pillai, S. C., Evaluating the Mechanism of Visible Light Activity for N, F-TiO_2 Using Photoelectrochemistry. *The Journal of Physical Chemistry C* **2014**, *118*(23), 12206-12215.
23. Pillai, S. C.; McGuinness, N. B.; Byrne, C.; Han, C.; Lalley, J.; Nadagouda, M.; Falaras, P.; Kontos, A. G.; Gracia-Pinilla, M. A.; OShea, K., Photocatalysis as an effective advanced oxidation process. *Advanced Oxidation Processes for Water Treatment: Fundamentals and Applications* **2017**, 333-381.
24. Padmanabhan, S. C.; Pillai, S. C.; Colreavy, J.; Balakrishnan, S.; McCormack, D. E.; Perova, T. S.; Gun'ko, Y.; Hinder, S. J.; Kelly, J. M., A simple sol-gel processing for the development of high-temperature stable photoactive anatase titania. *Chemistry of Materials* **2007,** *19* (18), 4474-4481.
25. Byrne, C.; Fagan, R.; Hinder, S.; McCormack, D. E.; Pillai, S. C., New Approach of Modifying the Anatase to Rutile Transition Temperature in TiO_2 Photocatalysts. *RSC Advances* **2016,** *6* (97), 95232-95238.
26. Sá, J.; Garlisi, C.; Palmisano, G.; Czapla-Masztafiak, J.; Kayser, Y.; Szlachetko, J., Differences between bulk and surface electronic structure of doped TiO_2 with soft-elements (C, N and S). *Materials Chemistry and Physics* **2018,** *208*, 281-288.
27. Van de Krol, R.; Grätzel, M., *Photoelectrochemical hydrogen production*. Springer: **2012**; Vol. 90.
28. Guo, Q.; Zhou, C.; Ma, Z.; Ren, Z.; Fan, H.; Yang, X., Fundamental Processes in Surface Photocatalysis on TiO_2. In *Heterogeneous Photocatalysis*, Springer: **2016;** pp 361-416.
29. Diebold, U., The surface science of titanium dioxide. *Surface Science Reports* **2003,** *48* (5), 53-229.
30. Ding, Y.; Chen, M.; Wu, W., Mechanical properties, hardness and electronic structures of new post-cotunnite phase (Fe_2 P-type) of TiO_2. *Physica. B, Condensed matter* , **2014,** *433*, 48.
31. Holm, B.; Swamy, V.; Harrison, N. M.; Johansson, B., Materials science - The hardest known oxide. *Nature (London)* **2001,** *410* (6829), 653.
32. Liu, Q.-J.; Ran, Z.; Liu, F.-S.; Liu, Z.-T., Phase transitions and mechanical stability of TiO_2 polymorphs under high pressure. *Journal of Alloys and Compounds* **2015,** *631*, 192-201.
33. Mattesini, M.; De Almeida, J. S.; Dubrovinsky, L.; Dubrovinskaia, N.; Johansson, B.; Ahuja, R., Cubic TiO_2 as a potential light absorber in solar-energy conversion. **2004,** *70* (11), 115101.
34. Mattesini, M.; De Almeida, J. S.; Dubrovinsky, L.; Dubrovinskaia, N.; Johansson, B.; Ahuja, R., High-pressure and high-temperature synthesis of the cubic TiO_2 polymorph. **2004,** *70* (21), 212101.
35. Simons, P.; Dachille, F., The structure of TiO_2II, a high-pressure phase of TiO_2. *Acta Crystallographica* **1967,** *23* (2), 334-336.
36. Sasaki, T., Watanabe, M.; Fujiki, Y., Structure of $K_{1.0}Ti_8O_{16}$ and $K_{0.0}Ti_8O_{16}$. **1993,** *49* (5), 838-841.
37. Latroche, M.; Brohan, L.; Marchand, R.; Tournoux, M., New hollandite oxides: TiO_2 (H) and $K_{0.06}TiO_2$. **1989,** *81* (1), 78-82.
38. Etacheri, V.; Di Valentin, C.; Schneider, J.; Bahnemann, D.; Pillai, S. C., Visible-light activation of TiO_2 photocatalysts: Advances in theory and experiments. *Journal of Photochemistry and Photobiology C: Photochemistry Reviews* **2015,** *25*, 1-29.
39. Neelgund, G. M.; Shivashankar, S. A.; Chethana, B. K.; Sahoo, P. P.; Rao, K. J., Nanocrystalline TiO_2 preparation by microwave route and nature of anatase–rutile phase transition in nano TiO_2. *Bulletin of Materials Science* **2011,** *34* (6), 1163-1171.
40. Zhang, H.; Banfield, J., Understanding polymorphic phase transformation behavior during growth of nanocrystalline aggregates: insights from TiO_2. **2000,** *104* (15), 3481-3487.

41. Won, D. J.; Wang, C. H.; Jang, H. K.; Choi, D. J., Effects of thermally induced anatase-to-rutile phase transition in MOCVD-grown TiO_2 films on structural and optical properties. *Applied Physics A Materials Science & Processing* **2001,** *73* (5), 595-600.
42. Wetchakun, N.; Phanichphant, S., Effect of temperature on the degree of anatase–rutile transformation in titanium dioxide nanoparticles synthesized by the modified sol–gel method. **2008,** *8* (3-4), 343-346.
43. Zallen, R.; Moret, M. P., The optical absorption edge of brookite TiO_2. *Solid State Communications* **2006,** *137* (3), 154-157.
44. Banfield, J., Thermodynamic analysis of phase stability of nanocrystalline titania. *Journal of Materials Chemistry* **1998,** *8* (9), 2073-2076.
45. Nahar, M. S.; Zhang, J.; Hasegawa, K.; Kagaya, S.; Kuroda, S., Phase transformation of anatase–rutile crystals in doped and undoped TiO_2 particles obtained by the oxidation of polycrystalline sulfide. *Materials Science in Semiconductor Processing* **2009,** *12* (4), 168-174.
46. Madras, G.; McCoy, B. J.; Navrotsky, A., Kinetic model for TiO_2 polymorphic transformation from anatase to rutile. *Journal of the American Ceramic Society* **2007,** *90* (1), 250-255.
47. Dvoranová, D.; Brezová, V.; Mazúr, M.; Malati, M. A., Investigations of metal-doped titanium dioxide photocatalysts. *Applied Catalysis B: Environmental* **2002,** *37* (2), 91-105.
48. Zhang, W.; Zhang, M.; Yin, Z.; Chen, Q., Photoluminescence in anatase titanium dioxide nanocrystals. *Applied Physics B* **2000,** *70* (2), 261-265.
49. Okada, K.; Yamamoto, N.; Kameshima, Y.; Yasumori, A.; MacKenzie, K. J. D., Effect of Silica Additive on the Anatase-to-Rutile Phase Transition. *Journal of the American Ceramic Society* **2001,** *84* (7), 1591-1596.
50. Matthews, A., The crystallization of anatase and rutile from amorphous titanium dioxide under hydrothermal conditions. *American Mineralogist* **1976,** *61* (5-6), 419-424.
51. Shin, H.; Jung, H. S.; Hong, K. S.; Lee, J.-K., Crystal phase evolution of TiO_2 nanoparticles with reaction time in acidic solutions studied via freeze-drying method. *Journal of Solid State Chemistry* **2005,** *178* (1), 15-21.
52. Ghosh, T.; Dhabal, S.; Datta, A., On crystallite size dependence of phase stability of nanocrystalline TiO_2. *Journal of applied physics* **2003,** *94* (7), 4577-4582.
53. Zhang, Z.; Wang, C. C.; Zakaria, R.; Ying, J. Y., Role of particle size in nanocrystalline TiO_2-based photocatalysts. *The Journal of Physical Chemistry B* **1998,** *102* (52), 10871-10878.
54. Bacsa, R.; Kiwi, J., Effect of rutile phase on the photocatalytic properties of nanocrystalline titania during the degradation of p-coumaric acid. *Applied Catalysis B: Environmental* **1998,** *16* (1), 19-29.
55. Li, G.; Li, L.; Boerio-Goates, J.; Woodfield, B. F., Grain-growth kinetics of rutile TiO_2 nanocrystals under hydrothermal conditions. *Journal of materials research* **2003,** *18* (11), 2664-2669.
56. Li, G.; Boerio-Goates, J.; Woodfield, B. F.; Li, L., Evidence of linear lattice expansion and covalency enhancement in rutile TiO_2 nanocrystals. **2004**.
57. Hirano, M.; Nakahara, C.; Ota, K.; Tanaike, O.; Inagaki, M., Photoactivity and phase stability of ZrO_2-doped anatase-type TiO_2 directly formed as nanometer-sized particles by hydrolysis under hydrothermal conditions. *Journal of Solid State Chemistry* **2003,** *170* (1), 39-47.
58. Gouma, P. I.; Mills, M. J., Anatase-to-Rutile Transformation in Titania Powders. *Journal of the American Ceramic Society* **2001,** *84* (3), 619-622.
59. Kim, J.; Song, K. C.; Foncillas, S.; Pratsinis, S. E., Dopants for synthesis of stable bimodally porous titania. *Journal of the European Ceramic Society* **2001,** *21* (16), 2863-2872.
60. Shannon, R. D.; Pask, J. A., Kinetics of the Anatase-Rutile Transformation. *Journal of the American Ceramic Society* **1965,** *48* (8), 391-398.
61. Zhang, J.; Huang, F.; Lin, Z. J. N., Progress of nanocrystalline growth kinetics based on oriented attachment. **2010,** *2* (1), 18-34.
62. Hummer, D. R.; Kubicki, J. D.; Kent, P. R.; Post, J. E.; Heaney, P. J., Origin of nanoscale phase stability reversals in titanium oxide polymorphs. **2009,** *113* (11), 4240-4245.

63. Raju, M.; Van Duin, A. C.; Fichthorn, K. A., Mechanisms of oriented attachment of TiO_2 nanocrystals in vacuum and humid environments: reactive molecular dynamics. **2014,** *14* (4), 1836-1842.
64. Zhang, Y.; Wu, L.; Zeng, Q.; Zhi, J., An approach for controllable synthesis of different-phase titanium dioxide nanocomposites with peroxotitanium complex as precursor. **2008,** *112* (42), 16457-16462.
65. Batzill, M.; Morales, E. H.; Diebold, U., Influence of nitrogen doping on the defect formation and surface properties of TiO_2 rutile and anatase. *Physical review letters* **2006,** *96* (2), 026103.
66. Sun, J.; Gao, L., pH Effect on Titania-Phase Transformation of Precipitates from Titanium Tetrachloride Solutions. **2002,** *85* (9), 2382-2384.
67. Sui, R.; Charpentier, P., Synthesis of metal oxide nanostructures by direct sol–gel chemistry in supercritical fluids. **2012,** *112* (6), 3057-3082.
68. Su, C.; Hong, B. Y.; Tseng, C. M., Sol–gel preparation and photocatalysis of titanium dioxide. **2004,** *96* (3), 119-126.
69. Akpan, U.; Hameed, B.., The advancements in sol–gel method of doped-TiO_2 photocatalysts. **2010,** *375* (1), 1-11.
70. Wang, C. C.; Ying, J. Y., Sol−gel synthesis and hydrothermal processing of anatase and rutile titania nanocrystals. **1999,** *11* (11), 3113-3120.
71. Hsiang, H.-I.; Lin, S.-C., Effects of aging on the phase transformation and sintering properties of TiO_2 gels. **2004,** *380* (1-2), 67-72.
72. Yang, J.; Mei, S.; Ferreira, J. M., Hydrothermal synthesis of nanosized titania powders: influence of peptization and peptizing agents on the crystalline phases and phase transitions. **2000,** *83* (6), 1361-1368.
73. Cristallo, G., Study of anatase–rutile transition phase in monolithic catalyst V_2O_5/TiO_2 and $V_2O_5–WO_3/TiO_2$. *Applied Catalysis A: General* **2001,** *209* (1-2), 249-256.
74. Smith, S. J.; Stevens, R.; Liu, S.; Li, G.; Navrotsky, A.; Boerio-Goates, J.; Woodfield, B. F., Heat capacities and thermodynamic functions of TiO_2 anatase and rutile: Analysis of phase stability. *American Mineralogist* **2009,** *94* (2-3), 236-243.
75. Muscat, J.; Swamy, V.; Harrison, N. M., First-principles calculations of the phase stability of TiO_2. *Physical Review B* **2002,** *65* (22), 224112.
76. Navrotsky, A.; Kleppa, O., Enthalpy of the Anatase-Rutile Transformation. *Journal of the American Ceramic Society* **1967,** *50* (11), 626-626.
77. Mitsuhashi, T.; Kleppa, O., Transformation enthalpies of the TiO_2 polymorphs. *Journal of the American Ceramic Society* **1979,** *62* (7-8), 356-357.
78. Jamieson, J. C.; Olinger, B.; Dachille, F.; Simons, P.; Roy, R., Pressure-Temperature Studies of Anatase, Brookite, Rutile and TiO_2 (II) - A Discussion. *Mineralogical Soc. Amer.*, 1015 Eighteenth St., NW Suite 601, Washington, DC 20036: 1969; Vol. 54, pp 1477.
79. Rao, C., Kinetics and thermodynamics of the crystal structure transformation of spectroscopically pure anatase to rutile. *Canadian Journal of Chemistry* **1961,** *39* (3), 498-500.
80. Dachille, F.; Simons, P.; Roy, R., Pressure-temperature studies of anatase, brookite, rutile and TiO_2-II. *Am Mineral* **1968,** *53*, 1929-1939.
81. Vargas, S.; Arroyo, R.; Haro, E.; Rodriguez, R., Effects of cationic dopants on the phase transition temperature of titania prepared by the sol-gel method. *Journal of materials research* **1999,** *14* (10), 3932-3937.
82. Liao, S.-C.; Chen, Y.-J.; Mayo, W.; Kear, B., Transformation-assisted consolidation of bulk nanocrystalline TiO_2. *Nanostructured materials* **1999,** *11* (4), 553-557.
83. Liao, S. C., Colaizzi, J., Chen, Y., Kear, B. H., Mayo, W. E., Refinement of Nanoscale Grain Structure in Bulk Titania via a Transformation-Assisted Consolidation (TAC) Method. *Journal of the American Ceramic Society* **2000,** *83* (9), 2163-2169.
84. Murray, J.; Wriedt, H., The O−Ti (oxygen-titanium) system. *Journal of Phase Equilibria* **1987,** *8* (2), 148-165.
85. Wang, H.; Lewis, J., Second-generation photocatalytic materials: anion-doped TiO_2. *Journal of Physics: Condensed Matter* **2005,** *18* (2), 421.

86. Dawei, M.; Xiuling, W.; Xiaoyu, F.; Zhengjie, Z.; Hong, C.; Xin, M.; Jianping, Z., High Pressure Response of Rutile Polymorphs and Its Significance for Indicating the Subduction Depth of Continental Crust. *Acta Geologica Sinica (English Edition)* **2008,** *82* (2), 371-376.
87. Dubrovinskaia, N. A.; Dubrovinsky, L. S.; Ahuja, R.; Prokopenko, V. B.; Dmitriev, V.; Weber, H.-P.; Osorio-Guillen, J.; Johansson, B., Experimental and theoretical identification of a new high-pressure TiO_2 polymorph. *Physical Review Letters* **2001,** *87* (27), 275501.
88. Mehranpour, H.; Askari, M.; Ghamsari, M. S.; Farzalibeik, H., Study on the phase transformation kinetics of sol-gel drived TiO_2 nanoparticles. **2010,** *2010*, 31.
89. Zhang, H.; Banfield, J. F., New kinetic model for the nanocrystalline anatase-to-rutile transformation revealing rate dependence on number of particles. **1999,** *84* (4), 528-535.
90. Kumar, K.N. P.; Keizer, K.; Burggraaf, A. J., Textural evolution and phase transformation in titania membranes: Part 1.—Unsupported membranes. **1993,** *3* (11), 1141-1149.
91. Riyas, S.; Krishnan, G.; Das, P. M., Anatase–rutile transformation in doped titania under argon and hydrogen atmospheres. *Advances in Applied Ceramics* **2007,** *106* (5), 255-264.
92. Ihara, T.; Miyoshi, M.; Iriyama, Y.; Matsumoto, O.; Sugihara, S., Visible-light-active titanium oxide photocatalyst realized by an oxygen-deficient structure and by nitrogen doping. *Applied Catalysis B: Environmental* **2003,** *42* (4), 403-409.
93. MacKenzie, K., Calcination of titania: IV, Effect of additives on the anataserutile transformation. *Transactions and Journal of the British Ceramic Society* **1975,** *74* (2), 29-34.
94. Mackenzie, K., Calcination of titania: V, Kinetics and mechanism of the anatase-rutile transformation in the presence of additives. *Transactions and Journal of the British Ceramic Society* **1975,** *74* (3), 77-84.
95. Ding, X.-z.; Liu, X. H., Correlation between anatase-to-rutile transformation and grain growth in nanocrystalline titania powders. *Journal of materials research* **1998,** *13* (09), 2556-2559.
96. Gilbert, B.; Zhang, H.; Huang, F.; Finnegan, M. P.; Waychunas, G. A.; Banfield, J. F., Special phase transformation and crystal growth pathways observed in nanoparticles. *Geochem. Trans* **2003,** *4* (4), 20-27.
97. Kumar, K.N. P.; Fray, D. J.; Nair, J.; Mizukami, F.; Okubo, T., Enhanced anatase-to-rutile phase transformation without exaggerated particle growth in nanostructured titania–tin oxide composites. *Scripta materialia* **2007,** *57* (8), 771-774.
98. Reidy, D.; Holmes, J.; Morris, M., The critical size mechanism for the anatase to rutile transformation in TiO_2 and doped-TiO_2. *Journal of the European Ceramic Society* **2006,** *26* (9), 1527-1534.
99. Kumar, S. R.; Pillai, S. C.; Hareesh, U.; Mukundan, P.; Warrier, K., Synthesis of thermally stable, high surface area anatase–alumina mixed oxides. *Materials letters* **2000,** *43* (5), 286-290.
100. Perera, S.; Gillan, E. G., High-temperature stabilized anatase TiO_2 from an aluminum-doped TiCl 3 precursor. *Chemical communications* **2005,** (48), 5988-5990.
101. Park, J.-K.; Ahn, J.-P.; Kim, G., Effect of compact structure on phase transformation kinetics from anatase phase to rutile phase and microstructure evolution during sintering of ultrafine titania powder compacts. *Metals and Materials* **1999,** *5* (2), 129-134.
102. Lee, G. H.; Zuo, J. M., Growth and Phase Transformation of Nanometer-Sized Titanium Oxide Powders Produced by the Precipitation Method. *Journal of the American Ceramic Society* **2004,** *87* (3), 473-479.
103. Zhang, Q.; Gao, L.; Guo, J., Effects of calcination on the photocatalytic properties of nanosized TiO_2 powders prepared by $TiCl_4$ hydrolysis. *Applied Catalysis B: Environmental* **2000,** *26* (3), 207-215.
104. Francisco, M. S. P.; Mastelaro, V. R., Inhibition of the anatase-rutile phase transformation with addition of CeO_2 to CuO-TiO_2 system: Raman spectroscopy, X-ray diffraction, and textural studies. *Chemistry of Materials* **2002,** *14* (6), 2514-2518.
105. Serpone, N., Is the band gap of pristine TiO_2 narrowed by anion-and cation-doping of titanium dioxide in second-generation photocatalysts? *The Journal of Physical Chemistry B* **2006,** *110* (48), 24287-24293.

106. Nagaveni, K.; Hegde, M.; Madras, G., Structure and Photocatalytic Activity of $Ti_{1-x}M_xO_{2\pm\delta}$ (M= W, V, Ce, Zr, Fe, and Cu) Synthesized by Solution Combustion Method. *The Journal of Physical Chemistry B* **2004,** *108* (52), 20204-20212.
107. Ranjit, K.; Cohen, H.; Willner, I.; Bossmann, S.; Braun, A., Lanthanide oxide-doped titanium dioxide: Effective photocatalysts for the degradation of organic pollutants. *Journal of Materials Science* **1999,** *34* (21), 5273-5280.
108. Nowotny, J.; Bak, T.; Sheppard, L.; Sorrell, C., Solar-hydrogen: a solid-state chemistry perspective. *Advances in Solar Energy: Volume 17: An Annual Review of Research and Development in Renewable Energy Technologies* **2015,** *17*, 169-215.
109. Sun, B.; Vorontsov, A. V.; Smirniotis, P. G., Role of platinum deposited on TiO_2 in phenol photocatalytic oxidation. *Langmuir* **2003,** *19* (8), 3151-3156.
110. Franch, M. I.; Peral, J.; Domènech, X.; Ayllón, J. A., Aluminium (III) adsorption: a soft and simple method to prevent TiO_2 deactivation during salicylic acid photodegradation. *Chemical communications* **2005,** (14), 1851-1853.
111. Fujishima, A.; Zhang, X., Titanium dioxide photocatalysis: present situation and future approaches. *Comptes Rendus Chimie* **2006,** *9* (5), 750-760.
112. Emeline, A. V.; Kuznetsov, V. N.; Rybchuk, V. K.; Serpone, N., Visible-Light-Active Titania Photocatalysts: The Case of N-Doped S—Properties and Some Fundamental Issues. *International Journal of Photoenergy* **2007,** *2008*.
113. Sato, S., Photocatalytic activity of NO_x-doped TiO_2 in the visible light region. *Chemical Physics Letters* **1986,** *123* (1), 126-128.
114. Sato, S.; Nakamura, R.; Abe, S., Visible-light sensitization of TiO_2 photocatalysts by wet-method N doping. *Applied Catalysis A: General* **2005,** *284* (1), 131-137.
115. Choi, H.; Antoniou, M. G.; Pelaez, M.; De la Cruz, A. A.; Shoemaker, J. A.; Dionysiou, D. D., Mesoporous nitrogen-doped TiO_2 for the photocatalytic destruction of the cyanobacterial toxin microcystin-LR under visible light irradiation. *Environmental science & technology* **2007,** *41* (21), 7530-7535.
116. Fang, X.; Zhang, Z.; Chen, Q.; Ji, H.; Gao, X., Dependence of nitrogen doping on TiO_2 precursor annealed under NH_3 flow. *Journal of Solid State Chemistry* **2007,** *180* (4), 1325-1332.
117. Oropeza, F. E.; Harmer, J.; Egdell, R.; Palgrave, R. G., A critical evaluation of the mode of incorporation of nitrogen in doped anatase photocatalysts. *Physical Chemistry Chemical Physics* **2010,** *12* (4), 960-969.
118. Irokawa, Y.; Morikawa, T.; Aoki, K.; Kosaka, S.; Ohwaki, T.; Taga, Y., Photodegradation of toluene over $TiO_{2-x}N_x$ under visible light irradiation. *Physical Chemistry Chemical Physics* **2006,** *8* (9), 1116-1121.
119. Irie, H.; Watanabe, Y.; Hashimoto, K., Carbon-doped anatase TiO_2 powders as a visible-light sensitive photocatalyst. *Chemistry Letters* **2003,** *32* (8), 772-773.
120. Sakthivel, S.; Kisch, H., Daylight photocatalysis by carbon-modified titanium dioxide. *Angewandte Chemie International Edition* **2003,** *42* (40), 4908-4911.
121. Etacheri, V.; Michlits, G.; Seery, M. K.; Hinder, S. J.; Pillai, S. C., A Highly Efficient $TiO_{2-x}C_x$ Nano-heterojunction Photocatalyst for Visible Light Induced Antibacterial Applications. *ACS applied materials & interfaces* **2013,** *5* (5), 1663-1672.
122. Czoska, A.; Livraghi, S.; Chiesa, M.; Giamello, E.; Agnoli, S.; Granozzi, G.; Finazzi, E.; Valentin, C. D.; Pacchioni, G., The nature of defects in fluorine-doped TiO_2. *The Journal of Physical Chemistry C* **2008,** *112* (24), 8951-8956.
123. Borgarello, E.; Kiwi, J.; Graetzel, M.; Pelizzetti, E.; Visca, M., Visible light induced water cleavage in colloidal solutions of chromium-doped titanium dioxide particles. *Journal of the American chemical society* **1982,** *104* (11), 2996-3002.
124. Iwasaki, M.; Hara, M.; Kawada, H.; Tada, H.; Ito, S., Cobalt ion-doped TiO_2 photocatalyst response to visible light. *Journal of Colloid and Interface Science* **2000,** *224* (1), 202-204.
125. Klosek, S.; Raftery, D., Visible light driven V-doped TiO_2 photocatalyst and its photooxidation of ethanol. *The Journal of Physical Chemistry B* **2001,** *105* (14), 2815-2819.

126. Morikawa, T.; Irokawa, Y.; Ohwaki, T., Enhanced photocatalytic activity of $TiO_{2-x}N_x$ loaded with copper ions under visible light irradiation. *Applied Catalysis A: General* **2006,** *314* (1), 123-127.
127. Yang, J.; Ferreira, J., Inhibitory effect of the Al_2O_3–SiO_2 mixed additives on the anatase–rutile phase transformation. *Materials Letters* **1998,** *36* (5), 320-324.
128. Debeila, M. A.; Raphulu, M. C.; Mokoena, E.; Avalos, M.; Petranovskii, V.; Coville, N. J.; Scurrell, M. S., The effect of gold on the phase transitions of titania. *Materials Science and Engineering: A* **2005,** *396* (1), 61-69.
129. Janes, R.; Knightley, L.; Harding, C., Structural and spectroscopic studies of iron (III) doped titania powders prepared by sol-gel synthesis and hydrothermal processing. *Dyes and pigments* **2004,** *62* (3), 199-212.
130. Heo, K. C.; Ok, C. I.; Kim, J. W.; Moon, B. K., The effects of manganese ions and their magnetic properties on the anatase-rutile phase transition of nanocrystalline TiO_2: Mn prepared by using the solvothermal method. *Journal of the Korean Physical Society* **2005,** *47* (5), 861-865.
131. Arroyo, R.; Cordoba, G.; Padilla, J.; Lara, V., Influence of manganese ions on the anatase–rutile phase transition of TiO_2 prepared by the sol–gel process. *Materials Letters* **2002,** *54* (5), 397-402.
132. Karvinen, S., The effects of trace elements on the crystal properties of TiO_2. *Solid state sciences* **2003,** *5* (5), 811-819.
133. Hishita, S.; Mutoh, I.; Koumoto, K.; Yanagida, H., Inhibition mechanism of the anatase-rutile phase transformation by rare earth oxides. *Ceramics International* **1983,** *9* (2), 61-67.
134. Zhang, Y.-H.; Reller, A., Phase transformation and grain growth of doped nanosized titania. *Materials Science and Engineering: C* **2002,** *19* (1), 323-326.
135. Nair, J.; Nair, P.; Mizukami, F.; Oosawa, Y.; Okubo, T., Microstructure and phase transformation behavior of doped nanostructured titania. *Materials research bulletin* **1999,** *34* (8), 1275-1290.
136. Bond, G. C.; Sárkány, A. J.; Parfitt, G. D., The vanadium pentoxide-titanium dioxide system: Structural investigation and activity for the oxidation of butadiene. *Journal of Catalysis* **1979,** *57* (3), 476-493.
137. Li, X.; Li, F., Study of Au/Au^{3+}-TiO_2 photocatalysts toward visible photooxidation for water and wastewater treatment. *Environmental science & technology* **2001,** *35* (11), 2381-2387.
138. Buso, D.; Pacifico, J.; Martucci, A.; Mulvaney, P., Gold-Nanoparticle-Doped TiO_2 Semiconductor Thin Films: Optical Characterization. *Advanced Functional Materials* **2007,** *17* (3), 347-354.
139. Li, H.; Bian, Z.; Zhu, J.; Huo, Y.; Li, H.; Lu, Y., Mesoporous Au/TiO_2 nanocomposites with enhanced photocatalytic activity. *Journal of the American Chemical Society* **2007,** *129* (15), 4538-4539.
140. Xu, J.; Sun, Y.; Zhao, Y.; Huang, J.; Chen, C.; Jiang, Z., Photocatalytic inactivation effect of gold-doped TiO_2 (Au/TiO_2) nanocomposites on human colon carcinoma LoVo cells. *International Journal of Photoenergy* **2007,** *2007*.
141. Rahulan, K. M.; Ganesan, S.; Aruna, P., Synthesis and optical limiting studies of Au-doped TiO_2 nanoparticles. *Advances in Natural Sciences: Nanoscience and Nanotechnology* **2011,** *2* (2), 025012.
142. Ismail, A. A.; Bahnemann, D. W.; Robben, L.; Yarovyi, V.; Wark, M., Palladium doped porous titania photocatalysts: impact of mesoporous order and crystallinity. *Chemistry of Materials* **2009,** *22* (1), 108-116.
143. Epifani, M.; Giannini, C.; Tapfer, L.; Vasanelli, L., Sol–gel synthesis and characterization of Ag and Au nanoparticles in SiO_2, TiO_2, and ZrO_2 thin films. *Journal of the American Ceramic Society* **2000,** *83* (10), 2385-2393.
144. Loganathan, K.; Bommusamy, P.; Muthaiahpillai, P.; Velayutham, M., The syntheses, characterizations, and photocatalytic activities of silver, platinum, and gold doped TiO_2 nanoparticles. *Environmental Engineering Research* **2011,** *16* (2), 81-90.
145. Mogyorósi, K.; Kmetykó, Á.; Czirbus, N.; Veréb, G.; Sipos, P.; Dombi, A., Comparison of the substrate dependent performance of Pt-, Au-and Ag-doped TiO_2 photocatalysts in H_2-

production and in decomposition of various organics. *Reaction Kinetics and Catalysis Letters* **2009,** *98* (2), 215-225.
146. Shaham-Waldmann, N.; Paz, Y., Away from TiO_2: a critical minireview on the developing of new photocatalysts for degradation of contaminants in water. *Materials Science in Semiconductor Processing* **2016,** *42*, 72-80.
147. Fujishima, A.; Honda, K., Photolysis-decomposition of water at the surface of an irradiated semiconductor. *Nature* **1972,** *238* (5385), 37-38.
148. Linsebigler, A. L.; Lu, G.; Yates Jr, J. T., Photocatalysis on TiO_2 surfaces: principles, mechanisms, and selected results. *Chemical reviews* **1995,** *95* (3), 735-758.
149. Scanlon, D. O.; Dunnill, C. W.; Buckeridge, J.; Shevlin, S. A.; Logsdail, A. J.; Woodley, S. M.; Catlow, C. R. A.; Powell, M. J.; Palgrave, R. G.; Parkin, I. P., Band alignment of rutile and anatase TiO_2. *Nature materials* **2013,** *12* (9), 798-801.
150. Etacheri, V.; Geiger, U.; Gofer, Y.; Roberts, G. A.; Stefan, I. C.; Fasching, R.; Aurbach, D., Exceptional electrochemical performance of Si-nanowires in 1, 3-dioxolane solutions: A surface chemical investigation. *Langmuir* **2012,** *28* (14), 6175-6184.
151. Blake, D. M., *Bibliography of work on the heterogeneous photocatalytic removal of hazardous compounds from water and air*. National Renewable Energy Laboratory: 1994; Vol. 1617.
152. Hustert, K.; Zepp, R. G., Photocatalytic degradation of selected azo dyes. *Chemosphere* **1992,** *24* (3), 335-342.
153. Ojani, R.; Raoof, J.-B.; Zarei, E., Electrochemical monitoring of photoelectrocatalytic degradation of rhodamine B using TiO_2 thin film modified graphite electrode. *Journal of Solid State Electrochemistry* **2012,** *16* (6), 2143-2149.
154. Banerjee, S.; Dionysiou, D. D.; Pillai, S. C., Self-cleaning applications of TiO_2 by photo-induced hydrophilicity and photocatalysis. *Applied Catalysis B: Environmental* **2015,** *176*, 396-428.
155. Gerischer, H.; Heller, A., The role of oxygen in photooxidation of organic molecules on semiconductor particles. *The Journal of Physical Chemistry* **1991,** *95* (13), 5261-5267.
156. Vinodgopal, K.; Bedja, I.; Hotchandani, S.; Kamat, P. V., A photocatalytic approach for the reductive decolorization of textile azo dyes in colloidal semiconductor suspensions. *Langmuir* **1994,** *10* (6), 1767-1771.
157. Vinodgopal, K.; Kamat, P. V., Photochemistry of textile azo dyes. Spectral characterization of excited state, reduced and oxidized forms of acid orange 7. *Journal of Photochemistry and Photobiology A: Chemistry* **1994,** *83* (2), 141-146.
158. Shemer, G.; Paz, Y., Interdigitated electrophotocatalytic cell for water purification. *International Journal of Photoenergy* **2011,** *2011*.
159. Schneider, J.; Matsuoka, M.; Takeuchi, M.; Zhang, J.; Horiuchi, Y.; Anpo, M.; Bahnemann, D. W., Understanding TiO_2 photocatalysis: mechanisms and materials. *Chemical reviews* **2014,** *114* (19), 9919-9986.
160. Abe, R., Recent progress on photocatalytic and photoelectrochemical water splitting under visible light irradiation. *Journal of Photochemistry and Photobiology C: Photochemistry Reviews* **2010,** *11* (4), 179-209.
161. Maeda, K.; Domen, K., Photocatalytic water splitting: recent progress and future challenges. *The Journal of Physical Chemistry Letters* **2010,** *1* (18), 2655-2661.
162. Fujishima, A.; Zhang, X.; Tryk, D. A., TiO_2 photocatalysis and related surface phenomena. *Surface Science Reports* **2008,** *63* (12), 515-582.
163. Peiró, A. M.; Colombo, C.; Doyle, G.; Nelson, J.; Mills, A.; Durrant, J. R., Photochemical reduction of oxygen adsorbed to nanocrystalline TiO_2 films: A transient absorption and oxygen scavenging study of different TiO_2 preparations. *The Journal of Physical Chemistry B* **2006,** *110* (46), 23255-23263.
164. Emeline, A.; Ryabchuk, V.; Serpone, N., Dogmas and misconceptions in heterogeneous photocatalysis. Some enlightened reflections. *The Journal of Physical Chemistry B* **2005,** *109* (39), 18515-18521.
165. Kamat, P. V., Photophysical, photochemical and photocatalytic aspects of metal nanoparticles. *ACS Publications*: **2002,** 7729-7744.

166. Kamat, P. V.; Bedja, I.; Hotchandani, S., Photoinduced charge transfer between carbon and semiconductor clusters. One-electron reduction of C60 in colloidal TiO_2 semiconductor suspensions. *The Journal of Physical Chemistry* **1994,** *98* (37), 9137-9142.
167. Yoshihara, T.; Katoh, R.; Furube, A.; Tamaki, Y.; Murai, M.; Hara, K.; Murata, S.; Arakawa, H.; Tachiya, M., Identification of reactive species in photoexcited nanocrystalline TiO_2 films by wide-wavelength-range (400− 2500 nm) transient absorption spectroscopy. *The Journal of Physical Chemistry B* **2004,** *108* (12), 3817-3823.
168. Serpone, N.; Lawless, D.; Khairutdinov, R., Size effects on the photophysical properties of colloidal anatase TiO_2 particles: size quantization versus direct transitions in this indirect semiconductor? *The journal of Physical Chemistry* **1995,** *99* (45), 16646-16654.
169. Lawless, D.; Serpone, N.; Meisel, D., Role of hydroxyl radicals and trapped holes in photocatalysis. A pulse radiolysis study. *The Journal of Physical Chemistry* **1991,** *95* (13), 5166-5170.
170. Bahnemann, D. W.; Hilgendorff, M.; Memming, R., Charge carrier dynamics at TiO_2 particles: reactivity of free and trapped holes. *The Journal of Physical Chemistry B* **1997,** *101* (21), 4265-4275.
171. Furube, A.; Asahi, T.; Masuhara, H.; Yamashita, H.; Anpo, M., Charge carrier dynamics of standard TiO_2 catalysts revealed by femtosecond diffuse reflectance spectroscopy. *The Journal of Physical Chemistry B* **1999,** *103* (16), 3120-3127.
172. Colombo, D. P.; Bowman, R. M., Does interfacial charge transfer compete with charge carrier recombination? A femtosecond diffuse reflectance investigation of TiO_2 nanoparticles. *The Journal of Physical Chemistry* **1996,** *100* (47), 18445-18449.
173. Iwata, K.; Takaya, T.; Hamaguchi, H.-o.; Yamakata, A.; Ishibashi, T.A.; Onishi, H.; Kuroda, H., Carrier Dynamics in TiO_2 and Pt/TiO_2 Powders Observed by Femtosecond Time-Resolved Near-Infrared Spectroscopy at a Spectral Region of 0.9−1.5 μm with the Direct Absorption Method. *The Journal of Physical Chemistry B* **2004,** *108* (52), 20233-20239.
174. Yamakata, A.; Ishibashi, T.A.; Takeshita, K.; Onishi, H., Time-resolved infrared absorption study of photochemical reactions over metal oxides. *Topics in catalysis* **2005,** *35* (3), 211-216.
175. Colbeau-Justin, C.; Kunst, M.; Huguenin, D., Structural influence on charge-carrier lifetimes in TiO_2 powders studied by microwave absorption. *Journal of Materials Science* **2003,** *38* (11), 2429-2437.
176. Martin, S. T.; Herrmann, H.; Choi, W.; Hoffmann, M. R., Time-resolved microwave conductivity. Part 1.—TiO_2 photoreactivity and size quantization. *Journal of the Chemical Society, Faraday Transactions* **1994,** *90* (21), 3315-3322.
177. Martin, S. T.; Herrmann, H.; Hoffmann, M. R., Time-resolved microwave conductivity. Part 2.—Quantum-sized TiO_2 and the effect of adsorbates and light intensity on charge-carrier dynamics. *Journal of the chemical society, Faraday transactions* **1994,** *90* (21), 3323-3330.
178. Furube, A.; Asahi, T.; Masuhara, H.; Yamashita, H.; Anpo, M., Direct observation of a picosecond charge separation process in photoexcited platinum-loaded TiO_2 particles by femtosecond diffuse reflectance spectroscopy. *Chemical physics letters* **2001,** *336* (5), 424-430.
179. Henglein, A., Small-particle research: physicochemical properties of extremely small colloidal metal and semiconductor particles. *Chemical Reviews* **1989,** *89* (8), 1861-1873.
180. Kolle, U.; Moser, J.; Gratzel, M., Dynamics of interfacial charge-transfer reactions in semiconductor dispersions. Reduction of cobaltoceniumdicarboxylate in colloidal TiO_2. *Inorganic chemistry* **1985,** *24* (14), 2253-2258.
181. Szczepankiewicz, S. H.; Colussi, A.; Hoffmann, M. R., Infrared spectra of photoinduced species on hydroxylated titania surfaces. *The Journal of Physical Chemistry B* **2000,** *104* (42), 9842-9850.
182. Bahnemann, D.; Henglein, A.; Lilie, J.; Spanhel, L., Flash photolysis observation of the absorption spectra of trapped positive holes and electrons in colloidal titanium dioxide. *The Journal of Physical Chemistry* **1984,** *88* (4), 709-711.
183. Martin, S. T.; Morrison, C. L.; Hoffmann, M. R., Photochemical mechanism of size-quantized vanadium-doped TiO_2 particles. *The Journal of Physical Chemistry* **1994,** *98* (51), 13695-13704.

184. Yang, X.; Tamai, N., How fast is interfacial hole transfer? In situ monitoring of carrier dynamics in anatase TiO_2 nanoparticles by femtosecond laser spectroscopy. *Physical Chemistry Chemical Physics* **2001,** *3* (16), 3393-3398.
185. Hoffmann, M. R.; Martin, S. T.; Choi, W.; Bahnemann, D. W., Environmental applications of semiconductor photocatalysis. *Chemical reviews* **1995,** *95* (1), 69-96.
186. Yamakata, A.; Ishibashi, T.-a.; Onishi, H., Water-and oxygen-induced decay kinetics of photogenerated electrons in TiO_2 and Pt/TiO_2: a time-resolved infrared absorption study. *The Journal of Physical Chemistry B* **2001,** *105* (30), 7258-7262.
187. Tamaki, Y.; Furube, A.; Katoh, R.; Murai, M.; Hara, K.; Arakawa, H.; Tachiya, M., Trapping dynamics of electrons and holes in a nanocrystalline TiO_2 film revealed by femtosecond visible/near-infrared transient absorption spectroscopy. *Comptes Rendus Chimie* **2006,** *9* (2), 268-274.
188. Tamaki, Y.; Furube, A.; Murai, M.; Hara, K.; Katoh, R.; Tachiya, M., Dynamics of efficient electron–hole separation in TiO_2 nanoparticles revealed by femtosecond transient absorption spectroscopy under the weak-excitation condition. *Physical Chemistry Chemical Physics* **2007,** *9* (12), 1453-1460.
189. Ohno, T.; Sarukawa, K.; Matsumura, M., Photocatalytic activities of pure rutile particles isolated from TiO_2 powder by dissolving the anatase component in HF solution. *The Journal of Physical Chemistry B* **2001,** *105* (12), 2417-2420.
190. Muggli, D. S.; Ding, L., Photocatalytic performance of sulfated TiO_2 and Degussa P-25 TiO_2 during oxidation of organics. *Applied Catalysis B: Environmental* **2001,** *32* (3), 181-194.
191. Bickley, R. I.; Gonzalez-Carreno, T.; Lees, J. S.; Palmisano, L.; Tilley, R. J., A structural investigation of titanium dioxide photocatalysts. *Journal of Solid State Chemistry* **1991,** *92* (1), 178-190.
192. Ohno, T.; Tokieda, K.; Higashida, S.; Matsumura, M., Synergism between rutile and anatase TiO_2 particles in photocatalytic oxidation of naphthalene. *Applied Catalysis A: General* **2003,** *244* (2), 383-391.
193. Hurum, D. C.; Agrios, A. G.; Gray, K. A.; Rajh, T.; Thurnauer, M. C., Explaining the enhanced photocatalytic activity of Degussa P25 mixed-phase TiO_2 using EPR. *The Journal of Physical Chemistry B* **2003,** *107* (19), 4545-4549.
194. Loddo, V.; Marci, G.; Palmisano, L.; Sclafani, A., Preparation and characterization of Al 2 O 3 supported TiO_2 catalysts employed for 4-nitrophenol photodegradation in aqueous medium. *Materials chemistry and physics* **1998,** *53* (3), 217-224.
195. Sclafani, A.; Herrmann, J., Comparison of the photoelectronic and photocatalytic activities of various anatase and rutile forms of titania in pure liquid organic phases and in aqueous solutions. *The Journal of Physical Chemistry* **1996,** *100* (32), 13655-13661.
196. Bessekhouad, Y.; Robert, D.; Weber, J., Preparation of TiO_2 nanoparticles by sol-gel route. *International journal of photoenergy* **2003,** *5* (3), 153-158.
197. Mills, A.; Elliott, N.; Hill, G.; Fallis, D.; Durrant, J. R.; Willis, R. L., Preparation and characterisation of novel thick sol–gel titania film photocatalysts. *Photochemical & Photobiological Sciences* **2003,** *2* (5), 591-596.
198. Zhang, H.; Banfield, J. F., Phase transformation of nanocrystalline anatase-to-rutile via combined interface and surface nucleation. *Journal of Materials Research* **2000,** *15* (02), 437-448.
199. Shi, Z.; Yan, L.; Jin, L.; Lu, X.; Zhao, G., The phase transformation behaviors of Sn^{2+}-doped Titania gels. *Journal of non-crystalline solids* **2007,** *353* (22), 2171-2178.
200. Suresh, C.; Biju, V.; Mukundan, P.; Warrier, K., Anatase to rutile transformation in sol-gel titania by modification of precursor. *Polyhedron* **1998,** *17* (18), 3131-3135.
201. Hu, L.; Yoko, T.; Kozuka, H.; Sakka, S., Effects of solvent on properties of sol-gel-derived TiO_2 coating films. *Thin solid films* **1992,** *219* (1-2), 18-23.
202. Asahi, R.; Morikawa, T.; Ohwaki, T.; Aoki, K.; Taga, Y., Visible-light photocatalysis in nitrogen-doped titanium oxides. *science* **2001,** *293* (5528), 269-271.
203. Yadav, H. M.; Otari, S. V.; Koli, V. B.; Mali, S. S.; Hong, C. K.; Pawar, S. H.; Delekar, S. D., Preparation and characterization of copper-doped anatase TiO_2 nanoparticles with visible

light photocatalytic antibacterial activity. *Journal of Photochemistry and Photobiology A: Chemistry* **2014,** *280*, 32-38.
204. Ho, W.; Jimmy, C. Y.; Lee, S., Low-temperature hydrothermal synthesis of S-doped TiO_2 with visible light photocatalytic activity. *Journal of solid state chemistry* **2006,** *179* (4), 1171-1176.
205. Li, D.; Haneda, H.; Labhsetwar, N. K.; Hishita, S.; Ohashi, N., Visible-light-driven photocatalysis on fluorine-doped TiO_2 powders by the creation of surface oxygen vacancies. *Chemical Physics Letters* **2005,** *401* (4), 579-584.
206. Kőrösi, L.; Papp, S.; Ménesi, J.; Illés, E.; Zöllmer, V.; Richardt, A.; Dékány, I., Photocatalytic activity of silver-modified titanium dioxide at solid–liquid and solid–gas interfaces. *Colloids and Surfaces A: Physicochemical and Engineering Aspects* **2008,** *319* (1), 136-142.
207. Etacheri, V.; Seery, M. K.; Hinder, S. J.; Pillai, S. C., Nanostructured $Ti_{1-x}S_xO_{2-y}N_y$ Heterojunctions for Efficient Visible-Light-Induced Photocatalysis. *Inorganic chemistry* **2012,** *51* (13), 7164-7173.
208. Koppenol, W.; Liebman, J. F., The oxidizing nature of the hydroxyl radical. A comparison with the ferryl ion (FeO^{2+}). *The journal of physical chemistry* **1984,** *88* (1), 99-101.
209. Serpone, N.; Pelizzetti, E., *Photocatalysis: fundamentals and applications*. Wiley-Interscience: 1989.
210. Chun, W.-J.; Ishikawa, A.; Fujisawa, H.; Takata, T.; Kondo, J. N.; Hara, M.; Kawai, M.; Matsumoto, Y.; Domen, K., Conduction and valence band positions of Ta_2O_5, TaON, and Ta_3N_5 by UPS and electrochemical methods. *The Journal of Physical Chemistry B* **2003,** *107* (8), 1798-1803.
211. Wang, L.; Wang, P.; Huang, B.; Ma, X.; Wang, G.; Dai, Y.; Zhang, X.; Qin, X., Synthesis of Mn-doped ZnS microspheres with enhanced visible light photocatalytic activity. *Applied Surface Science* **2017,** *391*, 557-564.
212. Chang, C.-J.; Chu, K.-W.; Hsu, M.-H.; Chen, C.-Y., Ni-doped ZnS decorated graphene composites with enhanced photocatalytic hydrogen-production performance. *International Journal of Hydrogen Energy* **2015,** *40* (42), 14498-14506.
213. Vinoth Kumar, J.; Saravanakumar, K.; Senthil Kumar, P.; Muthuraj, V., Visible Light Photocatalytic Activity of Rhombus Like α-Fe_2O_3 for Degradation of Organic Contaminants. *Energy and Environment Focus* **2016,** *5* (3), 222-228.
214. Huang, L. Y.; Zhang, R. X.; Sun, X. J.; Cheng, X. N. In *Synthesis and Characterization of g-C_3N_4/α-Fe_2O_3 Composites with Enhanced Photocatalytic Activity*, Key Engineering Materials, Trans Tech Publ: **2014**, 225-228.
215. Mahadik, M.; Shinde, S.; Mohite, V.; Kumbhar, S.; Rajpure, K.; Moholkar, A.; Kim, J.; Bhosale, C., Photoelectrocatalytic oxidation of Rhodamine B with sprayed α-Fe_2O_3 photocatalyst. *Materials express* **2013,** *3* (3), 247-255.
216. Pasternak, S.; Paz, Y., On the similarity and dissimilarity between photocatalytic water splitting and photocatalytic degradation of pollutants. *ChemPhysChem* **2013,** *14* (10), 2059-2070.
217. Bai, X.; Wang, L.; Zong, R.; Lv, Y.; Sun, Y.; Zhu, Y., Performance enhancement of ZnO photocatalyst via synergic effect of surface oxygen defect and graphene hybridization. *Langmuir* **2013,** *29* (9), 3097-3105.
218. Sun, J.-H.; Dong, S.-Y.; Wang, Y.-K.; Sun, S. P., Preparation and photocatalytic property of a novel dumbbell-shaped ZnO microcrystal photocatalyst. *Journal of Hazardous Materials* **2009,** *172* (2), 1520-1526.
219. Tian, C.; Zhang, Q.; Wu, A.; Jiang, M.; Liang, Z.; Jiang, B.; Fu, H., Cost-effective large-scale synthesis of ZnO photocatalyst with excellent performance for dye photodegradation. *Chemical Communications* **2012,** *48* (23), 2858-2860.
220. Wang, Y.; Shi, R.; Lin, J.; Zhu, Y., Enhancement of photocurrent and photocatalytic activity of ZnO hybridized with graphite-like C_3N_4. *Energy & Environmental Science* **2011,** *4* (8), 2922-2929.
221. Wu, C.; Shen, L.; Zhang, Y.-C.; Huang, Q., Solvothermal synthesis of Cr-doped ZnO nanowires with visible light-driven photocatalytic activity. *Materials Letters* **2011,** *65* (12), 1794-1796.

222. Xie, W.; Li, Y.; Sun, W.; Huang, J.; Xie, H.; Zhao, X., Surface modification of ZnO with Ag improves its photocatalytic efficiency and photostability. *Journal of Photochemistry and Photobiology A: chemistry* **2010,** *216* (2), 149-155.
223. Yang, L. Y.; Dong, S. Y.; Sun, J. H.; Feng, J. L.; Wu, Q. H.; Sun, S. P., Microwave-assisted preparation, characterization and photocatalytic properties of a dumbbell-shaped ZnO photocatalyst. *Journal of hazardous materials* **2010,** *179* (1), 438-443.
224. Ahmad, M.; Ahmed, E.; Zhang, Y.; Khalid, N.; Xu, J.; Ullah, M.; Hong, Z., Preparation of highly efficient Al-doped ZnO photocatalyst by combustion synthesis. *Current Applied Physics* **2013,** *13* (4), 697-704.
225. Sun, J. H.; Dong, S. Y.; Feng, J. L.; Yin, X. J.; Zhao, X. C., Enhanced sunlight photocatalytic performance of Sn-doped ZnO for Methylene Blue degradation. *Journal of Molecular Catalysis A: Chemical* **2011,** *335* (1), 145-150.
226. Xu, C.; Cao, L.; Su, G.; Liu, W.; Qu, X.; Yu, Y., Preparation, characterization and photocatalytic activity of Co-doped ZnO powders. *Journal of alloys and compounds* **2010,** *497* (1), 373-376.
227. Chen, G.; Li, F.; Fan, Y.; Luo, Y.; Li, D.; Meng, Q., A novel noble metal-free ZnS-WS_2/CdS composite photocatalyst for H_2 evolution under visible light irradiation. *Catalysis Communications* **2013,** *40*, 51-54.
228. Fu, J.; Chang, B.; Tian, Y.; Xi, F.; Dong, X., Novel C_3N_4–CdS composite photocatalysts with organic–inorganic heterojunctions: in situ synthesis, exceptional activity, high stability and photocatalytic mechanism. *Journal of Materials Chemistry A* **2013,** *1* (9), 3083-3090.
229. Hong, E.; Kim, D.; Kim, J. H., Heterostructured metal sulfide (ZnS–CuS–CdS) photocatalyst for high electron utilization in hydrogen production from solar water splitting. *Journal of Industrial and Engineering Chemistry* **2014,** *20* (5), 3869-3874.
230. Li, Q.; Guo, B.; Yu, J.; Ran, J.; Zhang, B.; Yan, H.; Gong, J. R., Highly efficient visible-light-driven photocatalytic hydrogen production of CdS-cluster-decorated graphene nanosheets. *Journal of the American Chemical Society* **2011,** *133* (28), 10878-10884.
231. Li, X.; Chen, J.; Li, H.; Li, J.; Xu, Y.; Liu, Y.; Zhou, J., Photoreduction of CO_2 to methanol over Bi_2S_3/CdS photocatalyst under visible light irradiation. *Journal of Natural Gas Chemistry* **2011,** *20* (4), 413-417.
232. Li, W.; Feng, C.; Dai, S.; Yue, J.; Hua, F.; Hou, H., Fabrication of sulfur-doped gC_3N_4/Au/CdS Z-scheme photocatalyst to improve the photocatalytic performance under visible light. *Applied Catalysis B: Environmental* **2015,** *168*, 465-471.
233. Wu, J.-C.; Zheng, J.; Wu, P.; Xu, R., Study of native defects and transition-metal (Mn, Fe, Co, and Ni) doping in a zinc-blende CdS photocatalyst by DFT and hybrid DFT calculations. *The Journal of Physical Chemistry C* **2011,** *115* (13), 5675-5682.
234. Yan, H.; Yang, J.; Ma, G.; Wu, G.; Zong, X.; Lei, Z.; Shi, J.; Li, C., Visible-light-driven hydrogen production with extremely high quantum efficiency on Pt–PdS/CdS photocatalyst. *Journal of Catalysis* **2009,** *266* (2), 165-168.
235. Yao, W.; Huang, C.; Muradov, N.; Ali, T., A novel Pd–Cr_2O_3/CdS photocatalyst for solar hydrogen production using a regenerable sacrificial donor. *international journal of hydrogen energy* **2011,** *36* (8), 4710-4715.
236. Zhang, W.; Wang, Y.; Wang, Z.; Zhong, Z.; Xu, R., Highly efficient and noble metal-free NiS/CdS photocatalysts for H_2 evolution from lactic acid sacrificial solution under visible light. *Chemical Communications* **2010,** *46* (40), 7631-7633.
237. Zhang, N.; Zhang, Y.; Pan, X.; Fu, X.; Liu, S.; Xu, Y. J., Assembly of CdS nanoparticles on the two-dimensional graphene scaffold as visible-light-driven photocatalyst for selective organic transformation under ambient conditions. *The Journal of Physical Chemistry C* **2011,** *115* (47), 23501-23511.
238. Cai, Q.; Hu, Z.; Zhang, Q.; Li, B.; Shen, Z., Fullerene (C60)/CdS nanocomposite with enhanced photocatalytic activity and stability. *Applied Surface Science* **2017**.
239. Wang, Q.; Lian, J.; Ma, Q.; Zhang, S.; He, J.; Zhong, J.; Li, J.; Huang, H.; Su, B., Preparation of carbon spheres supported CdS photocatalyst for enhancement its photocatalytic H 2 evolution. *Catalysis Today* **2017,** *281*, 662-668.

240. Yue, Z.; Liu, A.; Zhang, C.; Huang, J.; Zhu, M.; Du, Y.; Yang, P., Noble-metal-free hetero-structural CdS/Nb_2O_5/N-doped-graphene ternary photocatalytic system as visible-light-driven photocatalyst for hydrogen evolution. *Applied Catalysis B: Environmental* **2017,** *201*, 202-210.
241. Ning, X.; Meng, S.; Fu, X.; Ye, X.; Chen, S., Efficient utilization of photogenerated electrons and holes for photocatalytic selective organic syntheses in one reaction system using a narrow band gap CdS photocatalyst. *Green Chemistry* **2016,** *18* (12), 3628-3639.
242. Yoo, P. S.; Reddy, D. A.; Jia, Y.; Bae, S. E.; Huh, S.; Liu, C., Magnetic core-shell $ZnFe_2O_4$/ZnS nanocomposites for photocatalytic application under visible light. *Journal of Colloid and Interface Science* **2017,** *486*, 136-143.
243. Kong, L.; Li, Z.; Huang, S.; Jia, J.; Li, L., Boosting photocatalytic performance and stability of $CuInS_2$/ZnS-TiO_2 heterostructures *via* sol-gel processed integrate amorphous titania gel. *Applied Catalysis B: Environmental* **2017,** *204*, 403-410.
244. Madkour, M.; Al Sagheer, F., Au/ZnS and Ag/ZnS nanoheterostructures as regenerated nanophotocatalysts for photocatalytic degradation of organic dyes. *Optical Materials Express* **2017,** *7* (1), 158-169.
245. Samanta, D.; Chanu, T. I.; Chatterjee, S., Citrus limetta juice as capping agent in hydrothermal synthesis of ZnS nanosphere for photocatalytic activity. *Materials Research Bulletin* **2017,** *88*, 85-90.
246. Lee, G.-J.; Anandan, S.; Masten, S. J.; Wu, J. J., Photocatalytic hydrogen evolution from water splitting using Cu doped ZnS microspheres under visible light irradiation. *Renewable Energy* **2016,** *89*, 18-26.
247. Chang, C. J.; Chu, K.-W., ZnS/polyaniline composites with improved dispersing stability and high photocatalytic hydrogen production activity. *International Journal of Hydrogen Energy* **2016,** *41* (46), 21764-21773.
248. Chang, C. J.; Huang, K. L.; Chen, J. K.; Chu, K. W.; Hsu, M. H., Improved photocatalytic hydrogen production of ZnO/ZnS based photocatalysts by Ce doping. *Journal of the Taiwan Institute of Chemical Engineers* **2015,** *55*, 82-89.
249. Suyana, P.; Kumar, S. N.; Kumar, B. D.; Nair, B. N.; Pillai, S. C.; Mohamed, A. P.; Warrier, K.; Hareesh, U., Antifungal properties of nanosized ZnS particles synthesised by sonochemical precipitation. *RSC Advances* **2014,** *4* (17), 8439-8445.
250. Eyasu, A.; Yadav, O.; Bachheti, R., Photocatalytic degradation of methyl orange dye using Cr-doped ZnS nanoparticles under visible radiation. *Int. J. Chem. Tech. Res* **2013,** *5* (4), 1452-1461.
251. Nishimoto, S.; Bhushan, B., Bioinspired self-cleaning surfaces with superhydrophobicity, superoleophobicity, and superhydrophilicity. *RCS Advances* **2013,** *3* (3), 671-690.
252. Pillai, S. C.; McGuinness, N. B.; Byrne, C.; Han, C.; Lalley, J.; Nadagouda, M. N.; Falaras, P.; Kontos, A. G.; Gracia-Pinilla, M. A.; OShea, K; Mangalaraja, R. V.,Photocatalysis as an effective advanced oxidation process. **2017**, 333-381.
253. Cebeci, F. Ç.; Wu, Z.; Zhai, L.; Cohen, R. E.; Rubner, M. F., Nanoporosity-driven superhydrophilicity: a means to create multifunctional antifogging coatings. **2006,** *22* (6), 2856-2862.
254. Bayati, M.; Molaei, R.; Golestani-Fard, F., Enhancing photoinduced hydrophilicity of micro arc oxidized TiO_2 nanostructured porous layers by V-doping. **2011,** *373* (1-3), 51-60.
255. Wang, J. J.; Wang, D. S.; Wang, J.; Zhao, W. L.; Wang, C. W., High transmittance and superhydrophilicity of porous TiO_2/SiO_2 bi-layer films without UV irradiation. **2011,** *205* (12), 3596-3599.
256. Midtdal, K.; Jelle, B. P., Self-cleaning glazing products: A state-of-the-art review and future research pathways. **2013,** *109*, 126-141.
257. Malato, S.; Fernández-Ibáñez, P.; Maldonado, M.; Blanco, J.; Gernjak, W., Decontamination and disinfection of water by solar photocatalysis: recent overview and trends. *Catalysis Today* **2009,** *147* (1), 1-59.

258. Podporska-Carroll, J.; Panaitescu, E.; Quilty, B.; Wang, L.; Menon, L.; Pillai, S. C., Antimicrobial properties of highly efficient photocatalytic TiO_2 nanotubes. *Applied Catalysis B: Environmental* **2015,** *176*, 70-75.
259. Synnott, D. W.; Seery, M. K.; Hinder, S. J.; Michlits, G.; Pillai, S. C., Anti-bacterial activity of indoor-light activated photocatalysts. *Applied Catalysis B: Environmental* **2013,** *130*, 106-111.
260. Byrne, J. A.; Fernandez-Ibanez, P. A.; Dunlop, P. S.; Alrousan, D.; Hamilton, J. W., Photocatalytic enhancement for solar disinfection of water: a review. *International Journal of Photoenergy* **2011,** *2011*.
261. Dunnill, C. W.; Ansari, Z.; Kafizas, A.; Perni, S.; Morgan, D. J.; Wilson, M.; Parkin, I. P., Visible light photocatalysts - N-doped TiO_2 by sol–gel, enhanced with surface bound silver nanoparticle islands. *Journal of Materials Chemistry* **2011,** *21* (32), 11854-11861.
262. Wu, P.; Xie, R.; Imlay, K.; Shang, J. K., Visible-light-induced bactericidal activity of titanium dioxide codoped with nitrogen and silver. *Environmental science & technology* **2010,** *44* (18), 6992-6997.
263. Ashkarran, A. A.; Hamidinezhad, H.; Haddadi, H.; Mahmoudi, M., ,ouble-doped TiO_2 nanoparticles as an efficient visible-light-active photocatalyst and antibacterial agent under solar simulated light. *Applied Surface Science* **2014,** *301*, 338-345.
264. Yu, J. C.; Ho, W.; Yu, J.; Yip, H.; Wong, P. K.; Zhao, J., Efficient visible-light-induced photocatalytic disinfection on sulfur-doped nanocrystalline titania. *Environmental science & technology* **2005,** *39* (4), 1175-1179.
265. Leyland, N. S.; Podporska-Carroll, J.; Browne, J.; Hinder, S. J.; Quilty, B.; Pillai, S. C., Highly Efficient F, Cu doped TiO_2 anti-bacterial visible light active photocatalytic coatings to combat hospital-acquired infections. *Scientific Reports* **2016,** *6*, 24770.
266. Rengifo-Herrera, J.; Mielczarski, E.; Mielczarski, J.; Castillo, N.; Kiwi, J.; Pulgarin, C., Escherichia coli inactivation by N, S co-doped commercial TiO_2 powders under UV and visible light. *Applied Catalysis B: Environmental* **2008,** *84* (3), 448-456.
267. Rengifo-Herrera, J.; Pierzchała, K.; Sienkiewicz, A.; Forro, L.; Kiwi, J.; Pulgarin, C., Abatement of organics and Escherichia coli by N, S co-doped TiO_2 under UV and visible light. Implications of the formation of singlet oxygen ($^1O_2$) under visible light. *Applied Catalysis B: Environmental* **2009,** *88* (3), 398-406.
268. Rengifo-Herrera, J.; Kiwi, J.; Pulgarin, C., N, S co-doped and N-doped Degussa P-25 powders with visible light response prepared by mechanical mixing of thiourea and urea. Reactivity towards *E. coli* inactivation and phenol oxidation. *Journal of Photochemistry and Photobiology A: Chemistry* **2009,** *205* (2), 109-115.
269. Rengifo-Herrera, J. A.; Pulgarin, C., Photocatalytic activity of N, S co-doped and N-doped commercial anatase TiO_2 powders towards phenol oxidation and E. coli inactivation under simulated solar light irradiation. *Solar Energy* **2010,** *84* (1), 37-43.
270. Petrie, B.; Barden, R.; Kasprzyk-Hordern, B., A review on emerging contaminants in wastewaters and the environment: current knowledge, understudied areas and recommendations for future monitoring. *Water research* **2015,** *72*, 3-27.
271. Cesaro, A.; Belgiorno, V., Removal of endocrine disruptors from urban wastewater by advanced oxidation processes (AOPs): a review. *The Open Biotechnology Journal* **2016,** *10* (1).
272. Kumar, E.; Holt, W. V., Impacts of endocrine disrupting chemicals on reproduction in wildlife. In *Reproductive Sciences in Animal Conservation*, Springer: 2014; pp 55-70.
273. Hughes, S. R.; Kay, P.; Brown, L. E., Global synthesis and critical evaluation of pharmaceutical data sets collected from river systems. *Environmental science & technology* **2012,** *47* (2), 661-677.
274. Nakada, N.; Hanamoto, S.; Jürgens, M. D.; Johnson, A. C.; Bowes, M. J.; Tanaka, H., Assessing the population equivalent and performance of wastewater treatment through the ratios of pharmaceuticals and personal care products present in a river basin: Application to the River Thames basin, UK. *Science of the Total Environment* **2017,** *575*, 1100-1108.
275. Kay, P.; Hughes, S. R.; Ault, J. R.; Ashcroft, A. E.; Brown, L. E., Widespread, routine occurrence of pharmaceuticals in sewage effluent, combined sewer overflows and receiving waters. *Environmental Pollution* **2017,** *220*, 1447-1455.

276. Gaw, S.; Thomas, K. V.; Hutchinson, T. H., Sources, impacts and trends of pharmaceuticals in the marine and coastal environment. *Phil. Trans. R. Soc. B* **2014,** *369* (1656), 20130572.
277. Alvarez-Corena, J. R.; Bergendahl, J. A.; Hart, F. L., Advanced oxidation of five contaminants in water by UV/TiO_2 : Reaction kinetics and byproducts identification. *Journal of Environmental Management* **2016,** *181*, 544-551.
278. Pino, E.; Encinas, M. V., Photocatalytic degradation of chlorophenols on TiO_2-325mesh and TiO_2-P25. An extended kinetic study of photodegradation under competitive conditions. *Journal of Photochemistry and Photobiology A: Chemistry* **2012,** *242*, 20-27.
279. Miranda-García, N.; Suárez, S.; Sánchez, B.; Coronado, J. M.; Malato, S.; Maldonado, M. I., Photocatalytic degradation of emerging contaminants in municipal wastewater treatment plant effluents using immobilized TiO_2 in a solar pilot plant. *Applied Catalysis B: Environmental* **2011,** *103* (3–4), 294-301.
280. Barndõk, H.; Hermosilla, D.; Han, C.; Dionysiou, D. D.; Negro, C.; Blanco, Á., Degradation of 1, 4-dioxane from industrial wastewater by solar photocatalysis using immobilized NF-TiO_2 composite with monodisperse TiO_2 nanoparticles. *Applied Catalysis B: Environmental* **2016,** *180*, 44-52.
281. Barndõk, H.; Blanco, L.; Hermosilla, D.; Blanco, Á., Heterogeneous photo-Fenton processes using zero valent iron microspheres for the treatment of wastewaters contaminated with 1, 4-dioxane. *Chemical Engineering Journal* **2016,** *284*, 112-121.
282. Adams, C. D.; Scanlan, P. A.; Secrist, N. D., Oxidation and biodegradability enhancement of 1, 4-dioxane using hydrogen peroxide and ozone. *Environmental science & technology* **1994,** *28* (11), 1812-1818.
283. Choi, J. Y.; Lee, Y. J.; Shin, J.; Yang, J. W., Anodic oxidation of 1, 4-dioxane on boron-doped diamond electrodes for wastewater treatment. *Journal of hazardous materials* **2010,** *179* (1), 762-768.
284. Zenker, M. J.; Borden, R. C.; Barlaz, M. A., Occurrence and treatment of 1, 4-dioxane in aqueous environments. *Environmental Engineering Science* **2003,** *20* (5), 423-432.
285. Mohr, T. K.; Stickney, J. A.; DiGuiseppi, W. H., *Environmental investigation and remediation: 1, 4-dioxane and other solvent stabilizers*. CRC Press: 2016.
286. (ECB), E. C. B., E.U. risk assessment report: 1,4-dioxane, ISBN 92-894-1252-6, Second Priority List 21 (**2002**) 1-129 Office for Official Publications of the European Communities, Luxembourg.
287. Skadsen, J.; Rice, B.; Meyering, D., The occurrence and fate of pharmaceuticals, personal care products and endocrine disrupting compounds in a municipal water use cycle: a case study in the city of Ann Arbor. *Inc., City of Ann Arbor* **2004**, 22.
288. Han, T. H.; Han, J. S.; So, M. H.; Seo, J. W.; Ahn, C. M.; Min, D. H.; Yoo, Y. S.; Cha, D. K.; Kim, C. G., The removal of 1, 4-dioxane from polyester manufacturing process wastewater using an up-flow biological aerated filter (UBAF) packed with tire chips. *Journal of Environmental Science and Health, Part A* **2012,** *47* (1), 117-129.
289. Zenker, M. J.; Borden, R. C.; Barlaz, M. A., Biodegradation of 1, 4-dioxane using trickling filter. *Journal of environmental engineering* **2004,** *130* (9), 926-931.
290. Min, B. K.; Heo, J. E.; Youn, N. K.; Joo, O. S.; Lee, H.; Kim, J. H.; Kim, H. S., Tuning of the photocatalytic 1, 4-dioxane degradation with surface plasmon resonance of gold nanoparticles on titania. *Catalysis Communications* **2009,** *10* (5), 712-715.
291. Hill, R. R.; Jeffs, G. E.; Roberts, D. R., Photocatalytic degradation of 1, 4-dioxane in aqueous solution. *Journal of Photochemistry and Photobiology A: Chemistry* **1997,** *108* (1), 55-58.
292. Jasmann, J. R.; Borch, T.; Sale, T. C.; Blotevogel, J., Advanced electrochemical oxidation of 1, 4-dioxane via dark catalysis by novel titanium dioxide (TiO_2) pellets. *Environmental science & technology* **2016,** *50* (16), 8817-8826.
293. Spurr, R. A.; Myers, H., Quantitative analysis of anatase-rutile mixtures with an X-ray diffractometer. *Analytical Chemistry* **1957,** *29* (5), 760-762.
294. Scherrer, P., Determination of the internal structure and size of colloid particles by X-rays. In *Colloid Chemistry A textbook*, Springer, Berlin, Heidelberg. **1912**, 387-409.

295. Etacheri, V.; Seery, M. K.; Hinder, S. J.; Pillai, S. C., Highly Visible Light Active $TiO_{2-x}N_x$ Heterojunction Photocatalysts. *Chemistry of Materials* **2010,** *22* (13), 3843-3853.
296. Rao, C.; Turner, A.; Honig, J., Some observations concerning the effect of impurities on the anatase-rutile transition. *Journal of Physics and Chemistry of Solids* **1959,** *11* (1), 173-175.
297. Reidy, D. J.; Holmes, J. D.; Nagle, C.; Morris, M. A., A highly thermally stable anatase phase prepared by doping with zirconia and silica coupled to a mesoporous type synthesis technique. *Journal of Materials Chemistry* **2005,** *15* (34), 3494-3500.
298. Baiju, K. V.; Sibu, C. P.; Rajesh, K.; Pillai, P. K.; Mukundan, P.; Warrier, K. G. K.; Wunderlich, W., An aqueous sol–gel route to synthesize nanosized lanthana-doped titania having an increased anatase phase stability for photocatalytic application. *Materials Chemistry and Physics* **2005,** *90* (1), 123-127.
299. Fagan, R.; Synnott, D. W.; McCormack, D. E.; Pillai, S. C., An Effective Method for the Preparation of High Temperature Stable Anatase TiO_2 Photocatalysts. *Applied Surface Science* **2016**, *371*, 447-452.
300. Fagan, R.; McCormack, D. E.; Hinder, S.; Pillai, S. C., Improved high temperature stability of anatase TiO_2 photocatalysts by N, F, P co-doping. *Materials & Design* **2016,** *96*, 44-53.
301. Fagan, R.; McCormack, D. E.; Hinder, S. J.; Pillai, S. C., Photocatalytic Properties of g-C_3N_4–TiO_2 Heterojunctions under UV and Visible Light Conditions. *Materials* **2016,** *9* (4), 286.
302. Maruyama, S. A.; Lisboa, F. d. S.; Ramos, L. P.; Wypych, F., Alkaline earth layered benzoates as reusable heterogeneous catalysts for the methyl esterification of benzoic acid. *Química Nova* **2012,** *35* (8), 1510-1516.
303. Ohsaka, T.; Izumi, F.; Fujiki, Y., Raman spectrum of anatase, TiO_2. *Journal of Raman spectroscopy* **1978,** *7* (6), 321-324.
304. Tang, H.; Prasad, K.; Sanjines, R.; Schmid, P.; Levy, F., Electrical and optical properties of TiO_2 anatase thin films. *Journal of applied physics* **1994,** *75* (4), 2042-2047.
305. Berger, H.; Tang, H.; Lévy, F., Growth and Raman spectroscopic characterization of TiO_2 anatase single crystals. *Journal of crystal growth* **1993,** *130* (1-2), 108-112.
306. Shi, Z.; Ye, X.; Liang, K.; Gu, S.; Pan, F., XPS analysis of light elements (C, N) remaining in sol-gel derived TiO_2 films. *Journal of materials science letters* **2003,** *22* (18), 1255-1258.
307. Yang, J.; Bai, H.; Tan, X.; Lian, J., IR and XPS investigation of visible-light photocatalysis—Nitrogen–carbon-doped TiO_2 film. *Applied Surface Science* **2006,** *253* (4), 1988-1994.
308. Etacheri, V.; Haik, O.; Goffer, Y.; Roberts, G. A.; Stefan, I. C.; Fasching, R.; Aurbach, D., Effect of fluoroethylene carbonate (FEC) on the performance and surface chemistry of Si-nanowire Li-ion battery anodes. *Langmuir* **2011,** *28* (1), 965-976.
309. Akhavan, O.; Ghaderi, E.; Akhavan, A., Size-dependent genotoxicity of graphene nanoplatelets in human stem cells. *Biomaterials* **2012,** *33* (32), 8017-8025.
310. Zeleňák, V.; Vargová, Z.; Györyová, K., Correlation of infrared spectra of zinc (II) carboxylates with their structures. *Spectrochimica Acta Part A: Molecular and Biomolecular Spectroscopy* **2007,** *66* (2), 262-272.
311. Guan, X. H..; Chen, G. H.; Shang, C., ATR-FTIR and XPS study on the structure of complexes formed upon the adsorption of simple organic acids on aluminum hydroxide. *Journal of Environmental Sciences* **2007,** *19* (4), 438-443.
312. Nara, M.; Tasumi, M.; Tanokura, M.; Hiraoki, T.; Yazawa, M.; Tsutsumi, A., Infrared studies of interaction between metal ions and Ca^{2+}-binding proteins Marker bands for identifying the types of coordination of the side-chain COO^- groups to metal ions in pike parvalbumin (pI= 4.10). *FEBS letters* **1994,** *349* (1), 84-88.
313. Nakamoto, K., *Infrared and Raman spectra of inorganic and coordination compounds*. Wiley Online Library: **1986**.
314. Czakis-Sulikowska, D.; Czylkowska, A.; Malinowska, A., Thermal and other properties of new 4, 4'-bipyridine-trichloroacetato complexes of Mn (II), Ni (II) and Zn (II). *Journal of thermal analysis and calorimetry* **2002,** *67* (3), 667-678.

315. Deacon, G.; Phillips, R., Relationships between the carbon-oxygen stretching frequencies of carboxylato complexes and the type of carboxylate coordination. *Coordination Chemistry Reviews* **1980,** *33* (3), 227-250.
316. Lewandowski, W.; Kalinowska, M.; Lewandowska, H., The influence of metals on the electronic system of biologically important ligands. Spectroscopic study of benzoates, salicylates, nicotinates and isoorotates. Review. *Journal of inorganic biochemistry* **2005,** *99* (7), 1407-1423.
317. Manhas, B.; Trikha, A., Relationships between the direction of shifts in the carbon-oxygen stretching frequencies of carboxylato complexes and the type of carboxylate coordination. *Journal of the Indian Chemical Society* **1982,** *59* (2), 315-319.
318. Bezrodna, T.; Gavrilko, T.; Puchkovska, G.; Shimanovska, V.; Baran, J.; Marchewka, M., Spectroscopic study of TiO_2 (rutile)–benzophenone heterogeneous systems. *Journal of molecular structure* **2002,** *614* (1), 315-324.
319. Urlaub, R.; Posset, U.; Thull, R., FT-IR spectroscopic investigations on sol–gel-derived coatings from acid-modified titanium alkoxides. *Journal of non-crystalline solids* **2000,** *265* (3), 276-284.
320. Verma, A.; Samanta, S.; Bakhshi, A.; Agnihotry, S., Effect of stabilizer on structural, optical and electrochemical properties of sol–gel derived spin coated TiO_2 films. *Solar energy materials and solar cells* **2005,** *88* (1), 47-64.
321. Guillard, C.; Beaugiraud, B.; Dutriez, C.; Herrmann, J. M.; Jaffrezic, H.; Jaffrezic-Renault, N.; Lacroix, M., Physicochemical properties and photocatalytic activities of TiO_2-films prepared by sol–gel methods. *Applied Catalysis B: Environmental* **2002,** *39* (4), 331-342.
322. Kung, H. H.; Ko, E. I., Preparation of oxide catalysts and catalyst supports—a review of recent advances. *The Chemical Engineering Journal and the Biochemical Engineering Journal* **1996,** *64* (2), 203-214.
323. Woo, S.; Kim, W.; Kim, S.; Rhee, C., Photocatalytic behaviors of transition metal ion doped TiO_2 powder synthesized by mechanical alloying. *Materials Science and Engineering: A* **2007,** *449*, 1151-1154.
324. Devi, L. G.; Murthy, B. N.; Kumar, S. G., Photocatalytic activity of V^{5+}, Mo^{6+} and Th^{4+} doped polycrystalline TiO_2 for the degradation of chlorpyrifos under UV/solar light. *Journal of molecular catalysis A: Chemical* **2009,** *308* (1), 174-181.
325. Sobana, N.; Muruganadham, M.; Swaminathan, M., Nano-Ag particles doped TiO_2 for efficient photodegradation of direct azo dyes. *Journal of Molecular Catalysis A: Chemical* **2006,** *258* (1), 124-132.
326. Yu, H.; Wang, X.; Sun, H.; Huo, M., Photocatalytic degradation of malathion in aqueous solution using an Au–Pd–TiO_2 nanotube film. *Journal of hazardous materials* **2010,** *184* (1), 753-758.
327. Zhang, M.; An, T.; Liu, X.; Hu, X.; Sheng, G.; Fu, J., Preparation of a high-activity ZnO/TiO_2 photocatalyst via homogeneous hydrolysis method with low temperature crystallization. *Materials Letters* **2010,** *64* (17), 1883-1886.
328. Tian, J.; Chen, L.; Yin, Y.; Wang, X.; Dai, J.; Zhu, Z.; Liu, X.; Wu, P., Photocatalyst of TiO_2/ZnO nano composite film: preparation, characterization, and photodegradation activity of methyl orange. *Surface and Coatings Technology* **2009,** *204* (1), 205-214.
329. Qian, S.; Wang, C.; Liu, W.; Zhu, Y.; Yao, W.; Lu, X., An enhanced CdS/TiO_2 photocatalyst with high stability and activity: effect of mesoporous substrate and bifunctional linking molecule. *Journal of Materials Chemistry* **2011,** *21* (13), 4945-4952.
330. Tristão, J. C.; Magalhães, F.; Corio, P.; Sansiviero, M. T. C., Electronic characterization and photocatalytic properties of CdS/TiO_2 semiconductor composite. *Journal of Photochemistry and Photobiology A: Chemistry* **2006,** *181* (2), 152-157.
331. Xie, Y.; Li, Y.; Zhao, X., Low-temperature preparation and visible-light-induced catalytic activity of anatase F–N-codoped TiO_2. *Journal of Molecular Catalysis A: Chemical* **2007,** *277* (1), 119-126.
332. Liu, S.; Yu, J.; Wang, W., Effects of annealing on the microstructures and photoactivity of fluorinated N-doped TiO_2. *Physical Chemistry Chemical Physics* **2010,** *12* (38), 12308-12315.

333. Periyat, P.; McCormack, D. E.; Hinder, S. J.; Pillai, S. C., One-pot synthesis of anionic (nitrogen) and cationic (sulfur) codoped high-temperature stable, visible light active, anatase photocatalysts. *The Journal of Physical Chemistry C* **2009,** *113* (8), 3246-3253.
334. Chen, D.; Jiang, Z.; Geng, J.; Wang, Q.; Yang, D., Carbon and nitrogen co-doped TiO_2 with enhanced visible-light photocatalytic activity. *Industrial & engineering chemistry research* **2007,** *46* (9), 2741-2746.
335. Dong, F.; Zhao, W.; Wu, Z., Characterization and photocatalytic activities of C, N and S co-doped TiO_2 with 1D nanostructure prepared by the nano-confinement effect. *Nanotechnology* **2008,** *19* (36), 365607.
336. Yoong, L.; Chong, F. K.; Dutta, B. K., Development of copper-doped TiO_2 photocatalyst for hydrogen production under visible light. *Energy* **2009,** *34* (10), 1652-1661.
337. Li, X.; Li, F.; Yang, C.; Ge, W., Photocatalytic activity of WO_x-TiO_2 under visible light irradiation. *Journal of Photochemistry and Photobiology A: Chemistry* **2001,** *141* (2), 209-217.
338. Kwon, Y. T.; Song, K. Y.; Lee, W. I.; Choi, G. J.; Do, Y. R., Photocatalytic behavior of WO_3-loaded TiO_2 in an oxidation reaction. *Journal of Catalysis* **2000,** *191* (1), 192-199.
339. Ramos-Delgado, N.; Hinojosa-Reyes, L.; Guzman-Mar, I.; Gracia-Pinilla, M.; Hernández-Ramírez, A., Synthesis by sol–gel of WO_3/TiO_2 for solar photocatalytic degradation of malathion pesticide. *Catalysis today* **2013,** *209*, 35-40.
340. Smith, W.; Zhao, Y., Enhanced photocatalytic activity by aligned WO_3/TiO_2 two-layer nanorod arrays. *The Journal of Physical Chemistry C* **2008,** *112* (49), 19635-19641.
341. Liu, J.; Zhang, J.; Yue, G.; Lu, X.; Hu, Z.; Zhu, Y., W-doped TiO_2 photoanode for high performance perovskite solar cell. *Electrochimica Acta* **2016,** *195*, 143-149.
342. Couselo, N.; García Einschlag, F. S.; Candal, R. J.; Jobbágy, M., Tungsten-doped TiO_2 vs pure TiO_2 photocatalysts: effects on photobleaching kinetics and mechanism. *The Journal of Physical Chemistry C* **2008,** *112* (4), 1094-1100.
343. Sathasivam, S.; Bhachu, D. S.; Lu, Y.; Chadwick, N.; Althabaiti, S. A.; Alyoubi, A. O.; Basahel, S. N.; Carmalt, C. J.; Parkin, I. P., Tungsten doped TiO_2 with enhanced photocatalytic and optoelectrical properties via aerosol assisted chemical vapor deposition. *Scientific reports* **2015,** *5*, 10952.
344. Azadi, S.; Karimi-Jashni, A.; Javadpour, S., Photocatalytic Treatment of Landfill Leachate Using W-Doped TiO_2 Nanoparticles. *Journal of Environmental Engineering* **2017,** *143* (9), 04017049.
345. Álvaro, R. J.; Diana, N. D.; María, A. M., Effect of Cu on Optical Properties of TiO_2 Nanoparticles. **2017**.
346. Ullah, I.; Haider, A.; Khalid, N.; Ali, S.; Ahmed, S.; Khan, Y.; Ahmed, N.; Zubair, M., Tuning the band gap of TiO_2 by tungsten doping for efficient UV and visible photodegradation of Congo red dye. *Spectrochimica Acta Part A: Molecular and Biomolecular Spectroscopy* **2018**.
347. Bamwenda, G. R.; Arakawa, H., The visible light induced photocatalytic activity of tungsten trioxide powders. *Applied Catalysis A: General* **2001,** *210* (1), 181-191.
348. Yan, X.; Zong, X.; Lu, G. Q.; Wang, L., Ordered mesoporous tungsten oxide and titanium oxide composites and their photocatalytic degradation behavior. *Progress in Natural Science: Materials International* **2012,** *22* (6), 654-660.
349. Riboni, F.; Bettini, L. G.; Bahnemann, D. W.; Selli, E., WO_3–TiO_2 vs. TiO_2 photocatalysts: effect of the W precursor and amount on the photocatalytic activity of mixed oxides. *Catalysis Today* **2013,** *209*, 28-34.
350. Ismail, A. A.; Abdelfattah, I.; Helal, A.; Al-Sayari, S. A.; Robben, L.; Bahnemann, D. W., Ease synthesis of mesoporous WO_3–TiO_2 nanocomposites with enhanced photocatalytic performance for photodegradation of herbicide imazapyr under visible light and UV illumination. *Journal of Hazardous Materials* **2016,** *307*, 43-54.
351. Eibl, S.; Gates, B.; Knözinger, H., Structure of WO_x/TiO_2 Catalysts Prepared from Hydrous Titanium Oxide Hydroxide: Influence of Preparation Parameters. *Langmuir* **2001,** *17* (1), 107-115.
352. Szilágyi, I. M.; Santala, E.; Heikkilä, M.; Pore, V.; Kemell, M.; Nikitin, T.; Teucher, G.; Firkala, T.; Khriachtchev, L.; Räsänen, M., Photocatalytic properties of WO_3/TiO_2 core/shell

nanofibers prepared by electrospinning and atomic layer deposition. *Chemical Vapor Deposition* **2013,** *19* (4-6), 149-155.
353. Molenda, J.; Kubik, A., Transport properties and reactivity of tungsten trioxide. *Solid State Ionics* **1999,** *117* (1), 57-64.
354. Sahle, W.; Nygren, M., Electrical conductivity and high resolution electron microscopy studies of WO_{3-x} crystals with $0 \leq x \leq 0.28$. *Journal of Solid State Chemistry* **1983,** *48* (2), 154-160.
355. Aird, A.; Salje, E. K., Sheet superconductivity in twin walls: experimental evidence of. *Journal of Physics: Condensed Matter* **1998,** *10* (22), L377.
356. Ayyappan, S.; Subbanna, G.; Rao, C., Novel Metastable Structures of WO_3, MoO_3 and $W_{1-x}Mo_xO_3$ Obtained by the Deintercalation of Layered Amine Adducts. *Chemistry-A European Journal* **1995,** *1* (3), 165-170.
357. Zhu, Y.; Manthiram, A., New route for the synthesis of tungsten oxide bronzes. *Journal of Solid State Chemistry* **1994,** *110* (1), 187-189.
358. Siedle, A. R.; Wood, T. E.; Brostrom, M. L.; Koskenmaki, D. C.; Montez, B.; Oldfield, E., Solid-state polymerization of molecular metal oxide clusters: aluminum 12-tungstophosphate. *Journal of the American Chemical Society* **1989,** *111* (5), 1665-1669.
359. Kim, J. H.; Kim, K. L., A study of preparation of tungsten nitride catalysts with high surface area. *Applied Catalysis A: General* **1999,** *181* (1), 103-111.
360. Pintér, Z.; Sassi, Z.; Kornely, S.; Pion, C.; Perczel, I.; Kovács, K.; Bene, R.; Bureau, J.; Réti, F., Thermal behaviour of WO_3 and WO_3/TiO_2 materials. *Thin Solid Films* **2001,** *391* (2), 243-246.
361. Ke, D.; Liu, H.; Peng, T.; Liu, X.; Dai, K., Preparation and photocatalytic activity of WO_3/TiO_2 nanocomposite particles. *Materials Letters* **2008,** *62* (3), 447-450.
362. Saepurahman; Abdullah, M. A.; Chong, F. K., Preparation and characterization of tungsten-loaded titanium dioxide photocatalyst for enhanced dye degradation. *Journal of Hazardous Materials* **2010,** *176* (1), 451-458.
363. Szilágyi, I. M.; Madarász, J.; Pokol, G. r.; Király, P.; Tárkányi, G.; Saukko, S.; Mizsei, J.; Tóth, A. L.; Szabó, A.; Varga-Josepovits, K., Stability and controlled composition of hexagonal WO_3. *Chemistry of Materials* **2008,** *20* (12), 4116-4125.
364. Blackman, C. S.; Parkin, I. P., Atmospheric pressure chemical vapor deposition of crystalline monoclinic WO_3 and WO_{3-x} thin films from reaction of WCl_6 with O-containing solvents and their photochromic and electrochromic properties. *Chemistry of materials* **2005,** *17* (6), 1583-1590.
365. Slink, W. E.; DeGroot, P. B., Vanadium-titanium oxide catalysts for oxidation of butene to acetic acid. *Journal of Catalysis* **1981,** *68* (2), 423-432.
366. Shannon, R. D., Revised effective ionic radii and systematic studies of interatomic distances in halides and chalcogenides. *Acta crystallographica section A: crystal physics, diffraction, theoretical and general crystallography* **1976,** *32* (5), 751-767.
367. Hashimoto, S.; Murata, A.; Sakurada, T.; Tanaka, A., Alternation of Ti *2p* XPS spectrum for TiO_2 by Ar ion bombardment. *Journal of Surface Analysis* **2002,** *9* (3), 459-462.
368. Santara, B.; Giri, P.; Imakita, K.; Fujii, M., Microscopic origin of lattice contraction and expansion in undoped rutile TiO_2 nanostructures. *Journal of Physics D: Applied Physics* **2014,** *47* (21), 215302.
369. Neville, E. M.; Mattle, M. J.; Loughrey, D.; Rajesh, B.; Rahman, M.; MacElroy, J. D.; Sullivan, J. A.; Thampi, K. R., Carbon-doped TiO_2 and carbon, tungsten-codoped TiO_2 through sol–gel processes in the presence of melamine borate: reflections through photocatalysis. *The Journal of Physical Chemistry C* **2012,** *116* (31), 16511-16521.
370. Caruso, T.; Lenardi, C.; Agostino, R.; Amati, M.; Bongiorno, G.; Mazza, T.; Policicchio, A.; Formoso, V.; Maccallini, E.; Colavita, E., Electronic structure of cluster assembled nanostructured TiO_2 by resonant photoemission at the Ti $L_{2,3}$ edge. *The Journal of chemical physics* **2008,** *128* (9), 094704.
371. Pan, J. H.; Lee, W. I., Preparation of highly ordered cubic mesoporous WO_3/TiO_2 films and their photocatalytic properties. *Chemistry of Materials* **2006,** *18* (3), 847-853.

372. Zhao, D.; Chen, C.; Yu, C.; Ma, W.; Zhao, J., Photoinduced electron storage in WO_3/TiO_2 nanohybrid material in the presence of oxygen and postirradiated reduction of heavy metal ions. *The Journal of Physical Chemistry C* **2009,** *113* (30), 13160-13165.
373. Gui, Y.; Blackwood, D., Electrochromic enhancement of WO_3-TiO_2 composite films produced by electrochemical anodization. *Journal of The Electrochemical Society* **2014,** *161* (14), 191-201.
374. Shpak, A.; Korduban, A.; Medvedskij, M.; Kandyba, V., XPS studies of active elements surface of gas sensors based on WO_{3-x} nanoparticles. *Journal of electron spectroscopy and related phenomena* **2007,** *156*, 172-175.
375. Ho, S. F. Ion Beam Induced Chemical Changes in the Oxyanions (MOyn-) and Oxides (MOx) where M. University of Houston, **1987**.
376. Chen, D. M.; Xu, G.; Miao, L.; Chen, L. H.; Nakao, S.; Jin, P., W-doped anatase TiO_2 transparent conductive oxide films: Theory and experiment. *Journal of Applied Physics* **2010,** *107* (6), 063707.
377. Kafizas, A.; Parkin, I. P., Combinatorial atmospheric pressure chemical vapor deposition (cAPCVD): a route to functional property optimization. *Journal of the American Chemical Society* **2011,** *133* (50), 20458-20467.
378. Sundberg, J.; Nyberg, H.; Särhammar, E.; Gustavsson, F.; Kubart, T.; Nyberg, T.; Jacobson, S.; Jansson, U., Influence of Ti addition on the structure and properties of low-friction W–S–C coatings. *Surface and Coatings Technology* **2013,** *232*, 340-348.
379. Leftheriotis, G.; Papaefthimiou, S.; Yianoulis, P.; Siokou, A., Effect of the tungsten oxidation states in the thermal coloration and bleaching of amorphous WO_3 films. *Thin solid films* **2001,** *384* (2), 298-306.
380. Xiong, X.; Chen, H.; Xu, Y., Improved photocatalytic activity of TiO_2 on the Addition of $CuWO_4$. *The Journal of Physical Chemistry C* **2015,** *119* (11), 5946-5953.
381. Gong, J.; Yang, C.; Pu, W.; Zhang, J., Liquid phase deposition of tungsten doped TiO_2 films for visible light photoelectrocatalytic degradation of dodecyl-benzenesulfonate. *Chemical Engineering Journal* **2011,** *167* (1), 190-197.
382. Barndõk, H.; Merayo, N.; Blanco, L.; Hermosilla, D.; Blanco, Á., Application of on-line FTIR methodology to study the mechanisms of heterogeneous advanced oxidation processes. *Applied Catalysis B: Environmental* **2016,** *185*, 344-352.
383. Mehrvar, M.; Anderson, W. A.; Moo-Young, M., Photocatalytic degradation of aqueous tetrahydrofuran, 1, 4-dioxane, and their mixture with TiO_2. *International Journal of Photoenergy* **2000,** *2* (2), 67-80.
384. Stefan, M. I.; Bolton, J. R., Mechanism of the degradation of 1, 4-dioxane in dilute aqueous solution using the UV/hydrogen peroxide process. *Environmental Science & Technology* **1998,** *32* (11), 1588-1595.
385. Kim, H. S.; Kwon, B. H.; Yoa, S. J.; Kim, I. K., Degradation of 1, 4-dioxane by photo-Fenton processes. *Journal of chemical engineering of Japan* **2008,** *41* (8), 829-835.
386. Maurino, V.; Calza, P.; Minero, C.; Pelizzetti, E.; Vincenti, M., Light-assisted 1, 4-dioxane degradation. *Chemosphere* **1997,** *35* (11), 2675-2688.
387. Dozzi, M. V.; Livraghi, S.; Giamello, E.; Selli, E., Photocatalytic activity of S-and F-doped TiO_2 in formic acid mineralization. *Photochemical & Photobiological Sciences* **2011,** *10* (3), 343-349.
388. Dozzi, M. V.; Ohtani, B.; Selli, E., Absorption and action spectra analysis of ammonium fluoride-doped titania photocatalysts. *Physical Chemistry Chemical Physics* **2011,** *13* (40), 18217-18227.
389. Martin, C.; Solana, G.; Rives, V.; Marci, G.; Palmisano, L.; Sclafani, A., Physico-chemical properties of WO_3/TiO_2 systems employed for 4-nitrophenol photodegradation in aqueous medium. *Catalysis letters* **1997,** *49* (3-4), 235-243.
390. Sohn, J. R.; Bae, J. H., Characterization of tungsten oxide supported on TiO_2 and activity for acid catalysis. *Korean Journal of Chemical Engineering* **2000,** *17* (1), 86-92.
391. Di Paola, A.; Marci, G.; Palmisano, L.; Schiavello, M.; Uosaki, K.; Ikeda, S.; Ohtani, B., Preparation of polycrystalline TiO_2 photocatalysts impregnated with various transition metal

ions: characterization and photocatalytic activity for the degradation of 4-nitrophenol. *The Journal of Physical Chemistry B* **2002,** *106* (3), 637-645.
392. de Tacconi, N. R.; Chenthamarakshan, C.; Rajeshwar, K.; Pauporté, T.; Lincot, D., Pulsed electrodeposition of WO_3–TiO_2 composite films. *Electrochemistry Communications* **2003,** *5* (3), 220-224.
393. Rampaul, A.; Parkin, I. P.; O'Neill, S. A.; DeSouza, J.; Mills, A.; Elliott, N., Titania and tungsten doped titania thin films on glass; active photocatalysts. *Polyhedron* **2003,** *22* (1), 35-44.
394. Shifu, C.; Lei, C.; Shen, G.; Gengyu, C., The preparation of coupled WO_3/TiO_2 photocatalyst by ball milling. *Powder Technology* **2005,** *160* (3), 198-202.
395. Rengifo-Herrera, J. A.; Blanco, M. N.; Pizzio, L. R., Photocatalytic bleaching of aqueous malachite green solutions by UV-A and blue-light-illuminated TiO_2 spherical nanoparticles modified with tungstophosphoric acid. *Applied Catalysis B: Environmental* **2011,** *110*, 126-132.
396. Yadav, H. M.; Otari, S. V.; Koli, V. B.; Mali, S. S.; Hong, C. K.; Pawar, S. H.; Delekar, S. D., Preparation and characterization of copper-doped anatase TiO_2 nanoparticles with visible light photocatalytic antibacterial activity. *Journal of Photochemistry and Photobiology A: Chemistry* **2014,** *280*, 32-38.
397. Cong, Y.; Zhang, J.; Chen, F.; Anpo, M.; He, D., Preparation, photocatalytic activity, and mechanism of nano-TiO_2 co-doped with nitrogen and iron (III). *The Journal of Physical Chemistry C* **2007,** *111* (28), 10618-10623.
398. Shen, W.; Chen, H.; Pan, S., Anaerobic biodegradation of 1, 4-dioxane by sludge enriched with iron-reducing microorganisms. *Bioresource technology* **2008,** *99* (7), 2483-2487.
399. Wong, R. S.; Feng, J.; Hu, X.; Yue, P. L., Discoloration and mineralization of non-biodegradable azo dye orange II by copper-doped TiO_2 nanocatalysts. *Journal of Environmental Science and Health, Part A* **2004,** *39* (10), 2583-2595.
400. Raddaha, N. S.; Cordero-Arias, L.; Cabanas-Polo, S.; Virtanen, S.; Roether, J. A.; Boccaccini, A. R., Electrophoretic deposition of chitosan/*h*-BN and chitosan/*h*-BN/TiO_2 composite coatings on stainless steel (316L) substrates. *Materials* **2014,** *7* (3), 1814-1829.
401. Liu, D.; Zhang, M.; Xie, W.; Sun, L.; Chen, Y.; Lei, W., Porous BN/TiO_2 hybrid nanosheets as highly efficient visible-light-driven photocatalysts. *Applied Catalysis B: Environmental* **2017,** *207*, 72-78.
402. Su, C. Y.; Tang, H. Z.; Zhu, G. D.; Li, C. C.; Lin, C. K., The optical properties and sunscreen application of spherical *h*-BN–TiO_2/mica composite powder. *Ceramics International* **2014,** *40* (3), 4691-4696.
403. Fu, X.; Hu, Y.; Yang, Y.; Liu, W.; Chen, S., Ball milled *h*-BN: an efficient holes transfer promoter to enhance the photocatalytic performance of TiO_2. *Journal of hazardous materials* **2013,** *244*, 102-110.
404. Xie, W.; Zhang, M.; Liu, D.; Lei, W.; Sun, L.; Wang, X., Reactive Yellow 161 Decolorization by TiO_2/Porous Boron Nitride Nanosheet Composites in Cotton Dyeing Effluent. *ACS Sustainable Chemistry & Engineering* **2016,** *5* (2), 1392-1399.
405. Singh, B.; Singh, P.; Singh, K.; Sharma, J.; Kumar, M.; Bala, R.; Meena, R.; Sharma, S. K.; Kumar, A., Nanostructured BN–TiO_2 composite with ultra-high photocatalytic activity. *New Journal of Chemistry* **2017,** *41* (20), 11640-11646.
406. Matović, B.; Luković, J.; Nikolić, M.; Babić, B.; Stanković, N.; Jokić, B.; Jelenković, B., Synthesis and characterization of nanocrystaline hexagonal boron nitride powders: XRD and luminescence properties. *Ceramics International* **2016,** *42* (15), 16655-16658.
407. Chen, T.; Xiao, J.; Yang, G., Cubic boron nitride with an intrinsic peroxidase-like activity. *RSC Advances* **2016,** *6* (74), 70124-70132.
408. Deura, M.; Kutsukake, K.; Ohno, Y.; Yonenaga, I.; Taniguchi, T., Nanoindentation measurements of a highly oriented wurtzite-type boron nitride bulk crystal. *Japanese Journal of Applied Physics* **2017,** *56* (3), 030301.
409. Yuan, C.; Duan, B.; Li, L.; Xie, B.; Huang, M.; Luo, X., Thermal conductivity of polymer-based composites with magnetic aligned hexagonal boron nitride platelets. *ACS applied materials & interfaces* **2015,** *7* (23), 13000-13006.

410. Wang, X.; Wang, W.; Wang, X.; Zhang, J.; Zhao, J.; Gu, Z.; Zhou, L., Synthesis, structural characterization and evaluation of floating BN codoped TiO_2/expanded perlite composites with enhanced visible light photoactivity. *Applied Surface Science* **2015,** *349*, 264-271.
411. Lu, N.; Quan, X.; Li, J.; Chen, S.; Yu, H.; Chen, G., Fabrication of boron-doped TiO_2 nanotube array electrode and investigation of its photoelectrochemical capability. *The Journal of Physical Chemistry C* **2007,** *111* (32), 11836-11842.
412. Paine, R. T.; Narula, C. K., Synthetic routes to boron nitride. *Chemical Reviews* **1990,** *90* (1), 73-91.
413. Sheng, Y.; Yang, J.; Wang, F.; Liu, L.; Liu, H.; Yan, C.; Guo, Z., Sol-gel synthesized hexagonal boron nitride/titania nanocomposites with enhanced photocatalytic activity. *Applied Surface Science* **2019,** *465*, 154-163.
414. Li, D.; Jia, J.; Zhang, Y.; Wang, N.; Guo, X.; Yu, X., Preparation and characterization of Nano-graphite/TiO_2 composite photoelectrode for photoelectrocatalytic degradation of hazardous pollutant. *Journal of hazardous materials* **2016,** *315*, 1-10.
415. Elfeky, S. A.; Al-Sherbini, A. S., Photo-oxidation of rhodamine-6-G via TiO_2 and Au/TiO_2-bound polythene beads. *Journal of Nanomaterials* **2011,** *2011*, 74.
416. Bamwenda, G. R.; Tsubota, S.; Nakamura, T.; Haruta, M., Photoassisted hydrogen production from a water-ethanol solution: a comparison of activities of Au-TiO_2 and Pt-TiO_2. *Journal of Photochemistry and Photobiology A: Chemistry* **1995,** *89* (2), 177-189.
417. Ni, M.; Leung, M. K.; Leung, D. Y.; Sumathy, K., A review and recent developments in photocatalytic water-splitting using TiO_2 for hydrogen production. *Renewable and Sustainable Energy Reviews* **2007,** *11* (3), 401-425.
418. Rosseler, O.; Shankar, M. V.; Karkmaz-Le Du, M.; Schmidlin, L.; Keller, N.; Keller, V., Solar light photocatalytic hydrogen production from water over Pt and Au/TiO_2 (anatase/rutile) photocatalysts: Influence of noble metal and porogen promotion. *Journal of Catalysis* **2010,** *269* (1), 179-190.
419. Wang, C.; Hu, Q.; Huang, J.; Zhu, C.; Deng, Z.; Shi, H.; Wu, L.; Liu, Z.; Cao, Y., Enhanced hydrogen production by water splitting using Cu-doped TiO_2 film with preferred (0 0 1) orientation. *Applied Surface Science* **2014,** *292*, 161-164.
420. Zeng, P.; Zhang, Q.; Zhang, X.; Peng, T., Graphite oxide–TiO_2 nanocomposite and its efficient visible-light-driven photocatalytic hydrogen production. *Journal of Alloys and Compounds* **2011**.
421. Zhang, X.; Peng, T.; Song, S., Recent advances in dye-sensitized semiconductor systems for photocatalytic hydrogen production. *Journal of Materials Chemistry A* **2016,** *4* (7), 2365-2402.
422. Ismail, A. A.; Bahnemann, D. W., Photochemical splitting of water for hydrogen production by photocatalysis: a review. *Solar Energy Materials and Solar Cells* **2014,** *128*, 85-101.
423. Tong, H.; Ouyang, S.; Bi, Y.; Umezawa, N.; Oshikiri, M.; Ye, J., Nano-photocatalytic materials: possibilities and challenges. *Advanced materials* **2012,** *24* (2), 229-251.
424. Chen, X.; Shen, S.; Guo, L.; Mao, S. S., Semiconductor-based photocatalytic hydrogen generation. *Chemical reviews* **2010,** *110* (11), 6503-6570.
425. Niu, W.; Wang, G.; Liu, X.; Tang, J.; Bi, X., Preparation of WO_3-TiO_2 photo-anode and its performance of photocatalytic hydrogen production by water splitting. *Int J Electrochem Sc* **2015,** *10*, 8513-8521.
426. Chen, Y. L.; Lo, S. L.; Chang, H. L.; Yeh, H. M.; Sun, L.; Oiu, C., Photocatalytic hydrogen production of the CdS/TiO_2-WO_3 ternary hybrid under visible light irradiation. *Water science and technology* **2016,** *73* (7), 1667-1672.
427. Momeni, M. M.; Ghayeb, Y.; Davarzadeh, M., Single-step electrochemical anodization for synthesis of hierarchical WO_3–TiO_2 nanotube arrays on titanium foil as a good photoanode for water splitting with visible light. *Journal of Electroanalytical Chemistry* **2015,** *739*, 149-155.
428. Lai, C. W.; Sreekantan, S., Preparation of hybrid WO_3–TiO_2 nanotube photoelectrodes using anodization and wet impregnation: improved water-splitting hydrogen generation performance. *International Journal of Hydrogen Energy* **2013,** *38* (5), 2156-2166.

429. Lai, C. W.; Lau, K. S.; Abd Hamid, S. B. In *Controlled Growth of WO3-Loaded TiO_2 Nanotubes for Tandem Solar-Driven Water Splitting Cell*, Advanced Materials Research, Trans Tech Publ: **2015**; 243-247.
430. Low, J.; Yu, J.; Jaroniec, M.; Wageh, S.; Al-Ghamdi, A. A., Heterojunction photocatalysts. *Advanced Materials* **2017,** *29* (20), 1601694.
431. Society, I. C. Cancer statistics - Facts and figures on cancer rates in Ireland, including incidence, survival and mortality. https://www.cancer.ie/about-us/media-centre/cancer-statistics#sthash.UdN1ue7o.AQSzsboX.dpbs (accessed 21st of November 2018).
432. Shen, Y.; Shuhendler, A. J.; Ye, D.; Xu, J.-J.; Chen, H.-Y., Two-photon excitation nanoparticles for photodynamic therapy. *Chemical Society Reviews* **2016,** *45* (24), 6725-6741.
433. Liu, K.; Xing, R.; Zou, Q.; Ma, G.; Möhwald, H.; Yan, X., Simple Peptide-Tuned Self-Assembly of Photosensitizers towards Anticancer Photodynamic Therapy. *Angewandte Chemie* **2016,** *128* (9), 3088-3091.
434. Theodossiou, T. A.; Gonçalves, A. R.; Yannakopoulou, K.; Skarpen, E.; Berg, K., Photochemical Internalization of Tamoxifens Transported by a "Trojan-Horse" Nanoconjugate into Breast-Cancer Cell Lines. *Angewandte Chemie* **2015,** *127* (16), 4967-4971.
435. Castano, A. P.; Demidova, T. N.; Hamblin, M. R., Mechanisms in photodynamic therapy: part one—photosensitizers, photochemistry and cellular localization. *Photodiagnosis and photodynamic therapy* **2004,** *1* (4), 279-293.
436. Deda, D. K.; Araki, K., Nanotechnology, light and chemical action: An effective combination to kill cancer cells. *Journal of the Brazilian Chemical Society* **2015,** *26* (12), 2448-2470.

Appendix 1: Publications and Presentations

Publications

Peer-Review Papers

1. **Byrne, C.,** Moran, L., Hermosilla, D., Merayo, N., Blanco, Á., Rhatigan, S., ... & Pillai, S. C. (2019). Effect of Cu Doping on the Anatase-to-Rutile Phase Transition in TiO_2 Photocatalysts: Theory and Experiments. *Applied Catalysis B: Environmental. In Press.* **Impact Factor: 11.698**
2. Mathew, S., Ganguly, P., Rhatigan, S., Kumaravel, V., **Byrne, C.**, Hinder, S., ... & Pillai, S. (2018). Cu-Doped TiO_2: Visible Light Assisted Photocatalytic Antimicrobial Activity. *Applied Sciences*, *8*(11), 2067. **Impact factor: 1.484.**
3. **Byrne, C**., Subramanian, G., & Pillai, S. C. (2018). Recent advances in photocatalysis for environmental applications. *Journal of Environmental Chemical Engineering*, *6* (3), 3531-3555. **Impact Factor: Not Announced**
4. Ganguly, P., **Byrne, C**., Breen, A., & Pillai, S. C. (2018). Antimicrobial Activity of Photocatalysts: Fundamentals, Mechanisms, Kinetics and Recent Advances. *Applied Catalysis B: Environmental, 225*, 51-75. **Impact factor: 11.698**
5. **Byrne, C.,** Fagan, R., Hinder, S., McCormack, D. E., & Pillai, S. C. (2016). New approach of modifying the anatase to rutile transition temperature in TiO_2 photocatalysts. *RSC Advances*, *6* (97), 95232-95238. **Impact factor: 2.936**
6. Garvey, M., Panaitescu, E., Menon, L., **Byrne, C.,** Dervin, S., Hinder, S. J., & Pillai, S. C. (2016). Titania nanotube photocatalysts for effectively treating waterborne microbial pathogens. *Journal of Catalysis*, *344*, 631-639. **Impact factor: 6.759**

Book Chapters

7. Pillai, S. C., McGuinness, N. B., **Byrne, C**., Han, C., Lalley, J., Nadagouda, M., & Mangalaraja, R. V. (2017). Photocatalysis as an effective advanced oxidation process. *Advanced Oxidation Processes for Water Treatment: Fundamentals and Applications*, 333-381.
8. **Byrne, C.,** Nolan, M., Banerjee, S., John, H., Josef, S., Periyat, P. & Pillai, S. C. (2018). Advances in the Development of Novel Photocatalysts for Detoxification. *Visible Light-Active Photocatalysis: Nanostructured Catalyst Design, Mechanisms, and Applications*, 283-327.

Manuscripts under Revision

1. TiO_2 and WO_3 for the effective photocatalytic decomposition of 1,4-dioxane. **Byrne, C.,** Dervin, S., Hermosilla, D., Merayo, N., Blanco, A., Hinder, S. J., Cao, Z., Harb, M., Cavallo, L., Dionysiou, D. D. & Pillai, S. C.
2. Increased Photocatalytic Degradation of 1,4-dioxane with Boron Nitride Doped TiO_2. **Byrne, C.,** Hermosilla, D., Merayod, N., Blancod, A., Hinder, S. J., & Pillai, S. C.
3. Gold doped TiO_2 for the Photocatalytic Degradation of 1,4-dioxane. **Byrne, C.,** Hermosilla, D., Merayod, N., Blancod, A., Hinder, S. J., & Pillai, S. C.
4. Review of the Anatase to Rutile Transition in Titanium Dioxide Nanomaterials. **Byrne, C.,** Rhatigan, S., Nolan, M. & Pillai S. C.

Conference Proceedings

1. **Short Oral Communication & Poster**. "The Impact of Tungsten Doped Titanium Dioxide on the Phase Transition and Photocatalytic Properties" at 2nd Summer School on Environmental Applications of Advanced Oxidation Processes of the European PhD School on AOPs and NEREUS COST Action ES1403 Summer School on Advanced Treatment Technologies and Contaminants of Emerging Concern, 10th-14th July 2017, Auditorium of the Almeida Garrett Municipal Library (Porto, Portugal)
2. **Oral Presentation.** "Titanium Dioxide Nanomaterials for Healthcare Applications" at the Biomedical Postgraduate Research Conference, 20th-21st June 2017, IT Sligo, Ireland.
3. **Oral Presentation.** "The impact of copper on the anatase to rutile transition in titanium dioxide and the photocatalytic properties" at The 2017 E-MRS Spring Meeting and Exhibit in Symposium F Photocatalytic materials for energy and environment, 22nd-26th May 2017, Convention Centre of Strasbourg (France).
4. **Oral Presentation.** "Anatase to Rutile Transition in TiO_2 Nanomaterials for Environmental Applications" at the 27th Irish Environmental Researcher's Colloquium (ENVIRON) in Nanotechnology 10th- 12th April 2017, Athlone IT, Ireland.
5. **Oral Presentation.** "Anatase to Rutile transition in titanium dioxide nanomaterials for environmental applications" at the 26th Irish Environmental

Researcher's Colloquium (ENVIRON) in Nanotechnology, 22nd-24th March, 2016, University of Limerick, Ireland.

6. **Oral Presentation.** "Synthesis of Titanium Dioxide Nanomaterials for Environmental Applications" at the 25th Irish Environmental Researcher's Colloquium (ENVIRON) in Nanotechnology, 8th-10th April 2015, IT Sligo, Ireland.